

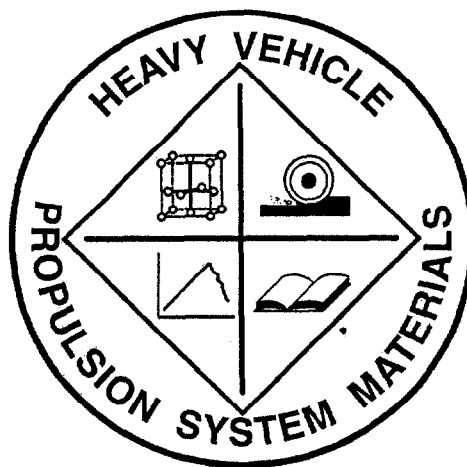
OAK RIDGE
NATIONAL LABORATORY

MANAGED BY UT-BATTELLE
FOR THE DEPARTMENT OF ENERGY

ORNL/TM-2000/233

**Heavy Vehicle Propulsion System
Materials Program
Semiannual Progress Report for
October 1999 Through March 2000**

Prepared for
U.S. Department of Energy
Assistant Secretary for
Energy Efficiency and Renewable Energy
Office of Transportation Technologies




UT-BATTELLE

ORNL/TM-2000/233

Metals and Ceramics Division

**HEAVY VEHICLE PROPULSION SYSTEM MATERIALS PROGRAM
SEMIANNUAL PROGRESS REPORT FOR
OCTOBER 1999 THROUGH MARCH 2000**

**D. R. Johnson
Program Manager**

Date Published: August 2000

NOTICE:

This document contains information of a preliminary nature. It is subject to revision or correction and therefore does not represent a final report.

**Prepared for
U.S. Department of Energy
Assistant Secretary for Energy Efficiency and Renewable Energy
Office of Transportation Technologies
EE 07 01 000**

**Prepared by the
OAK RIDGE NATIONAL LABORATORY
Oak Ridge, Tennessee 37831-6285
managed by
UT-Battelle, LLC
for the
U.S. DEPARTMENT OF ENERGY
under Contract DE-AC05-00OR22725**

REPORTS PREVIOUSLY ISSUED

ORNL/TM-9325	Period March 1983-September 1983
ORNL/TM-9466	Period October 1983-March 1984
ORNL/TM-9497	Period April 1984-September 1984
ORNL/TM-9673	Period October 1984-March 1985
ORNL/IM-9947	Period April 1985-September 1985
ORNL/TM-10079	Period October 1985-March 1986
ORNL/TM-10308	Period April 1986-September 1986
ORNL/TM-10469	Period October 1986-March 1987
ORNL/TM-10705	Period April 1987-September 1987
ORNL/TM-10838	Period October 1987-March 1988
ORNL/TM-11116	Period April 1988-September 1988
ORNL/TM-11239	Period October 1988-March 1989
ORNL/TM-11489	Period April 1989-September 1989
ORNL/TM-11586	Period October 1989-March 1990
ORNL/TM-11719	Period April 1990-September 1990
ORNL/TM-11859	Period October 1990-March 1991
ORNL/TM-11984	Period April 1991-September 1991
ORNL/TM-12133	Period October 1991-March 1992
ORNL/TM-12363	Period April 1992-September 1992
ORNL/TM-12428	Period October 1992-March 1993
ORNL/TM-12674	Period April 1993-September 1993
ORNL/TM-12778	Period October 1993-March 1994
ORNL/TM-12924	Period April 1994-September 1994
ORNL/TM-13046	Period October 1994-March 1995
ORNL/TM-13219	Period April 1995-September 1995
ORNL/TM-13262	Period October 1995-March 1996
ORNL/TM-13395	Period April 1996-September 1996
ORNL/TM-13467	Period October 1996-March 1997
ORNL/TM-13562	Period April 1997-September 1997
ORNL/TM-13648	Period October 1997-March 1998
ORNL/TM-13735	Period April 1998-September 1998
ORNL/TM-1999/95	Period October 1998-March 1999
ORNL/TM-2000/16	Period April 1999-September 1999

Research sponsored by the U.S. Department of Energy, Assistant Secretary for Energy Efficiency and Renewable Energy, Office of Transportation Technologies, as part of the Heavy Vehicle Propulsion System Materials Program, under contract DE-AC05-00OR22725 with UT-Battelle, LLC.

CONTENTS

SUMMARY AND INTRODUCTION	1
COST EFFECTIVE HIGH PERFORMANCE MATERIALS AND PROCESSING.....	3
<i>Cost-Effective Smart Materials for Diesel Engine Applications (ORNL)</i>	<i>5</i>
<i>Low Cost High Toughness Ceramics (ORNL).....</i>	<i>27</i>
<i>Cost-Effective Sintering of Silicon Nitride Ceramics (SIU-C)</i>	<i>37</i>
<i>Diesel Particulate Trap Development (ORNL).....</i>	<i>45</i>
ADVANCED MANUFACTURING TECHNOLOGY	49
<i>Durability of Diesel Engine Component Materials (ORNL).....</i>	<i>51</i>
<i>NDE of Ceramic Valves for Diesel Engines (Argonne National Laboratory)</i>	<i>54</i>
<i>Intermetallic -Bonded Cermets (ORNL)</i>	<i>60</i>
<i>Cost Effective Machining of Ceramic Engine Components (ORNL)</i>	<i>66</i>
TESTING AND CHARACTERIZATION	69
<i>NDE Technology for Fuel Delivery and Insulating Materials (Argonne National Laboratory)</i>	<i>71</i>
<i>Testing and Evaluation of Advanced Ceramics at High Temperature (North Carolina A&T State University)</i>	<i>73</i>
<i>Life Prediction of Ceramic Diesel Engine Components (ORNL)</i>	<i>82</i>
<i>Field Emission Analytical Electron Microscopy for Characterization of Catalyst Microstructures (ORNL)</i>	<i>91</i>
MATERIALS AND TESTING STANDARDS	93
<i>IEA ANNEX II Management (ORNL).....</i>	<i>95</i>
<i>Standards for High Temperature Transportation Materials (NIST)</i>	<i>100</i>
<i>Ceramic Mechanical Property Test Method Development (NIST).....</i>	<i>103</i>

HEAVY VEHICLE PROPULSION SYSTEM MATERIALS PROGRAM
SEMIANNUAL PROGRESS REPORT
FOR OCTOBER 1999 THROUGH MARCH 2000

SUMMARY AND INTRODUCTION

The purpose of the Heavy Vehicle Propulsion System Materials Program is the development of materials: ceramics, intermetallics, metal alloys, and metal and ceramic coatings, to support the dieselization of class 1-3 trucks to realize a 35% fuel-economy improvement over current gasoline-fueled trucks and to support commercialization of fuel-flexible LE-55 low-emissions, high-efficiency diesel engines for class 7-8 trucks.

The Office of Transportation Technologies, Office of Heavy Vehicle Technologies (OTT OHVT) has an active program to develop the technology for advanced LE-55 diesel engines with 55% efficiency and low emissions levels of 2.0 g/bhp-h NOx and 0.05 g/bhp-h particulates. The goal is also for the LE-55 engine to run on natural gas with efficiency approaching that of diesel fuel. The LE-55 program is being completed in FY 1997 and, after approximately 10 years of effort, has largely met the program goals of 55% efficiency and low emissions. However, the commercialization of the LE-55 technology requires more durable materials than those that have been used to demonstrate the goals. Heavy Vehicle Propulsion System Materials will, in concert with the heavy duty diesel engine companies, develop the durable materials required to commercialize the LE-55 technologies.

OTT OHVT also recognizes a significant opportunity for reduction in petroleum consumption by dieselization of pickup trucks, vans, and sport utility vehicles. Application of the diesel engine to class 1, 2, and 3 trucks is expected to yield a 35% increase in fuel economy per vehicle. The foremost barrier to diesel use in this market is emission control. Once an engine is made certifiable, subsequent challenges will be in cost; noise, vibration, and harshness (NVH); and performance.

The design of advanced components for high-efficiency diesel engines has, in some cases, pushed the performance envelope for materials of construction past the point of reliable operation. Higher mechanical and tribological stresses and higher temperatures of advanced designs limit the engine designer; advanced materials allow the design of components that may operate reliably at higher stresses and temperatures, thus enabling more efficient engine designs. Advanced materials also offer the opportunity to improve the emissions, NVH, and performance of diesel engines for pickup trucks, vans, and sport utility vehicles.

The principal areas of research are:

Cost Effective High Performance Materials and Processing
Advanced Manufacturing Technology
Testing and Characterization
Materials and Testing Standards

**COST EFFECTIVE HIGH PERFORMANCE
MATERIALS AND PROCESSING**

Cost-Effective Smart Materials for Diesel Engine Applications

J. O. Kiggans, Jr., T. N. Tiegs,

F. C. Montgomery, L. C. Maxey, and A. R. Steffans

Oak Ridge National Laboratory

Oak Ridge, TN 37831

Objective / Scope

There are two objectives for this project. The first is to evaluate the cost-effectiveness and maturity of various "Smart Materials Technologies," which are under consideration for diesel engine applications, such as fuel injection systems. The second is to develop "Smart Materials," to be incorporated into working actuators and sensors.

Task 1 a - Fabrication of PZT laminates

Introduction

It is now believed that cost-effective actuators will consist of thin multi-layered PZT structures constructed from tape cast PZT layers containing internal screen printed electrodes. The present task was initiated to develop the fabrication steps necessary for construction of these multi-layered actuators. The first part of this task is to tape cast PZT-4 material, and to study the lamination of the tapes.

Experimental

Tape cast materials were fabricated using a Mistler Co. TTC-1000 tape casting machine. The polyvinyl butyral (PVB) tape slurries consisted of 78.6 wt. % PZT-4 (APC Ceramics), 7.4 wt. % xylene (J. T. Baker), 7.4 wt. % anhydrous ethanol (J. T. Baker), 1.0 wt. % menhaden fish oil (Tape Cast Warehouse), 1.6 wt. % butyl benzyl phthalate (Tape Cast Warehouse), 1.6 wt. % polyethylene glycol 400 (PEG 400, Chemcentral), and 2.5 wt. % PVB (Butvar-98, Monsanto Chemical Co.). Tapes were cast at a speed of 20 cm/min onto a mylar film using a 15.25 cm wide doctor blade adjusted to a thickness of 0.03 cm. The thickness of the dried green tapes was ~0.20 to 0.25 mm thick. A metal punch was used to cut 2.7 cm diameter discs from the tape. The discs were stored in a dessicator separated by wax weighing paper for stable storage prior to use. Multiple tape laminates were made from each stock tape using the following procedure: 4 to 6 slices of the PVB tape, with 2.7 cm diameter mylar discs placed on each end of each PZT stack. Table 1 shows the $L_9(3^4)$ Taguchi

orthogonal array used for the lamination study. A total of 9 lamination trials and samples were needed to test the four experimental variables at three levels. The variables used for this study were temperature, lamination pressure, lamination time, and pre-heat time at temperature for tape slices stacked in the steel die prior to lamination. All samples were heated to 600 °C remove the binders and then sintered at 1125°C for 24 h. After sintering sample weight losses and final densities were determined using the Archimedes immersion density method.

Results

Table 2 lists the green and sintered density values for the 9 samples that were laminated and sintered in the Taguchi test. These data show that all samples sintered to >96 % T.D. Figure 1 is a set of four plots which show the average density values for PZT-4 tape laminates sintered in the Taguchi experimental array as a function of a) lamination temperature, b) lamination time, c) lamination pressure, and d) preheat time of die and tape layers prior to die lamination. The four plots indicate that the most robust conditions for lamination include: a 60 min preheat of laminate samples in the steel die at 70 °C, followed by pressing at 6.9 MPa pressure for 10 min.

Task 1 B - Fabrication of PZT laminates

Introduction

Recent collaborative work between ORNL and Ceradyne Inc. has demonstrated that the “Elvacite 2010” tape cast binder “unzips” and is easily burned-out from thick (> 2.5 cm) ceramic laminates. Our previous research has shown that PVB, our present tape cast binder, can be difficult to remove. These findings pose the question as to whether the Elvacite binder may be a better binder system than the PVB binder system that is presently employed to make PZT laminates. . A set of experiments was designed to address this question. In addition, since the final densities of sintered PZT laminates are strongly influenced by the green densities of the laminates, samples containing Elvacite and PVB were isopressed to increase green densities prior to binder burn-out and sintering. Also, since the high amounts of lubricants and binders necessary for tape casting could inhibit the isopress process, we are testing a novel idea to partially remove the lubricants and binders in the laminates using a low temperature binder burn-out step prior to the isopress process.

Experimental

Both PVB and Elvacite 2010 tapes were fabricated for this study. The procedures for preparing PZT-4 tapes with the PVB binder were discussed in the previous section. The following describes the preparation of Elvacite tapes: The Elvacite

tapes were made from slurries which consisted of 82.8 wt. % PZT-4, 8.9 wt. % toluene (Mallinckrodt), 1.8 wt. % anhydrous ethanol, 0.4 wt. % menhaden fish oil, 3.0 wt. % n-benzyl phthalate (Tape Cast Warehouse), and 3.1 wt. % Elvacite 2010 (ICI Acrylics, Inc.). Multiple tape laminates were made from each stock tape using the following procedure: 4 to 6 slices of the Elvacite 2010 tape were laminated using a 60 min preheat of laminate samples in the 2.7 cm diameter steel die at 90 °C, followed by pressing at 6.9 MPa pressure for 10 min. The PVB laminates are designated PVB-L and the Elvacite laminates are designated Elv-L. Two samples of each type were isopressed on top of an alumina setter in a latex rubber bag at 206 MPa. These samples are designated as PVB-L-IP and Elv-L-IP. Two laminated samples of each type were heated in an AD 998 alumina tray with tabular alumina between the laminate and tray at 5 °C/min to 225°C, held at 225°C for 30 min, and cooled at 5 °C/min to room temperature. These samples were isopressed under the same conditions as previous samples. These samples are designated PVB-L-225C-L and Elv-L-225C-L. All samples were heated to 600 °C remove the binders and then sintered at 1125°C for 24 h.

Results

Figure 2 is a summary graph showing the sintered densities of the tape laminates. The data show that the two PVB-L samples sintered to higher average density, 95.0 % T.D. compared to 92.6 % T.D. for the Elv-L samples. The isopress treatment of laminated samples resulted in a slightly higher average density for the Elv-L-IP samples at 97.85 % T.D. compared to 97.09 % T. D. for the PVB-L-IP samples. This is expected, since the isopress step should increase the green densities of the laminates, and result in higher sintered densities. The final group of samples which were laminated, heated tom 225°C, and then isopressed had the highest sintered densities of the samples tested. The Elv-L-225C-IP samples had an average density of 99.23 % T.D. and the PVB-L-225C-IP had an average density of 98.33 % T.D. Both the Elv-L-225C-IP and the PVB-L-225C-IP lost approximately 3.3 % of the initial weight during the 225°C heat treatment, which approximates the amount of lubricants, butyl benzyl phthlate and PEG 400 for the PVB laminates, and n-butyl phthlate for the Elvacite laminates. It is postulated that the loss of these lubricants from the laminates may allow more open pore space that can be compacted during the isopress step that follows.

Task 1 C– Fabrication of PZT laminates

This task is directed towards the determination of the optimal conditions for preparing multilayered PZT laminates. This study compares Elvacite 2010 and PVB binders that are employed in our lab to fabricate PZT tapes, and is an extension of the previous

section. The basic idea is to increase the sinterability of PZT laminates by increasing their green densities via heat treatment and isostatic pressing. Others have shown that one can increase the green density of ceramic tapes by pressing techniques.^{1,2} The effectiveness of the pressing treatment was highly depended on the percent of organic content relative to the ceramic material in the tapes. Our work extends the referenced work by increasing the powder to organic ratio by removing organic materials by heat treatments. Tape laminates are green bodies that contain ceramic particles, binders, bound solvents, liquid plasticizers, and gas molecules. The laminate can act somewhat like a "balloon" filled with liquid and suspended particles that merely move around on compression without increasing in density. By removing excess liquids from the tape, it is hoped that the balloon-like structure can be transformed into a compressible sponge structure containing binders for strength.

Experimental Procedure:

The preparation of PVB and Elvacite tapes and laminates was discussed in the previous sections. Duplicate samples were made for each experiment. A flow diagram of this lamination study is given in Figure 3. Samples were either not heated (control = C) or heated to 125, 175, 225, or 250 °C prior to the isopress step. The 125 and 175 °C heat treatments included a 72 h hold period at temperature in air. An additional set of samples was heated to 175 °C in vacuum and held in vacuum for 72 h. The 225 and 250 °C sample groups were heated at 1 °C / min and held at temperature for 1 h. Samples were then: a) isopressed in latex bags on top of a alumina setter at 206 MPa (IPSD206MPa); b) isopressed also at 206 MPa but without a setter disc (IPND206MPa); c) isopressed at 344 MPa without a setter disc (IPND344MPa); or d) uniaxial die pressed at 69 MPa (DP69MPa). After the final pressing treatment the samples were heated in a alumina crucible to 600°C to remove the binder. Samples were then sintered at 1125°C for 24 h under conditions discussed in previous reports.

Results

Figure 4 shows the densities as per cent of theoretical density (% T. D.) for the sintered laminates processed by the various treatments. The control sample L, which did not receive any processing after lamination, had a much lower density than all samples that were isopressed prior to sintering. The laminated sample that was heated to 225°C and then was die pressed at 69 MPa (L-225C-DP69MPa) also had a lower density than the other samples. In general, it is noted that samples processed with the PVB binder had higher densities than laminates made using the Elvacite binder. The best density was obtained for the PVB laminate designated L-225C-IPND206MPa. This sample was heated to 225°C and then

isopressed at 206 MPa with no disc support. The samples that were laminated or heated to less than 225°C warped during the isopress treatment unless a support disc was provided. Also, when support discs were used during the isopress treatment, the samples did not undergo the same degree of radial compaction than when the disc was not present. Weight loss data for each sample type was recorded, but the data was not easily correlated, because of unpredictable differences in solvent retained in the tapes. Overall, the results show that a heat treatment step prior to isopressing laminated PZT samples can result in improved densification. This is due to an increase in the green densities of these parts, although the densities of the green laminates were difficult to quantitate.

Task 2 a - Alternative Low Temperature Sinterable PZT Compositions

Introduction

The second task of the project for is the study of cost-effective alternative PZT compositions and processing methods to allow low temperature (~1125 °C) sintering and grain growth of PZT materials. Various sintering additives and grain growth enhancers were selected for testing from literature references for this study.

Experimental

Seventeen sample types were made using PZT-4 powder (PZT 840, APC International, Inc.) with the additions listed in Tables 3, 4, and 5. Control samples from the as-received powder were made by the following procedures: 1) pressing the received powder into discs; 2) mixing PZT-4 powder with binders and a lubricant, then milling, drying, grinding, and pressing the powder into green discs (DP-1 PZT 840); or 3) mixing PZT-4 powder with a binder, lubricant, and chemical(s), then milling, drying, grinding, and pressing the powder into green discs. Exact conditions for adding chemical additions and sample preparation are discussed in the previous reports. Samples were sintered at 1125 °C for 3, 24, or 48 h. The sintered density of each sample was measured, and electromechanical measurements were made using previously described methods. Samples were etched for 30 sec at room temperature with a solution containing 2.3 wt. % hydrochloric acid and 0.12 wt. % hydrofluoric acid. Samples were examined using a Nikon Epiphot – TME inverted microscope.

Results

Table 3 lists the density values and electromechanical measurements for PZT materials sintered at 1125 °C for 3 h. There are several important points noted in this 3 h data:

- 1) Samples with no chemical additions, PZT 840 (79.9%T.D.) and DP-1 PZT 840

(84.1 %T.D.), exhibited low densities. 2) Additions of Ag_2CO_3 (98.8 %T.D.) Bi_2O_3 (101.5 %T.D.), PbO (several above 93 % T.D.), and Cr_2O_3 (90.4 % T.D.) resulted in increased densification of PZT 4 powder. Mixtures of additives did not result in greater increases in densification than the most active component of the mixture. 3) Only the sample with Bi_2O_3 addition achieved acceptable d_{33} value. >0.28 . (The manufacturer's literature d_{33} value is 0.3 for materials sintered at $1275\text{ }^\circ\text{C}$). 4) The control PZT 840 and the samples containing 2 wt. % Bi_2O_3 had K_t values >0.5 ; although the high K_t for the control samples does not correlate well with the low densities of the PZT 840 samples. 5) The Bi_2O_3 addition resulted in a very high relative dielectric constant (K_{33}^T), 1724, compared to the PZT 840 value of 650.

Table 4 lists the density values and electromechanical measurements for PZT materials sintered at $1125\text{ }^\circ\text{C}$ for 24 h. There are several important points also noted in this 24 h data: 1) Greater than 98 % densification was obtained for nearly all sample types, including the controls. 2) Several sample types achieved acceptable d_{33} values (>0.28). 3) Only samples containing Bi_2O_3 or $\text{Bi}_4\text{Ti}_3\text{O}_{12}$ had K_t values >0.5 . 4) The Bi_2O_3 , Ag_2CO_3 , and $\text{Bi}_4\text{Ti}_3\text{O}_{12}$ additions resulted in higher relative dielectric constants compared to the control sample.

Table 5 lists the density values and electromechanical measurements for PZT materials sintered at $1125\text{ }^\circ\text{C}$ for 48 h. There are several important points in this 48 h data: 1) Greater than 99 % densification was obtained for nearly all sample types, including the controls. 2) All samples except the control PZT 840 types achieved a d_{33} value >0.28 . 3) Both the samples containing Bi_2O_3 and Ag_2CO_3 had K_t values (>0.5). 4) The Bi_2O_3 and Ag_2CO_3 additions resulted in higher relative dielectric constants than the PZT 840 sample.

Further samples with chemical additions are being fabricated. The present data show that the densification temperature of PZT materials can be easily lowered below $1125\text{ }^\circ\text{C}$; however this comes with a trade-off in the electromechanical properties with higher K_{33}^T and lower Q_m values.

Table 6 lists the densities of the samples that were examined in this study. All samples discussed in this section had densities over 98 % T.D., and the differences between the densities of the test samples fall within statistical deviation limits. Figure 5a and 5b show the optical images of control PZT-4 (no additives) sintered for 24 and 48 h, respectively. The average grain sizes of the control samples sintered for 24 and 48 h are very similar at about 1 – 2 μm . Figure 5c shows the optical image of PZT-4 which

contained 2 wt. % PbO and was sintered for 24 h. There is very little difference between the average grain size of this material and the control sample sintered for 24 h. Figure 6a and 6b show photos of samples containing 0.1 wt. % Ag_2CO_3 and sintered for 24 and 48 h, respectively. Once again these have microstructures similar to the controls. Silver (Ag) is of interest because its addition, even at very low levels, appears to enhance low temperature sintering of PZT. Reports have also indicated that Ag can improve the reliability of PZT materials. Figure 6c and 6d show samples containing 2.0 wt. % Ag_2CO_3 and 0.1% wt. % Cr_2O_3 , respectively. Cr_2O_3 is of interest because it can increase the mechanical quality factor, Q_m , and reduce the rate of aging in PZT materials. Also, both grain growth and grain inhibition have been reported for Cr_2O_3 additions to ceramic materials. The microstructures of both the samples that contained Ag and Cr_2O_3 are again similar to the controls. Neither additive stimulates grain growth in PZT-4 at 1125 °C. Figure 7a and 7b show images of PZT samples containing 0.1% wt. % Cr_2O_3 + 0.1 wt. % Ag_2CO_3 . The microstructures of these samples are again similar to the controls, showing that there are no combination effects from these two additives on PZT grain growth. Figure 8a and 8b show images of PZT-4 containing 2 wt. % Bi_2O_3 and sintered for 24 and 48 h, respectively. It is noted that the Bi_2O_3 has caused grain growth in both samples, with grain sizes ranging from 5 to 30 μm in the 24 h sample, and grains up to 40 μm in the 48 h sample. Thus, the grain growth was related to time of sintering. Figures 8c and 8d show images of samples containing 2 wt. % Bi_2O_3 + 0.1% wt. % Cr_2O_3 and sintered for 24 and 48 h, respectively. It is apparent that the Cr_2O_3 addition did not arrest the grain growth caused by the Bi_2O_3 addition. It is hoped that the growth stimulated by the Bi_2O_3 addition can be used to an advantage for actuator materials.

Task 3 - Testing of a Multilayer Stack Actuator

Introduction

A piezoelectric stack actuator was evaluated to assess its performance at various frequencies and voltage levels with a fixed applied load. A switched voltage source was used to supply the driving excitation. Displacement was monitored with a fiber optic displacement probe coupled to a digital oscilloscope. A resistive network was used to monitor the voltage and current applied to the piezoelectric stack. The measured performance was compared to the specifications for the system components.

Experimental Procedures:

A piezoelectric stack was purchased from EDO Acoustic Products for evaluation purposes. The device, model no 400P-4, is nominally 2.36 inches (60 mm) long with a specified nominal displacement of about 0.1% or 60 μm at a maximum voltage of 800 v.

A compressive fixture (Figure 9) was developed to secure the stack for testing purposes. The fixture was designed to provide a protective preload to the stack, to prevent debonding during excitation. A Belleville washer was used to supply a spring force to keep the preload constant and a load cell was included to monitor the preload in situ.

A preload of approximately 133 pounds was applied to the piezo stack device (EDO recommends a minimum of 100 pounds and a maximum of 1000 pounds). A mirror was affixed to the top of the actuator assembly to provide an optical target for the fiber optic probe. The fixture was bolted to a stiff honeycombed base plate (Newport corp.). A large (1.5" diameter) damped post was bolted in place adjacent to the fixture to provide a robust support for the optical probe.

A positive high-voltage square wave generator, Trek model P0678, was selected as an economical drive option for testing the piezo stack actuator. The maximum output voltage of this driver was 1000 v, with a maximum peak current of 10 A and a maximum average current of 100 mA at 1000v.

The supply voltage and drive current from the Trek generator were monitored using a voltage divider and current sampling resistor. Displacement, voltage and current were simultaneously measured on digital oscilloscopes.

Experimental Results:

The peak unloaded output voltage of the Trek generator was measured and found to be in very good agreement with the settings on the voltage level output adjustment knob. During testing under load, however, the peak voltage was observed to be significantly lower or higher than the indicated output setting and was influenced both by frequency and amplitude. Consequently, peak measured voltages are used for all calculations.

The lowest frequency at which the actuator was tested was 100 Hz. At that frequency, the displacement was very linear with respect to the peak, applied voltage, as shown in Figure 10. The maximum peak voltage that could be applied using the Trek amplifier was 748 v. This output was obtained at an indicated output control setting of approximately 660 volts. Further increases in the control setting did not produce any increases in applied voltage. The peak current observed at this level was about 6.25 A. The peak current specification for the Trek generator is given as "less than or equal to 10A" but the measured peak current is significantly lower (37.5%) than the 10 A maximum.

The maximum voltage and current achievable into the piezoelectric load was observed to decrease rapidly with frequency. At frequencies of 100, 200, and 500 Hz, maximum voltages of 748, 383, and 174 volts were achieved. The corresponding peak currents were 6.24, 3.47 and 1.68 amps. This decline in performance with frequency appears to be due to the inability of the Trek generator to supply the necessary average current. Reliable measurement of the average currents could not be obtained with the available instrumentation, due to the extremely fast rise times and short pulse widths of the current signals.

The maximum measured deflection of the EDO piezoelectric stack was 39.3 μm . This was the deflection measured at 100 Hz and a maximum developed drive voltage of 748 v. Based on the specified deflection of 60 μm at 800 v, a peak voltage of 748 v should have resulted in a peak displacement of 56 μm . The actual measured displacement was 30% lower than the displacement predicted by the specification.

The rise time associated with the test system was determined graphically from some of the displacement waveforms (Figure 11). Displacement rates were measured as low as 3 $\mu\text{s}/\mu\text{m}$ and as high as 7 $\mu\text{s}/\mu\text{m}$. Taking an average of 5 $\mu\text{s}/\mu\text{m}$, a displacement of, for example 40 μm , would require 200 μs .

Discussion:

The performance of this particular piezoelectric stack actuator and associated driver illustrate some of the advantages and disadvantages of this type of actuator. Although the maximum displacement of the actuator was less than predicted by the specifications, the actuator achieved significant displacements with relatively short rise times. For comparison purposes, a magnetostrictive actuator that was characterized previously in this program required over 2 ms to achieve a 40 μm displacement (Figure 12). The piezo stack actuator appears capable of achieving approximately an order of magnitude faster response.

It is worth noting that the limiting factors in the performance of the piezoelectric stack actuator appear to be primarily associated with the driver electronics. The Trek generator has a minimum output impedance of 100 Ω . If a lower output impedance driver could be applied to the actuator, the rise times could probably be reduced even further. Without question, the current limitations of the generator were responsible for the poor response at frequencies above 100 Hz. The high-frequency capabilities of this actuator were beyond the testing capabilities that could be achieved with this generator.

To a first approximation, the mechanical response of the piezoelectric stack actuator is directly related to the movement of charge into and out of the stack. Consequently, the design demands for a drive system are substantial. A tremendous reservoir of charge must be available to sustain the large average currents associated with high frequency operation. In addition, the output impedance of the supply must be extremely low both to maximize the mechanical rise time of the actuator and to minimize the power dissipation in the drive electronics.

References

- ¹J. A. Biggers, T. R. Shrout, and W. A. Schultze, "Densification of PZT cast tape by Pressing," *Ceramic Bulletin*, Vol. 58, No. 5, pp. 516-521, 1979.
- ²M. Chen et. al., "Study on Isopressing of YSZ Membrane fabricated by Tape Casting," *Wuji Cailiao Xuebao*, Vol. 14 No. 5, pp 745-750, 1999.

Travel

Travel by T. N. Tieg to University of Missouri, Rolla on Dec. 9th, 1999, to discuss PZT research topics with Prof. Wayne Hubner.

Table 1. L₉ Orthogonal Array

Sample#	Temp (C)	Pressure (MPa)	Lam. Time (min)	Preheat Time (min)
1	60	6.9	5	20
2	60	17.2	10	30
3	60	34.5	20	60
4	70	6.9	10	60
5	70	17.2	20	20
6	70	34.5	5	30
7	80	6.9	20	30
8	80	17.2	5	20
9	80	34.5	10	60

Table 2. Density values for Taguchi samples 1 through 9.

Sample #	Green Dens. (g/cm ³)	Sint. Dens. (g/cm ³)	Sint. Dens. (% T. D.)
1	4.12	7.551	99.4
2	4.28	7.505	98.8
3	4.5	7.429	97.8
4	4.25	7.587	99.8
5	4.46	7.571	99.6
6	4.64	7.422	97.7
7	4.31	7.586	99.8
8	4.34	7.327	96.4
9	4.6	7.52	98.9

*T.D.=7.6 g/cm³

Table 3. Physical and electromechanical measurements for PZT materials sintered at 1125 °C for 3 h.

Sample*	Wt. Loss (%)	T. D (%)	d ₃₃ (10 ⁻¹² m/V)	K _t	K _t ^T ₃₃
PZT 840	-0.6	79.9%	0.19	0.59	650
DP-1 PZT 840	-0.7	84.1	0.23	0.55	648
0.5% Ag ₂ CO ₃	-0.8	98.8	0.21	0.43	1074
0.1% Ag ₂ CO ₃ / 2% PbO	-2.3	96.9	0.18	0.38	946
0.1% Ag ₂ CO ₃ / 0.1% Cr ₂ O ₃ / 2% PbO	-2	97.1	0.18	0.36	947
0.5% Cr ₂ O ₃	-1.1	90.4	0.12	0.38	623
0.5% Cr ₂ O ₃ / 2% PbO	-0.2	93.7	0.2	0.4	659
0.1% Cr ₂ O ₃ / 2% PbO	-1.8	93.3	0.16	0.43	882
2% Bi ₂ O ₃	-1.6	101.5	0.38	0.55	1724

* PZT 840 + wt. % addition

Table 4. Physical and electromechanical measurements for PZT materials sintered at 1125 °C for 24h.

Sample*	Wt. Loss (%)	T. D. (%)	d ₃₃ (10 ⁻¹² m/V)	K _t	K ₃₃ ^T
PZT 840 DP	-0.70	98.60	0.21	0.48	1079
PZT 840	-0.90	99.30	0.26	0.53	1151
2% Ag ₂ CO ₃	-1.70	100.90	0.25	0.37	1202
0.1% Ag ₂ CO ₃	-1.00	100.90	0.19	nm**	nm
0.1% Ag ₂ CO ₃ / 2% PbO	-2.90	100.10	0.17	0.45	1071
0.1% Ag ₂ CO ₃ / 0.5% Cr ₂ O ₃	-1.70	98.80	0.2	0.40	912
0.1% Ag ₂ CO ₃ / 0.25% Cr ₂ O ₃	-0.20	98.00	0.24	0.50	1034
0.1% Ag ₂ CO ₃ / 0.1% Cr ₂ O ₃	-0.60	101.20	0.29	0.47	1265
0.1% Ag ₂ CO ₃ / 0.1% Cr ₂ O ₃ / 2% PbO	-2.40	100.80	0.28	0.41	1198
0.1% Ag ₂ CO ₃ / 2% Bi ₂ O ₃	-2.40	99.70	0.41	0.58	1895
0.1% Cr ₂ O ₃	-0.30	99.10	0.26	0.42	1130
0.5% Cr ₂ O ₃ / 2% PbO	-0.90	99.50	0.22	0.46	954
0.1% Cr ₂ O ₃ / 2% PbO	-2.47	97.90	0.23	0.37	1072
0.1% Cr ₂ O ₃ / 2% Bi ₂ O ₃	-1.90	99.40	0.4	0.58	1852
2% Bi ₂ O ₃	-2.20	100.90	0.38	nm	nm
0.5% Bi ₂ O ₃	-0.60	100.20	0.22	0.36	1407
2% Bi ₄ Ti ₃ O ₁₂	-0.80	99.30	0.32	0.55	1602

*PZT 840 + wt. % additive

**nm = not measured (broken or chipped sample)

Table 5. Physical and electromechanical measurements for PZT materials sintered at 1125 °C for 48 h.

Sample*	Wt. Loss (%)	T. D. (%)	d ₃₃ (10 ⁻¹² m/V)	K _t	K ₃₃ ^T
PZT 840	-0.7	100.2	0.24	0.48	1097
0.1% Ag ₂ CO ₃	-1	101.1	0.29	0.55	1169
0.1% Ag ₂ CO ₃ / 0.1% Cr ₂ O ₃	-0.6	101.5	0.29	0.5	1238
0.1% Ag ₂ CO ₃ / 2% Bi ₂ O ₃	-2.8	99.3	0.39	0.55	1822
0.1% Cr ₂ O ₃ / 2% Bi ₂ O ₃	-2.4	99.1	0.41	0.57	1800

• PZT 840 + wt. % additive

Table 6. Data from PZT Composition Study

Sample	Sintering Time (h)	Density (% T. D.)
PZT-4 Control	24	98.6
PZT-4 Control	48	100.2
+ 2 wt. % PbO	24	101.2
+ 0.1% wt. % Ag_2CO_3	24	100.9
+ 0.1 wt.% Ag_2CO_3	48	101.1
+ 2.0 wt.% Ag_2CO_3	24	100.9
+ 0.1% wt. % Cr_2O_3	24	99.2
+ 0.1% wt. % Cr_2O_3 + 0.1 wt.% Ag_2CO_3	24	101.0
+ 0.1% wt. % Cr_2O_3 + 0.1 wt.% Ag_2CO_3	48	100.5
+ 2 wt. % Bi_2O_3	24	100.9
+ 2 wt. % Bi_2O_3	48	99.3
+ 2 wt. % Bi_2O_3 + 0.1% wt. % Cr_2O_3	24	99.3
+ 2 wt. % Bi_2O_3 + 0.1% wt. % Cr_2O_3	48	99.1

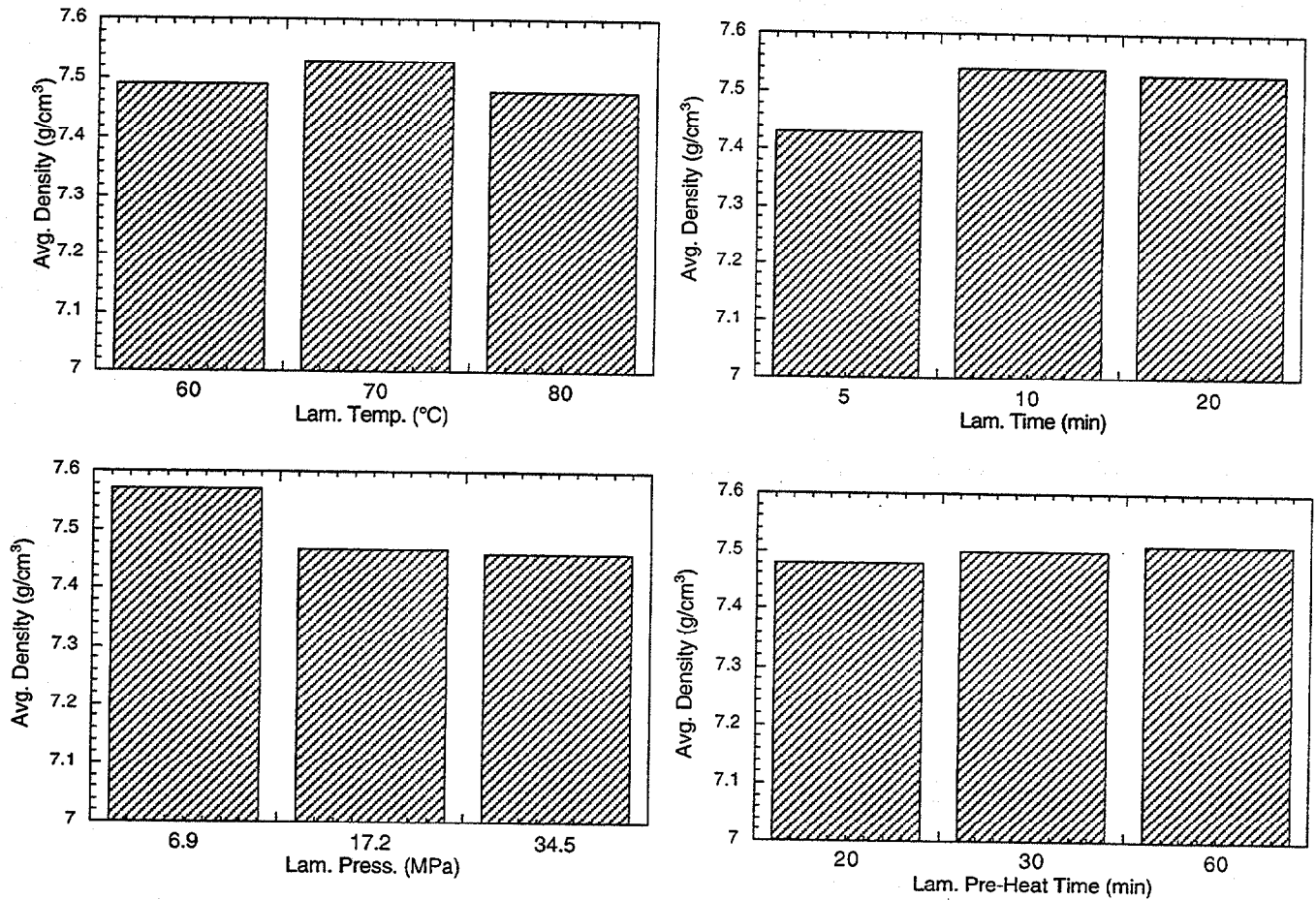


Figure 1. Average density values for PZT-4 tape laminates sintered in a Taguchi experimental array as a function of a) lamination temperature, b) lamination time, c) lamination pressure, and d) preheat time of die and tape layers prior to die lamination.

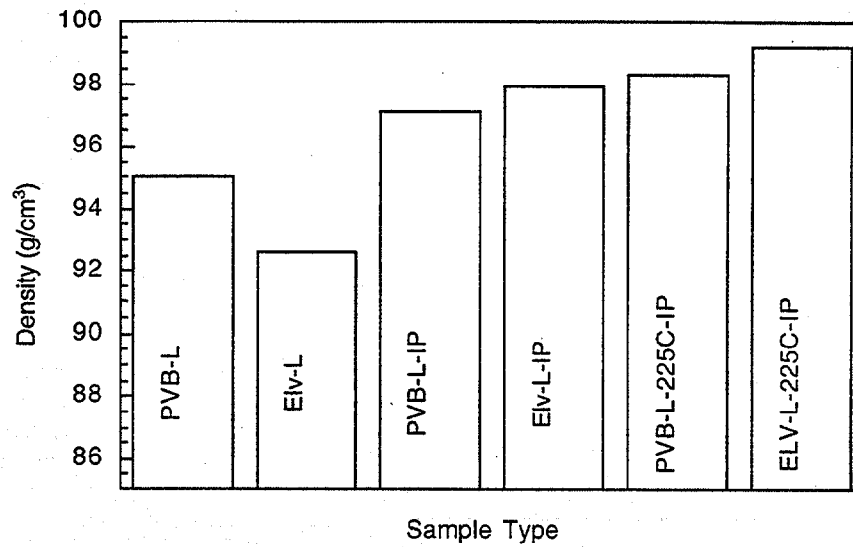


Figure 2. Sintered densities of PZT-4 laminates prepared by various methods

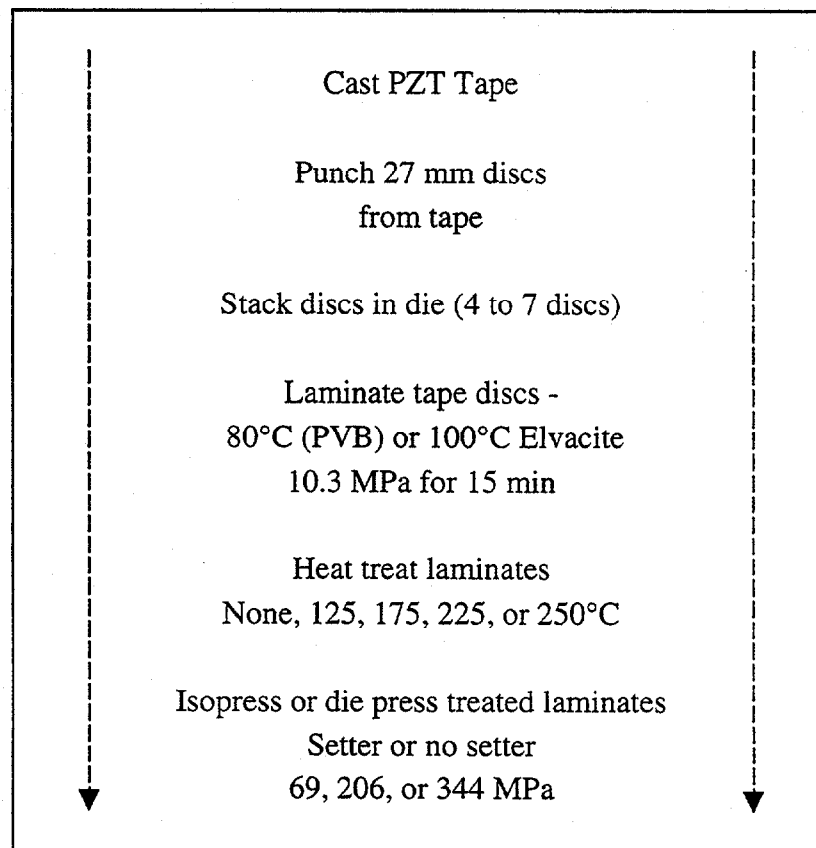


Figure 3. Flow diagram of PZT tape cast and lamination study.

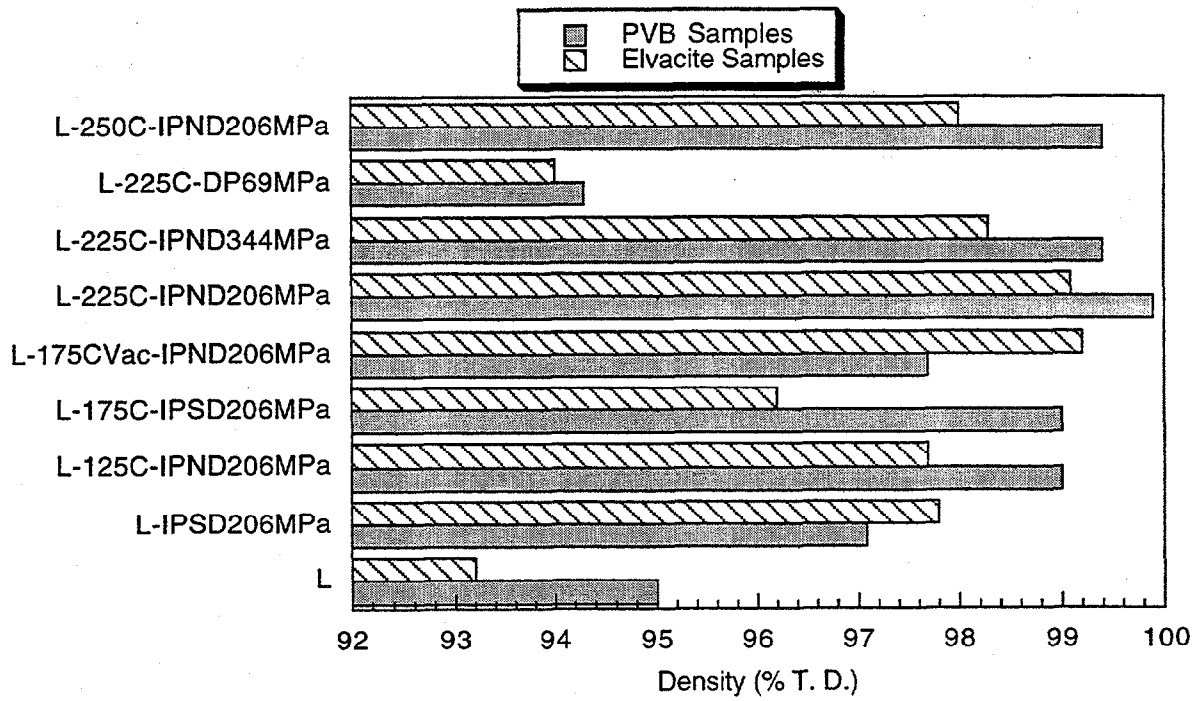
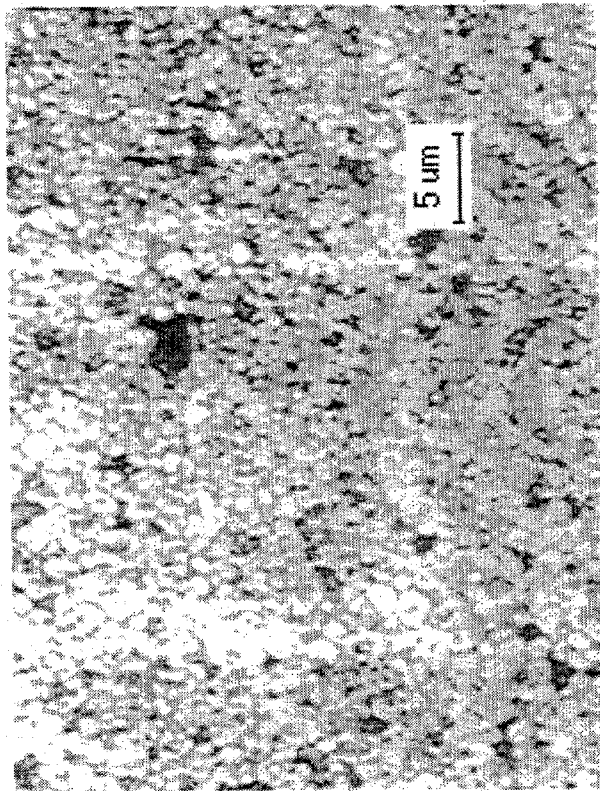
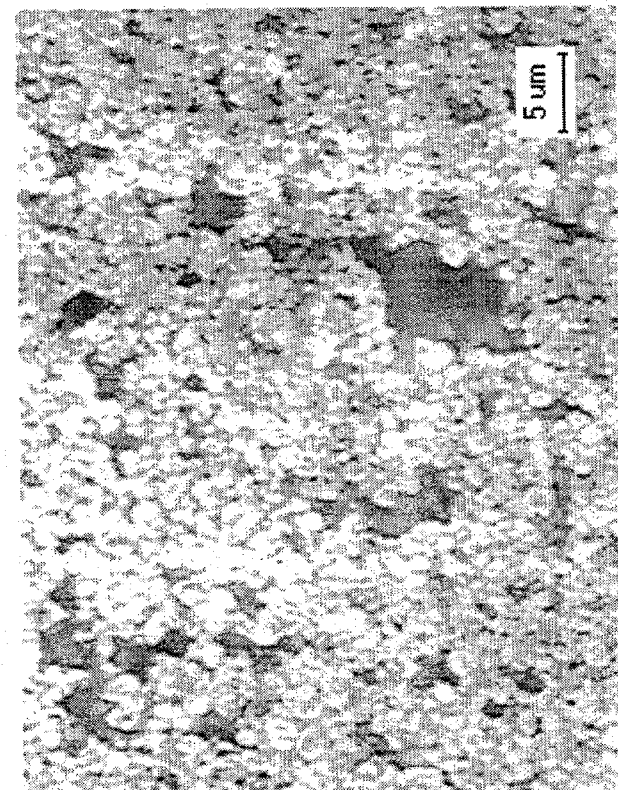


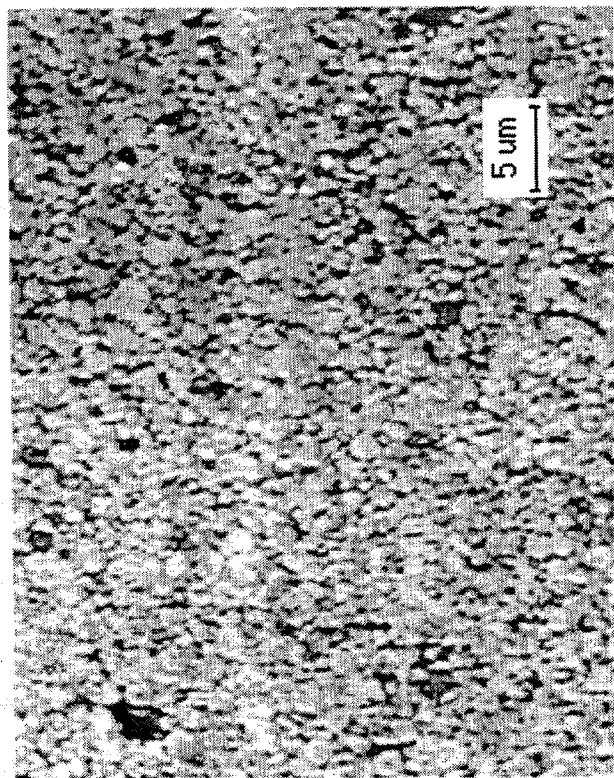
Figure 4. Graph of sintered density data from lamination study.



Control - No Additive - 48 h

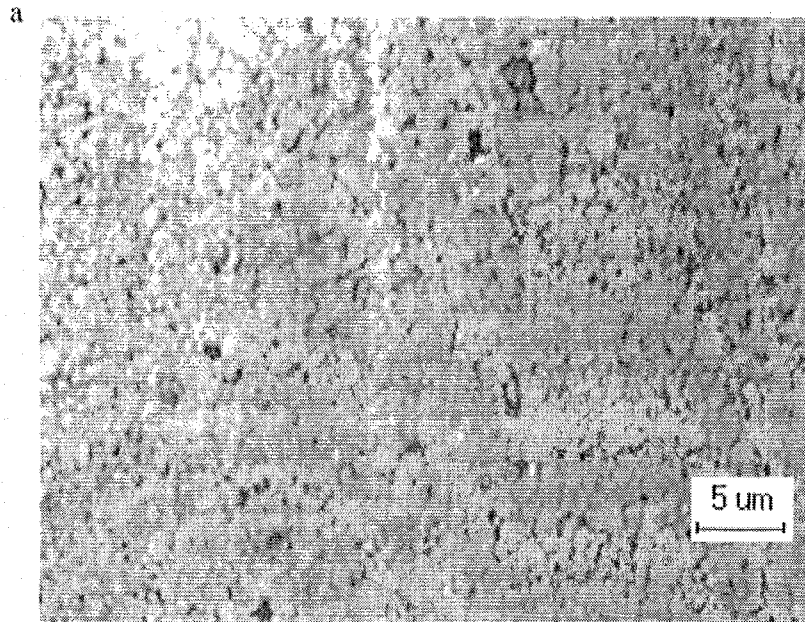


Control - No Additive - 24 h

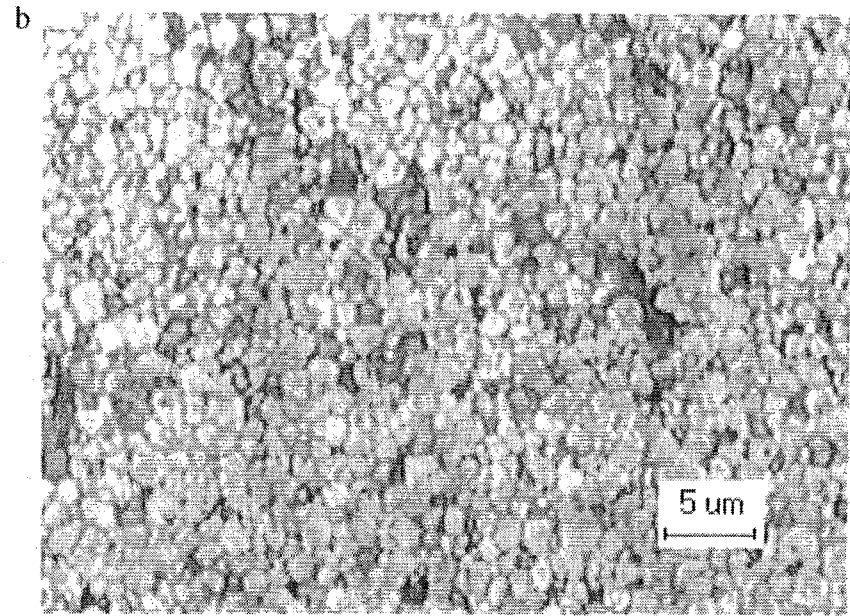


2 wt. % PbO - 24 h

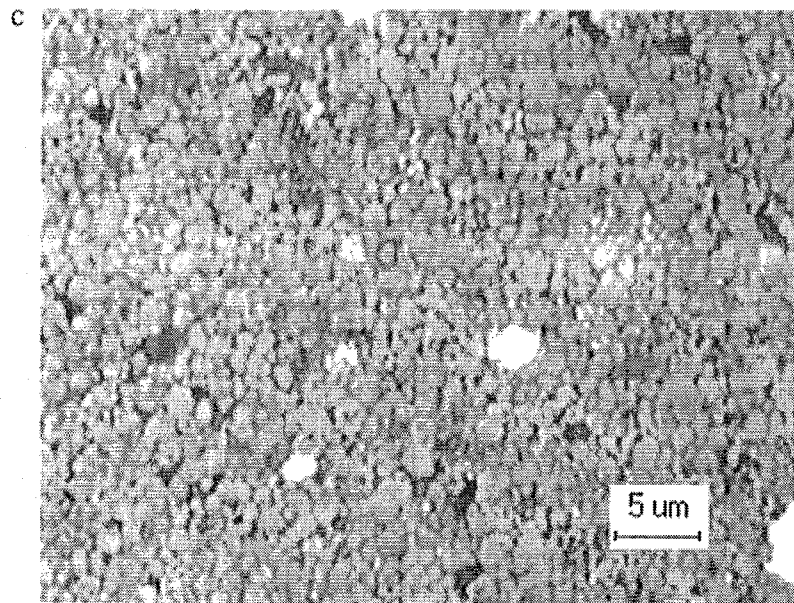
Figure 5 . Optical photographs of PZT-4 with additives sintered at 1125 °C for the indicated times.



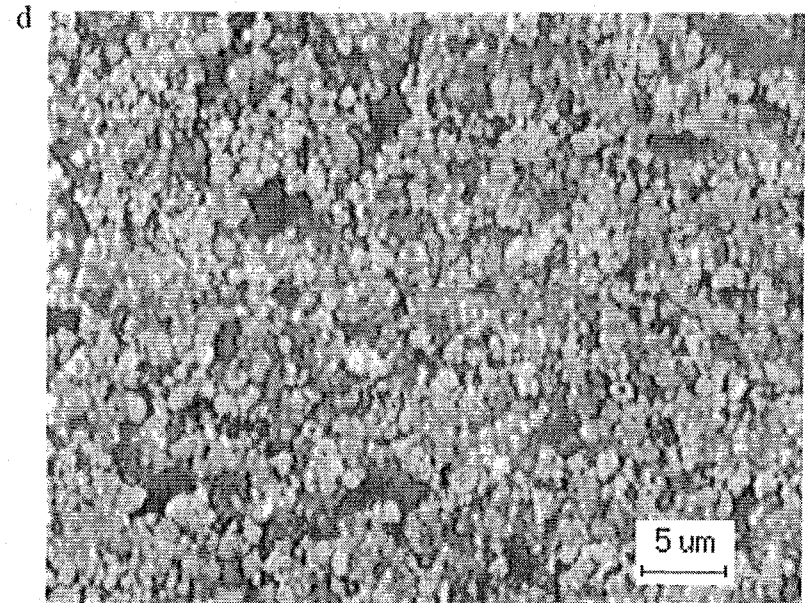
0.1 wt. % Ag - 24 h



0.1 wt. % Ag - 48 h

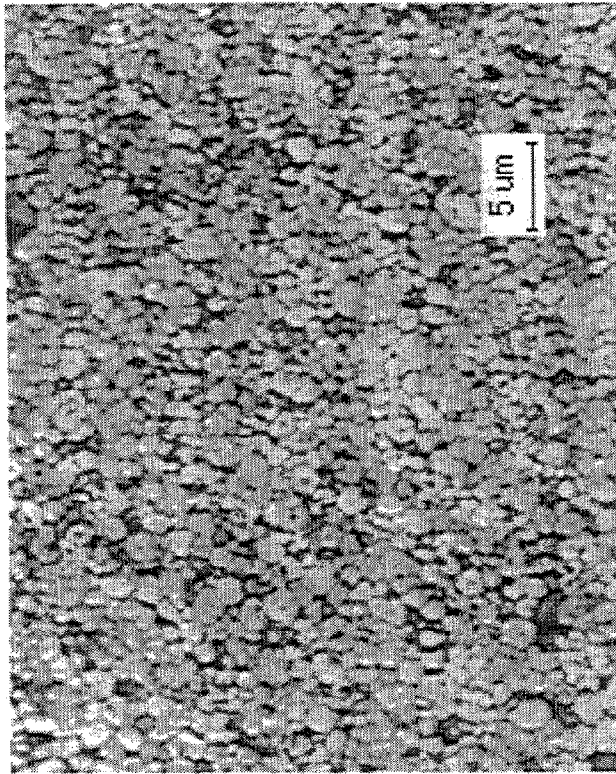


2 wt. % Ag - 24 h

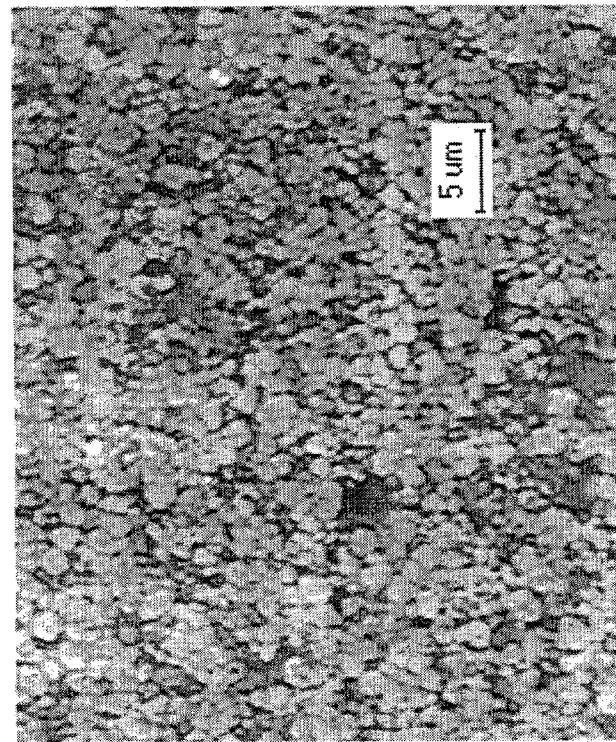


0.1 wt. % Cr - 24h

Figure 6. Optical photographs at 1000X of PZT-4 with additives sintered at 1125 °C for the indicated times.



0.1 wt. % Cr, 0.1 wt. % Ag - 48 h



0.1 wt. % Cr, 0.1 wt. % Ag - 24 h

Figure 7. Optical photographs of PZT-4 with additives sintered at 1125 °C for the indicated times.

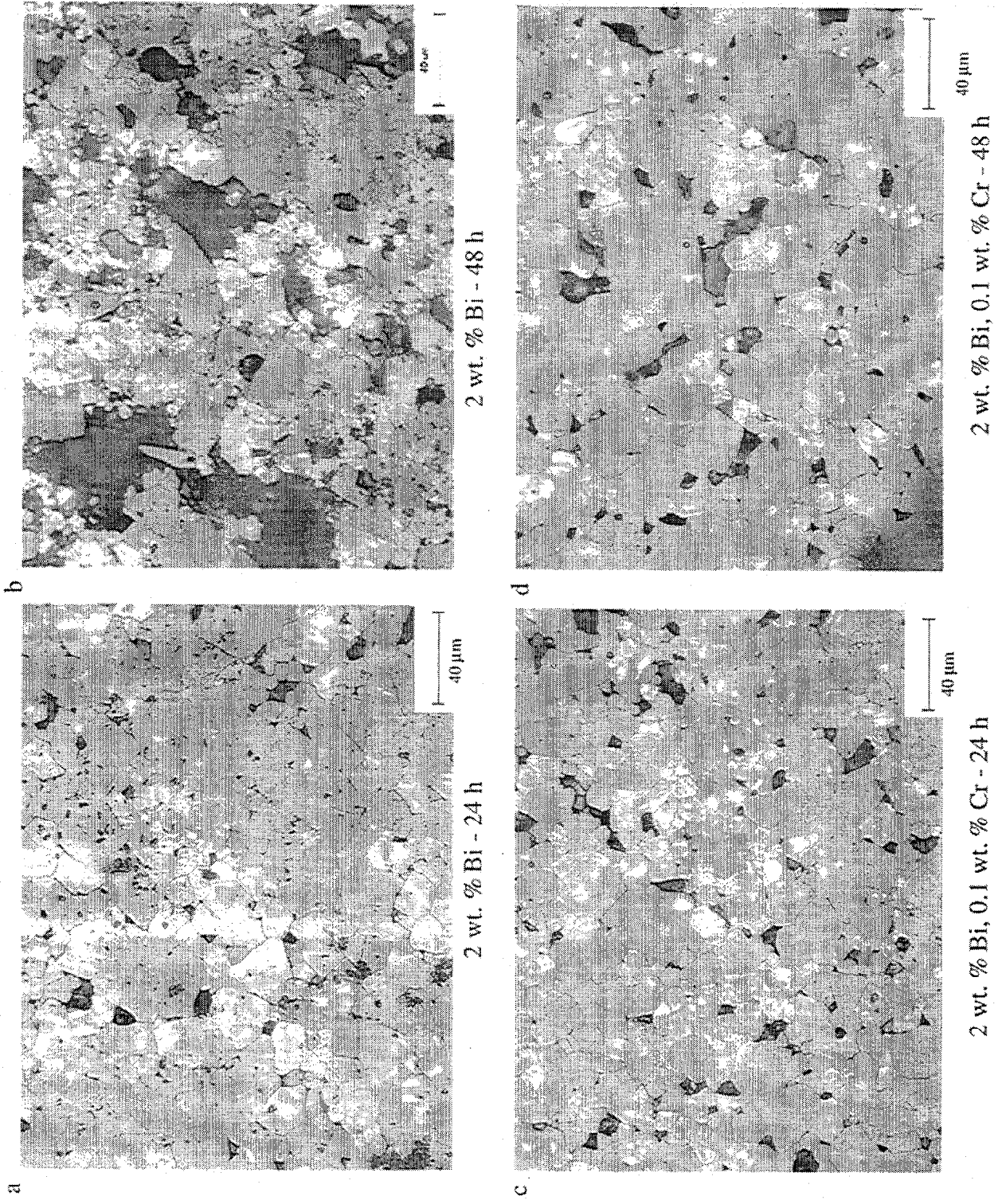


Figure 8. Optical photographs of PZT-4 with additives sintered at 1125 °C for the indicated times.

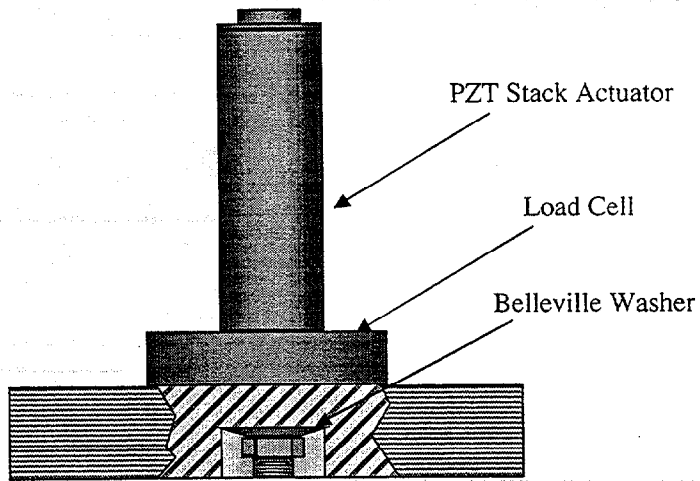


Figure 9 – Compressive mounting fixture for piezoelectric stack

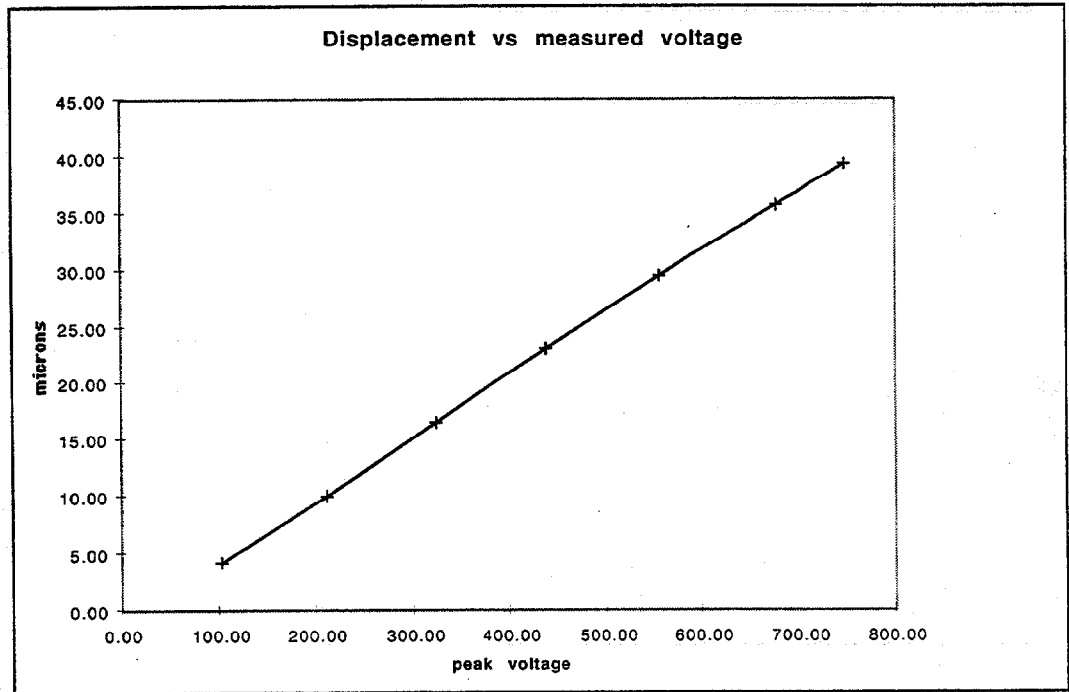


Figure 10 – Peak displacement of EDO stack actuator as a function of peak voltage

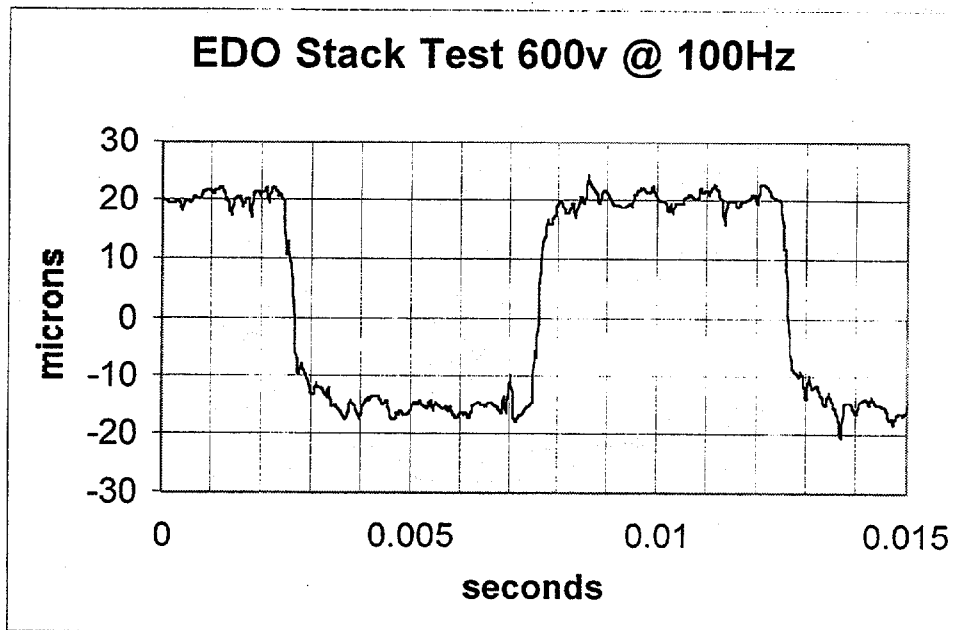


Figure 11 – Representative displacement waveform obtained with EDO stack actuator

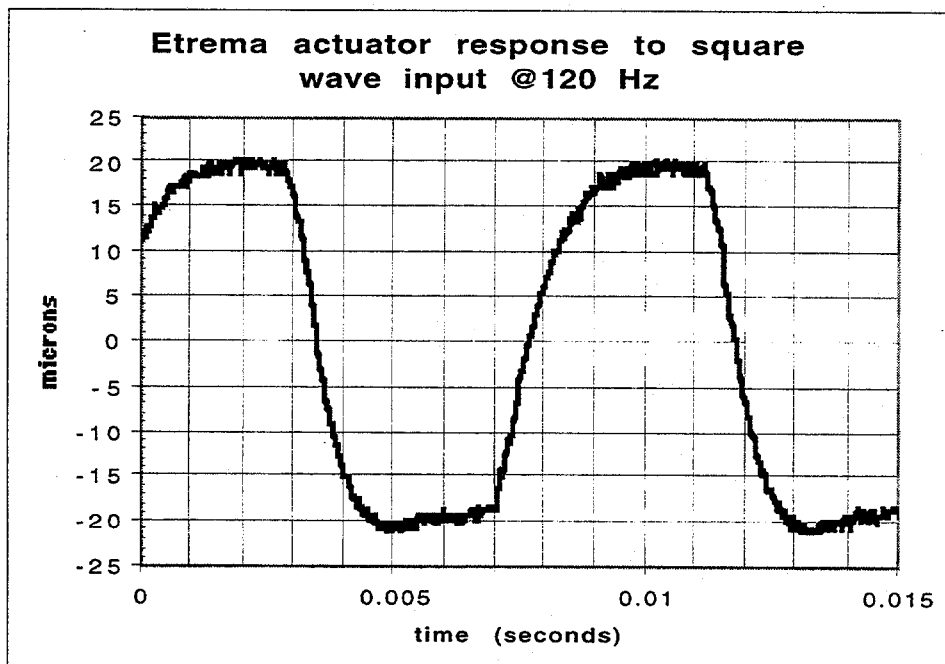


Figure 12 – Representative displacement waveform obtained with Etrema magnetostrictive actuator.

LOW COST-HIGH TOUGHNESS CERAMICS

T. N. Tiegs, F. Goransson, F. C. Montgomery, P. A. Menchhofer and D. L. Barker

Oak Ridge National Laboratory

Oak Ridge, TN 37831

Objective/Scope

Significant improvement in the reliability of structural ceramics for advanced diesel engine applications could be attained if the critical fracture toughness (K_{Ic}) were increased without strength degradation. Early results from ORNL research showed that significant increases in fracture toughness could be achieved by manipulating the microstructure to promote toughening mechanisms such as crack bridging. Excellent properties were obtained in this manner for the alumina and mullite matrix systems reinforced with SiC whiskers. In silicon nitride, mechanical property improvements were achieved by promoting acicular or elongated grain growth and these provided significant toughening on the same order as the whisker reinforced materials. Currently, the project is initiating studies on toughening of ceramics by two methods: microstructure development in oxide-based ceramics, and incorporation of ductile intermetallic phases.

Technical Highlights

Aluminide-Bonded Ceramics

Previous studies have shown that the properties of the aluminide-bonded ceramics (ABC) are attractive for diesel engine applications and consequently, development of these materials was started. Issues to be studied include the fabrication of parts using cost-effective processing, effect of alloying elements on the properties and fabrication of near-net-shape parts for testing. Initially, a study was done to examine the sintering behavior of the aluminide-bonded ceramics at high binder contents. Most of the previous work on ABC's was done at binder contents of 10-30 vol. %. However, higher binder contents on the order of 30-50 vol. % are necessary for these composites to match the thermal expansion of steel. Currently, the TiC-40 vol. % Ni₃Al composites appear to have the expansion characteristics very close to those for steel.

Preliminary testing indicates that improved wear resistance could be achieved by decreasing the grain size of the TiC. In addition, it was thought that changing the TiC grain shape from a highly faceted one to a more rounded equiaxed grain would increase abrasion resistance from any wear debris. Several approaches were examined to control the final TiC grain size. These include:

- (1) reduction of the initial TiC particle size;
- (2) use of additives to change the interface behavior of the growing TiC grains;
- (3) employing additives to physically inhibit grain growth;
- (4) rapid sintering to minimize high temperature exposure;
- (5) and post-densification thermal treatments.

Milling and Densification – The most obvious approach to grain refinement is to reduce the initial grain size. This is typically done by milling in conventional ball mills or by using high energy attrition mills that significantly reduce the particle size in a short time. This study examined several milling conditions and variables using both conventional ball milling and high energy attritor milling. The Ni₃Al powder characteristics used in fabrication of the composites are shown in Table 1. Note the large size of the prealloyed Ni₃Al powder produced by inert gas atomization. This is in contrast to the fine TiC powder used in all of the composites, which had an average particle size of 1.2-1.5 μ m. The Ni₃Al content for all the composites in the study was 40 vol. %. This composition was chosen because the thermal expansion of the composites is similar to that of steel.

The different milling conditions are described in Table 2. Media wear during milling contributed some ZrO_2 contamination to each of the compositions as shown in the table. The TiC particle size reduction during ball milling was not determined, but it is a low energy process and the particle size should not change drastically with time. However, attritor milling is a high energy process. The change in TiC particle size with milling time in the attritor is shown in Fig. 1. Significant particle size is realized in ≤ 4 hours and reaches a steady state at ~ 7 hours. During milling, the oxygen content of the TiC is increased and media wear is added to the batches as indicated in Table 2.

The effect of the milling conditions on densification is shown in Fig. 2. Obviously, as the TiC particle size is reduced and the oxygen increases, the densification is inhibited. The presence of the surface oxides decreases wetting by the Ni_3Al alloy during liquid phase sintering and would also contribute to greater off-gassing of CO from the TiC at elevated temperature. Both effects would result in decreased sintering. In addition, there is some oxidation of the Ni_3Al particles as well during milling, which would also, result in decreased sintering behavior. Besides oxidation of the TiC and Ni_3Al powders, the more intense milling also resulted in higher media wear and ZrO_2 contamination added to the compositions. The poor wetting behavior of the Ni_3Al with the oxide contamination would also contribute to inhibited densification. Milling with TiC-cermet media is being pursued as a way to minimize the effects of contamination.

The densification of the composites with the different Ni_3Al alloys types is shown in Fig. 3. Both the IC-50 and IC-218 based composites exhibited high densities with the vacuum-low pressure hot-isostatic pressing (V-LPHIP) firing schedule. On the other hand, the composites with IC-264 and IC-396M alloys, exhibited decreased densification. Both these alloys contained higher Zr contents than the other alloys and, in the case of IC-396M, Mo was also present. These amounts of Zr should have only a minor effect on the solubility of TiC and diffusion in the liquid phase. However, the Zr would act as a powerful oxygen getter in the system due to the high free energy of formation and stability of ZrO_2 . This oxygen gettering could significantly influence the wetting between the TiC and the liquid phase and thus affect the solution-reprecipitation kinetics. Small amounts of surface oxygen are well known to adversely affect the wetting between carbides and molten metals and in a similar fashion, minor additions of Mo to Ni have been shown to reduce the contact angle with TiC from 17° to 0° . Previous results have suggested inhibited sintering with Zr additions to Ni_3Al alloys.

The results on the continuous belt sintering are also shown in Fig. 3. In general, lower densities were obtained for the continuous sintered samples compared to the V-LPHIP processed ones. Previous work had found roughly equivalent densification between the two methods. However, in the present study, no definitive explanation has been found for the differences. The continuous sintering did not have a degassing hold step at $1200^\circ C$, nor a pressurization step at the end of the firing schedule. Further work is being done to determine the reasons for the discrepancies.

Microstructure – The effect of milling conditions on the microstructure of the TiC- Ni_3Al composites is shown in Fig. 4. As expected, as the milling intensity increased (and the initial TiC particle size decreased), the final TiC grain size becomes finer. However, in the present case, it was observed that the TiC grains contained increasing amounts of inclusions with the increase in milling intensity. This is exemplified in Fig. 5. Energy dispersive x-ray analysis (EDAX) of the inclusions identified them as ZrO_2 from the mill media contamination. These were evidently incorporated into the TiC grains during precipitation of the secondary TiC that forms during liquid phase sintering.

The effects of the different Ni_3Al alloys on the microstructure are shown in Fig. 6. [These should be compared to Fig. 3a which is the IC-50 alloy processed under similar conditions.] As can be seen, the Cr additions from the IC-218 and IC-264 alloys, results in a rounding of the TiC grains as compared to the faceted grains associated with the IC-50 alloy. In the case of the IC-218 alloy, some grain refinement is also evident. This alloy contains low Zr content and previous work had speculated that high Zr contents contributed to enhancing TiC grain growth during sintering. Further evidence of the effect of Zr is noted in the IC-264 microstructure, which has a comparable

Cr content to the IC-218 alloy, but significantly higher Zr content. The TiC grain size in that case was larger for the IC-264 containing composition.

The effect of the Mo addition (with the IC-396M alloy) on the microstructure is shown in Fig. 6c. Rounding of the grains was obvious. The IC-396M containing composition exhibited poor densification at 1450°C and the particular sample shown in Fig. 6c was sintered at 1500°C. A comparable sample using IC-50 alloy and sintered at 1500°C is shown in Fig. 6d. As shown, some grain refinement is evident. Previous work had reported grain refinement when Mo additions were made to the Ni₃Al. While the IC-396M alloy contains Mo, it also contains an appreciable amount of Zr. Thus, the Zr may have contributed to some grain growth in these samples.

Typical microstructures observed from the continuous belt sintered composites are shown in Fig. 7. While the example is for the materials containing IC-264 alloy, similar observations were made with the other composite types. A comparison of Fig. 7a and Fig. 4b indicates that as the heating rate increases (and the time at temperature remains constant), the TiC grain size is decreased. Further increase in the heating rate (and a decrease in the time at temperature) as shown in Fig. 7b, results in a further refinement of the TiC grains.

Mechanical Properties – The mechanical properties were determined for composites that achieved a density $\geq 95\%$ T. D. The effect of milling conditions on the flexural strength, fracture toughness and hardness are shown in Fig. 8. The strength is directly related to the densities (and inversely to the milling intensity); higher strengths were associated with the higher densities and lower milling intensity. In a similar fashion, the fracture toughness decreased with increasing milling intensity, which may be due to the higher levels of milling media contamination introduced into the batches. The hardness was in the range of 8-10 GPa with the highest value for the lowest density sample, which is unusual. While the attritor milled (4 h) sample had lower density, it also had a very fine grain size, which contributed to the high hardness value.

Excellent flexural strength, fracture toughness and hardness were observed for the samples fabricated with the different Ni₃Al alloys as shown in Fig. 9. The IC-218 alloy sample exhibited slightly higher strength and hardness probably due to the slightly finer grain size of these composites. Some contribution from solid solution hardening of the matrix may also have made a difference.

Laser Surface Treatment – Samples of dense TiC-50 vol. % Ni₃Al (IC-50 alloy, sintered at 1450°C by V-LPHIP process) were surface treated by a ruby laser operated at 18.5 kW in a pulsed mode (7 ms at 40 pulses/s) and rastered at 0.84 cm/s. The surfaces had been machined prior to the laser treatment. Laser surface treatments are characterized by extremely high heating and cooling rates on the order of 1000°C/s. The effect on the microstructure is shown in Fig. 10. As shown, there is a dramatic change from the base material (Fig. 10a) compared to the microstructure in the laser affected zone, LAZ (Fig. 10b). Melting of the composite occurs locally within the LAZ and during cooling dendritic growth of the TiC occurs as it precipitates from solution.

Because the laser was operated in a pulsed mode with overlapping spots, some areas were melted and remelted as the laser was rastered across the surface. The overlapping spots are seen in Fig. 10c. The interface between the melt-remelt areas reveals interesting differences in the TiC grain size depending on the local heating and cooling conditions experienced. In the remelt area, the TiC dendrites are very fine because of the high cooling rate adjacent to the material that was not remelted. Whereas, the dendrites in the area not remelted has grown in size because of the heat-treatment received from being near the laser spot. Indent hardness measurements in the LAZ (indent sizes were $\sim 200 \mu\text{m}$) showed the hardness increased slightly from 7.1 GPa for the baseline to 7.5 GPa in the LAZ. These preliminary tests indicate that laser surface treatments made be applicable to refining the grains size in TiC-Ni₃Al composites.

Coors CRADA - As part of the CRADA with Coors Ceramics, large batches of TiC (1000 g batch size of previously jet-milled material) were attritor milled in ethanol with zirconia media (3 mm diameter) or tungsten carbide media (4.9 mm diameter). Media-to-TiC charge ratio was different for the two media types because of the higher density of the WC, but the volume ratio between the media types was basically the same. The milling in the larger mill was held constant at 300 rpm, which produced essentially equivalent tip speeds on the rotor to those in the previous study on the zirconia media milled powders discussed above. Particle sizes were determined as a function of milling time as shown in Table 3. In this case for equivalent conditions, the tungsten carbide media resulted in higher milling efficiency due to its high density.

For both cases, milling of the TiC powders resulted in significant media wear. In turn, this adds considerable amounts of media material to the composition. As shown in Table 1, at the end of milling for 12 hours, the TiC either contained ~6.5 wt. % WC or ~4.6 wt. % ZrO₂. Previous work, where milling was done with more conventional ball milling and larger media sizes (>10 mm), milling resulted in about 0.5-1 wt. % addition of WC into the TiC compositions for milling times of 16 hours. The changes in the composition observed in the current study need to be taken into account when interpreting densification behavior and properties. TiC powders produced by these conditions are being fabricated into Ni₃Al-based composites to determine the effect on grain size reduction in the sintered materials.

Status of Milestones

On schedule.

Communications/Visits/Travel

Travel by T. N. Tiegs to attend the American Ceramic Society Pacific Coast Meeting in Bellevue, WA, Oct. 27-29, 1999 and present a paper entitled, "Processing and Properties of TiC-Ni₃Al Cermets."

Travel by T. N. Tiegs to Orlando, FL, Nov. 16-17, 1999 to attend a Program Coordination Meeting for the Metal Powder Industries Federation 2000 International Conference on Powder Metallurgy and Particulate Materials.

Travel by T. N. Tiegs to University of Missouri in Rolla, MO, Dec. 9, 1999 to discuss collaborative work with the faculty and to present a graduate student seminar entitled, "Processing and Properties of TiC-Ni₃Al Cermets."

Travel by T. N. Tiegs to Cocoa Beach, FL, Jan. 24-27, 2000 to attend the American Ceramic Society Meeting on Advanced Materials and Composites and present a paper entitled, "Microstructure and Properties of TiC-Ni₃Al Composites With Alternate Binder Compositions."

James Stephen, representing Coors Ceramics Co., visited ORNL on February 16 and 17 to discuss development of intermetallic-bonded TiC composites and the status of the CRADA between ORNL and Coors.

Problems Encountered

None.

Publications

T. N. Tiegs, F. Montgomery, F. L. Goranson, P. A. Menchhofer, D. L. Barker, and D. Wittmer, "Microstructure and Properties of TiC-Ni₃Al Composites With Alternate Binder Compositions," to be published in *Ceram. Eng. Sci. Proc.*, Am. Ceram. Soc., Westerville, OH (2000).

T. N. Tiegs, F. Montgomery, P. A. Menchhofer, D. L. Barker, F. L. Goranson, and D. Wittmer, "Grain Growth Inhibitors In Intermetallic-Bonded TiC Composites," to be published in Ceramic Transaction, Am. Ceram. Soc., Westerville, OH (2000).

Table 1. Samples of TiC-Ni₃Al composites fabricated to determine the effect of Ni₃Al-binder composition on the sintering behavior and properties. Balance of compositions is nickel. Samples contained 40 vol. % Ni₃Al.

Sample ID	Binder Type	Particle Size (μm)	Binder Composition (wt. %)				
			Al	Zr	Cr	Mo	B
DC-43B	IC-50	<65	11.3	0.6	--	--	0.02
DC-44	IC-218	<44	8.7	0.2	8.1	--	0.02
DC-45	IC-264	<44	8.4	1.7	7.8	--	0.02
DC-46	IC-396M	<65	8.0	0.9	7.7	3.0	0.01

Table 2. Fabrication of TiC-Ni₃Al composites using different milling conditions. Samples contained 40 vol. % Ni₃Al (IC-50).

Sample ID	Mill Type	Milling Time (h)	Media Wear (wt. %)	Estimated TiC Oxygen Content (wt. %)
DC-43B	Ball	24	0.5	0.7
DC-43A	Ball	89	2.2	1.9
DC-47	Attritor	4	1.9	1.5
DC-48	Attritor	9	4.1	2.1

Table 3. Summary of TiC particle size results on large scale milling of TiC powders.

Milling Time (h)	WC Media		ZrO ₂ Media	
	Mean Diameter (μm)	D90 Diameter (μm)	Mean Diameter (μm)	D90 Diameter (μm)
0	1.0±0.32	2.2	1.0±0.32	2.2
2	0.78±0.26	1.8	0.92±0.30	2.0
4	0.65±0.22	1.5	0.70±0.22	1.52
6	0.61±0.20	1.3	0.64±0.21	1.4
8	0.57±0.19	1.2	---	---
10	0.45±0.14	0.9	0.58±0.18	1.2
12	0.47±0.14	0.9	0.55±0.18	1.2
Milling Parameters				
Media/ TiC Charge Ratio (wt. Fraction)	23:1		10:1	
Media Wear Rate (wt. %/h)	0.025		0.040	
Media Addition to Batch (wt. %)*	6.5		4.6	

* Defined as Media Wear (g)/ [TiC Charge (g) + Media Wear (g)] X 100

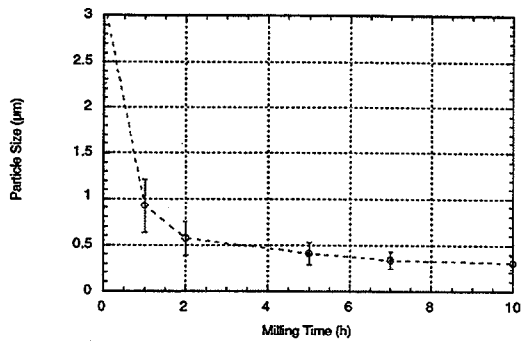


Fig. 1. Particle size reduction with attritor milling.

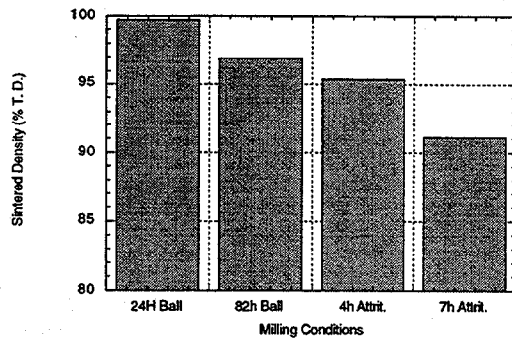


Fig. 2. Densification of TiC-40 vol. % Ni₃Al (IC-50) composites fabricated by different milling conditions. Sintered at 1450°C by V-LPHIP.

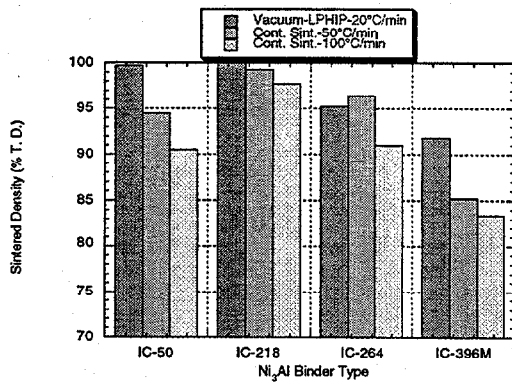


Fig. 3. Densification of TiC-40 vol. % Ni₃Al composites fabricated with different alloys. Sintered at 1450°C by V-LPHIP.

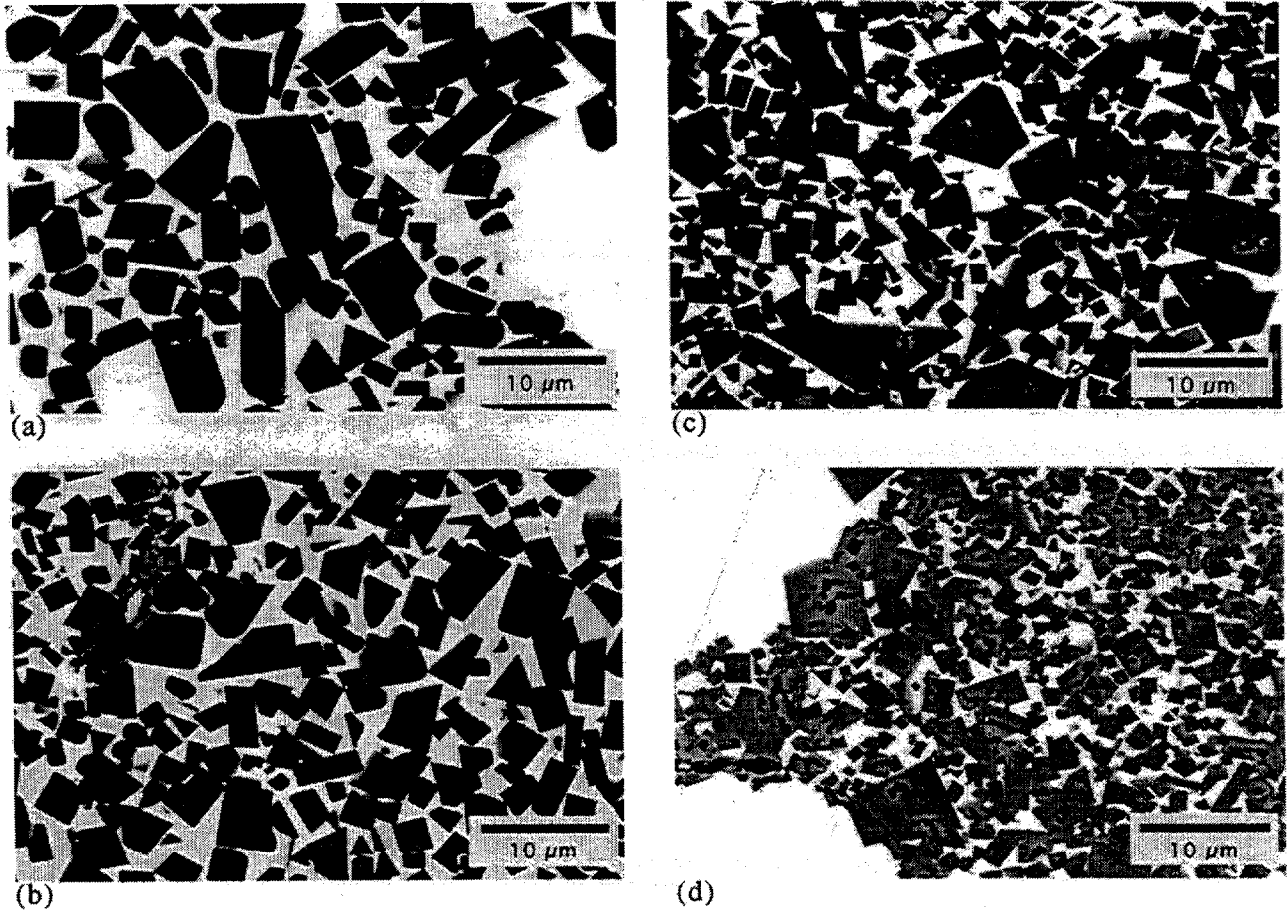


Fig. 4 Microstructures of TiC-40 vol. % Ni₃Al (IC-50) fabricated using different milling conditions: (a) ball mill 24 h; (b) ball mill 89 h; (c) attritor mill 4 h, and (d) attritor mill 9 h. Samples sintered by V-LPHIP at 1450°C.

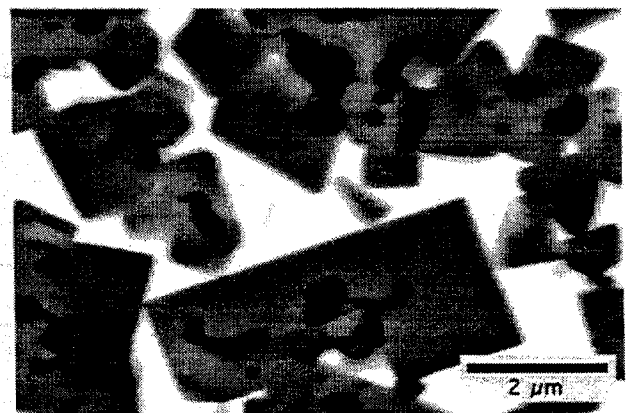


Fig. 5. Microstructure of attritor mill 9 h composite showing inclusions with TiC grains.

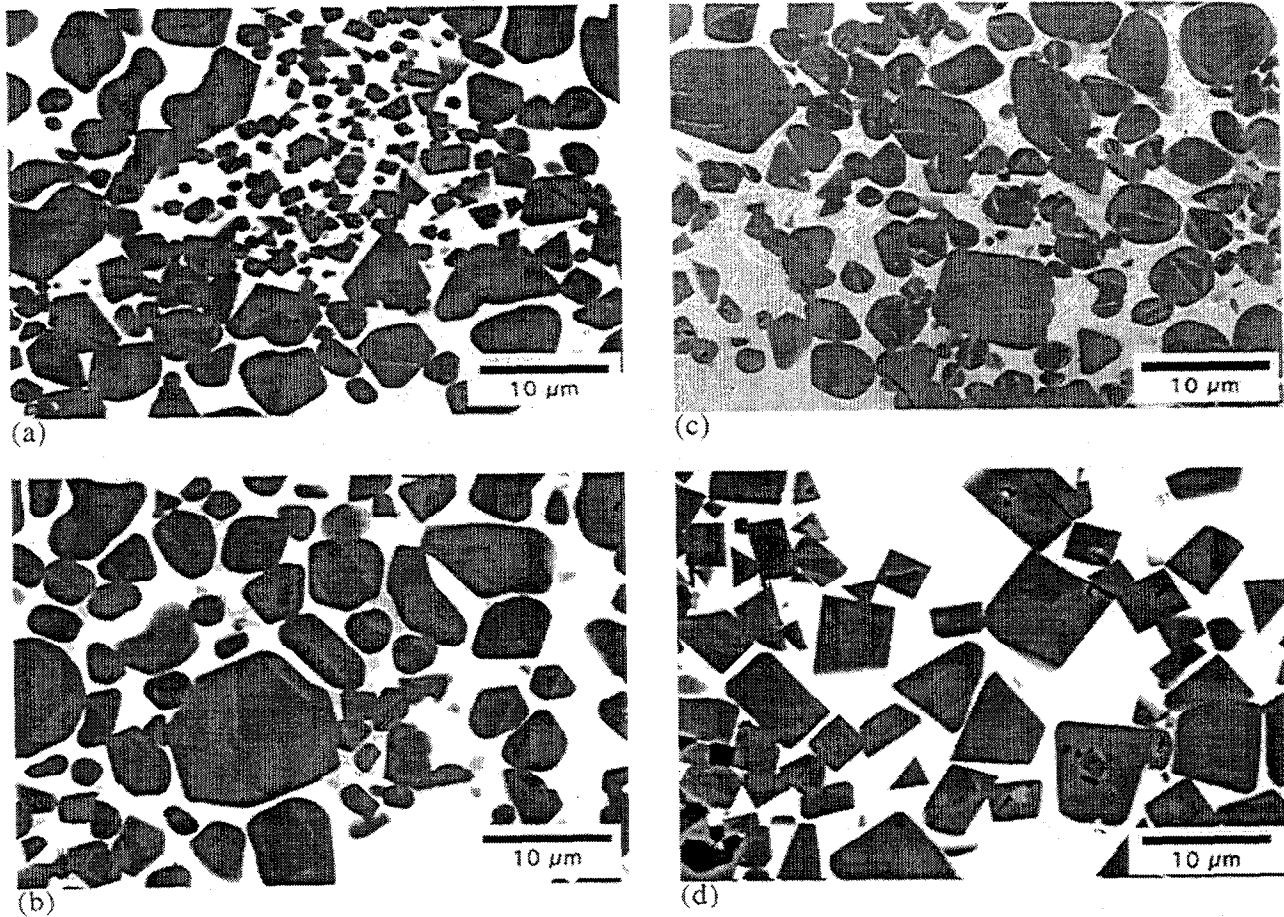


Fig. 6. Microstructures of TiC-40 vol. % Ni_3Al composites with different Ni_3Al alloy types, (a) IC-218; (b) IC-264, (c) IC-396M, and (d) IC-50. Samples ball milled 24h and sintered by V-LPHIP, (a) and (b) were sintered at 1450°C ; (c) and (d) were sintered at 1500°C .

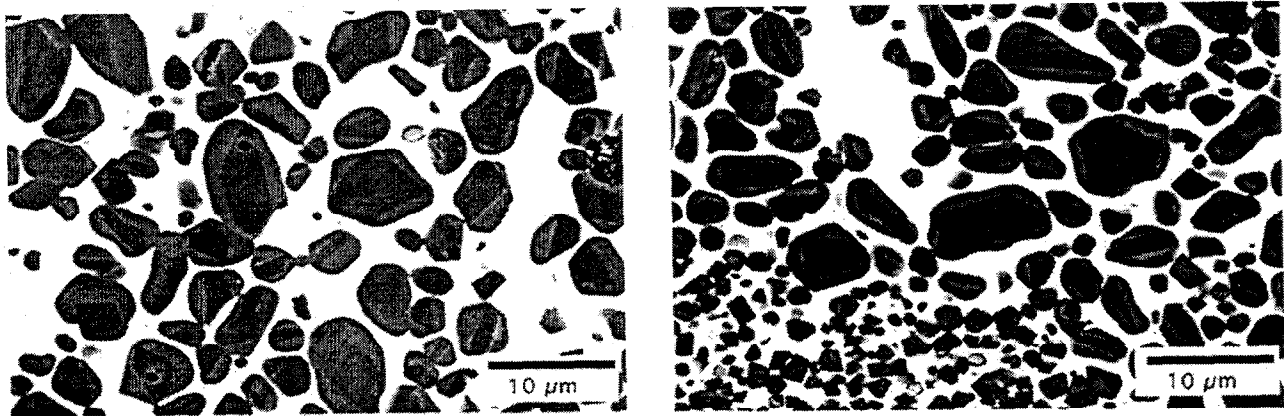
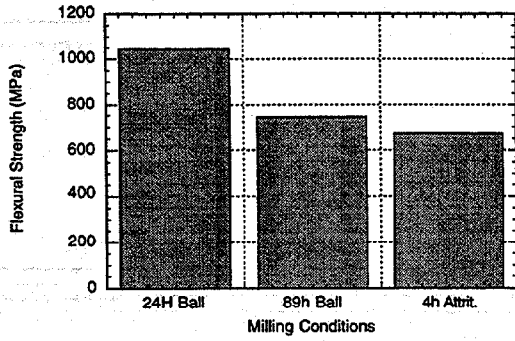
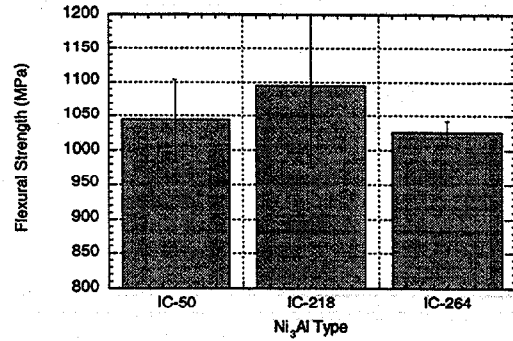


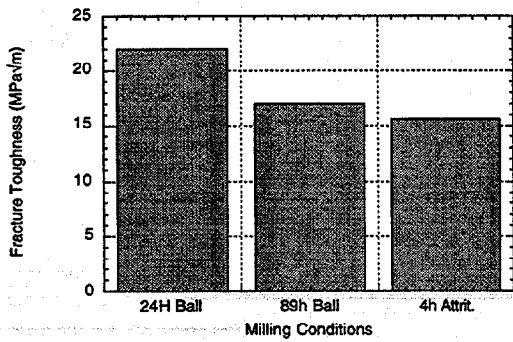
Fig. 7. Microstructures of TiC-40 vol. % Ni_3Al sintered at 1450°C in the continuous belt furnace; (a) $50^\circ\text{C}/\text{min}$ and 50 min hold, (b) $100^\circ\text{C}/\text{min}$ and 25 min hold. Samples ball milled 24h and used IC-264 Ni_3Al alloy. Fig. 6b is comparison photomicrograph with V-LPHIP process.



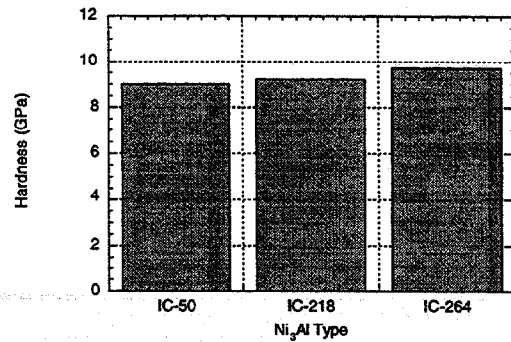
(a)



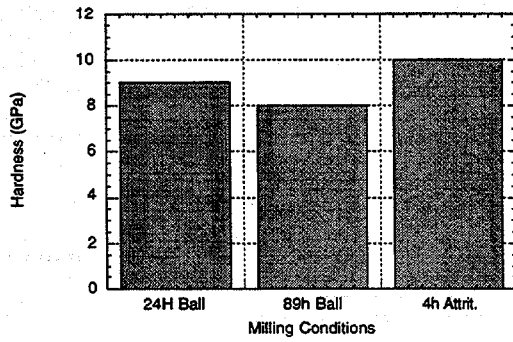
(a)



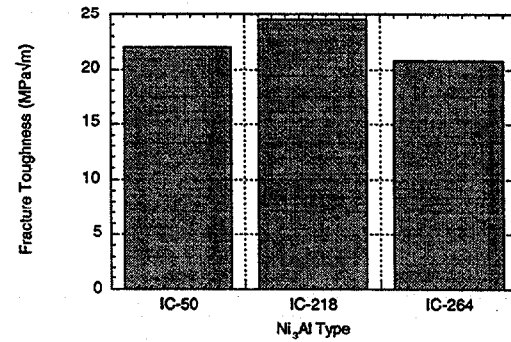
(b)



(b)



(c)



(c)

Fig. 8. Flexural strength, fracture toughness and hardness of composites fabricated with different milling conditions. Sintered at 1450°C by V-LPHIP. Fig. 9. Flexural strength, fracture toughness and hardness of composites fabricated with different Ni₃Al types. Sintered at 1450°C by V-LPHIP.

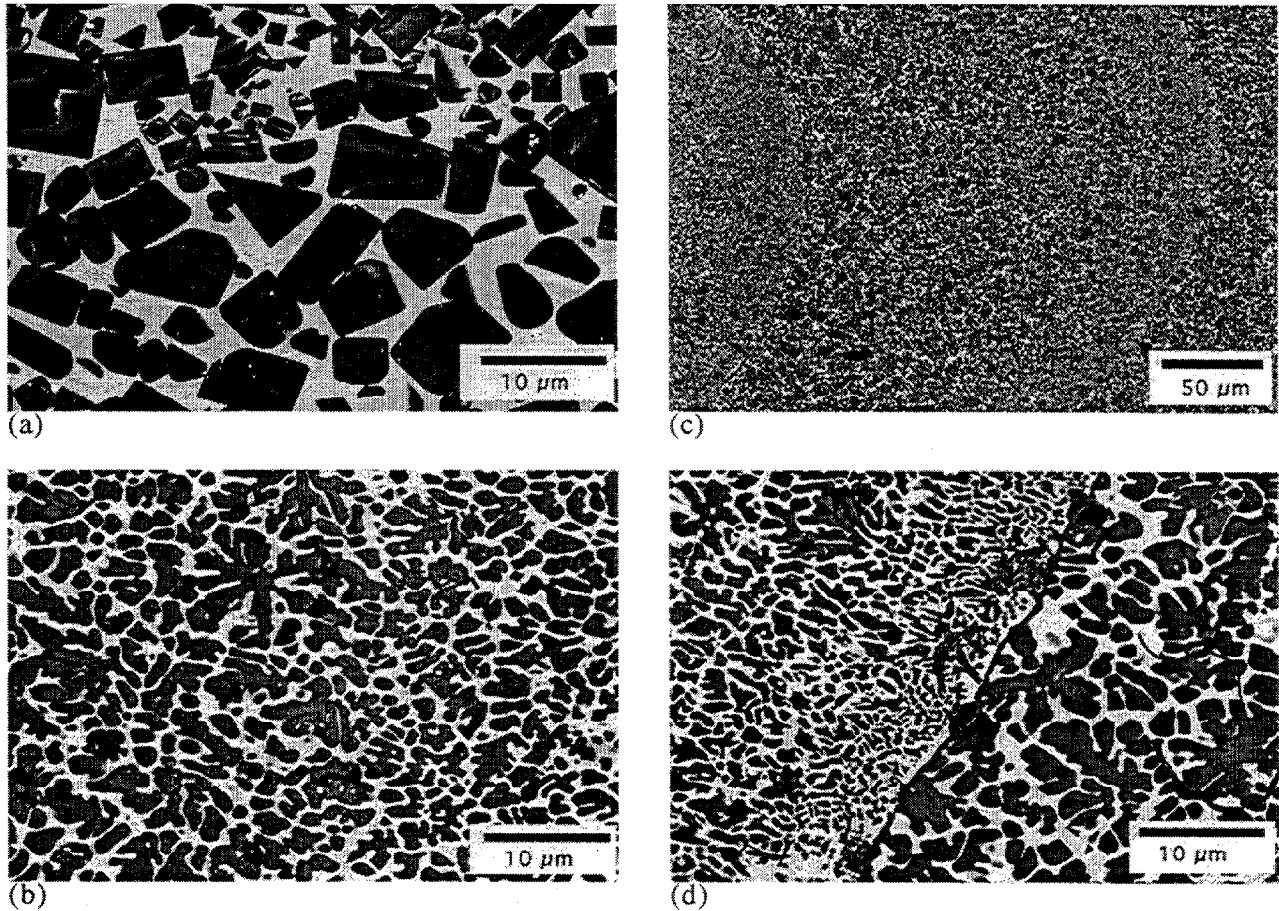


Fig. 10. Microstructures of TiC-50 vol. % Ni₃Al (IC-50) before and after laser surface treatment: (a) as-fabricated base materials, (b) laser affected zone, (c) overlap of laser spots, and (d) interface between a melt-remelt zone. Samples ball milled 24h and sintered at 1450°C by V-LPHIP,

Cost Effective Sintering of Silicon Nitride Ceramics (SIU-C)-

D. E. Wittmer, Southern Illinois University, Carbondale, IL 62901

Objective/Scope

The purpose of this work is to investigate the potential of cost effective sintering of Si_3N_4 and inter-metallic bonded carbides through the development of continuous sintering techniques.

Technical Highlights**Task 1. Refine Economic Model and Design for Chosen Furnace Configuration**

This task was completed as reported in a previous semiannual report.

Task 2. Continue evaluation of sintering parameters on properties of selected Si_3N_4 compositions**1. Prototype Belt Furnace**

Centorr Vacuum Industries, Inc. has redesigned the graphite hot zone of the continuous furnace to provide better insulation and thermal uniformity. During this reporting period a completely redesigned hot zone was received and installed. In addition, the ends of the interior of the hot zone were provided with an erosion/oxidation barrier to improve the hot zone life. One of the operation limitations with graphite hot zones is the short thermocouple lifetime experienced because of the Mo-C reaction. During the hot zone installation, all three expensive thermocouples required replacement, even though they only had roughly 50 hours of high temperature usage. This is similar to that experienced in batch furnaces containing graphite insulation.

During the past three months, the continuous furnace was in operation for approximately 300 hours with the new graphite insulation installed. The temperature uniformity has been noticeably improved and the thermal loading of the exterior of the furnace chamber has been reduced. Several materials were processed in the furnace including: intermetallic bonded TiC, silicon nitride composites, Co Bonded WC and partially stabilized Zirconia. The furnace continues to operate efficiently without any major problems. The only concern with the graphite hot zone will be the reduced life time and associated cost involving thermocouple replacement.

2. Collaboration with Industrial Partners and Affiliates

Work continues according to plan to develop collaborations with industrial partners. Due to the proprietary/confidential relationships established, the results of these collaborations will be reported as part of their individual programs.

3. Evaluation of Continuous Sintering of Silicon Nitride-Titanium Carbide

Graduate student Jason Smith has finished his thesis work and copies of his thesis have been sent to the program manager and project monitor. The major accomplishment of this work was producing silicon nitride containing TiN with improved fracture toughness and significantly improved thermal shock resistance, compared with the baseline A3Y9 silicon nitride. The summary of data is given in Table I. These results show that very high density silicon nitride can be produced through the addition of up to 10 wt% TiN without sacrificing strength or toughness. In many cases the fracture toughness was higher than the baseline composition which did not contain any TiN. Milling the TiN for 24 hours was found to increase the density with improved strength over the as-received TiN, however fracture toughness was not markedly improved. Obtaining densities greater than the target density was most likely due to a pickup of oxygen during the turbomilling process.

Task 3. Continue Evaluation of Low Cost Si_3N_4 Powders

Nothing to report this reporting period.

Task 4. Design and Construct Prototype Belt Furnace

This task has been completed.

Task 5. Continuous Sintering of Inter-metallic Bonded Carbides

During this reporting period Mr. Frederik Goransson finished his M.S. thesis and copies of his thesis have been submitted to the program manager and project monitor. This work has provided the initial motivation for continuance of continuous sintering of cermets as a means of reducing cost and potentially improving performance in the process. The following conclusions were made in this work:

- High densities and good mechanical properties can be achieved by both the vacuum-LPHIP process and the continuous sintering. The most promising systems for continuous sintering were TiC with 40 vol% binder, where the binder was reaction sintered Fe-Ni₃Al, pre-alloyed NiCr or pre-alloyed NiCrFe.
- TiC bonded with 30 vol.% reaction sintered Ni₃Al sintered well in both the belt furnace and the batch-pressure furnace for equal sintering times, reaching near full densities, while pre-alloyed Ni₃Al bonded TiC generally showed lower densities when continuously sintered.
- Metal elemental additions to the reaction sintered Ni₃Al significantly altered the sintered densities, with Fe, Si, Mo and Ti additions providing the best densification, using both continuous sintering and vacuum-LPHIP.
- High heating rate and short sintering time in the belt furnace generally had a negative effect on the sintered densities, hardness and fracture toughness for the reaction sintered Ni₃Al samples. However, high amounts of Fe additives produced better properties at the higher heating rate and shorter sintering times.
- Continuously sintered, TiC bonded with 30 vol.% reaction sintered Ni₃Al, highly doped with Fe, showed significantly higher sintered densities, hardness and fracture toughness when compared to all alloy additives. The high fracture toughness values achieved might be due to the tendency towards a more intergranular fracture behavior and a change .
- TiC - 40 vol.% pre-alloyed Ni₃Al showed significantly better densification using vacuum-LPHIP compared to continuous sintering, with lower mechanical properties recorded for continuous sintering, as a result of the low sintered densities.
- Pre-alloyed Cr doped Ni₃Al and pre-alloyed NiCr and NiCrFe bonded TiC showed high densification in both furnaces and all furnace settings, reaching near theoretical densities. Significantly finer TiC grains were observed for continuous sintering, processed at high heating rates and short sintering times, which could also explain the higher hardness and fracture toughness values achieved; leading to the conclusion that Cr in TiC systems increases densification and improves the mechanical properties.
- Generally low densities and poorer mechanical properties were achieved for 6 vol.% TaC, VC, Cr₂₃C₆ and Mo₂C additions to the pre-alloyed Ni₃Al baseline compositions, with significantly lower densities and properties attained for continuously sintered materials.

- TiN added at the 6 vol.% level to baseline pre-alloyed Ni₃Al produced full density using vacuum-LPHIP processing, while extremely low densities were achieved for continuous sintering. Slightly higher hardness and fracture toughness values were recorded for TiN additions fabricated by the vacuum-LPHIP process when compared to the baseline composition.
- Micrographs of sintered ball milled and attrition milled compositions showed differences in the shape of the carbide free regions, which are resulting from the large sized, pre-alloyed, Ni₃Al starting powders. Attrition milling produced round shaped regions, which compared to elliptical regions produced by ball milling, suggesting that the shape difference was caused by the type of milling.
- The baseline reaction sintered Ni₃Al bonded TiC performed best in the corrosion test in all acid solutions, hydrochloric, sulfuric and nitric acid solutions compositions with 30 vol.% binder. The 40 vol.% NiCr bonded TiC showed outstanding corrosion resistance in all acid solutions, outperforming the baseline pre-alloyed Ni₃Al TiC. NiCrFe also showed extremely good corrosion resistance.
- The thermal expansion was increased with increasing binder content. The highest thermal expansion coefficient was achieved for the 40 vol.% NiCr bonded TiC, which showed a thermal expansion coefficient of $10.9 \cdot 10^{-6}$ mm/mm °C for a temperature interval of 25 to 1000 °C.

Based on these conclusions, the following recommendations for future work are:

- Prepare larger samples of TiC bonded with 40 vol.% IC-50, IC-218, NiCr and NiCrFe in order to be able to machine test bars for strength and fracture toughness measurements.
- Use turbomilling in order to investigate the possibilities of reducing the carbide and intermetallic grain size efficiently without increasing oxygen contamination.
- Prepare samples with higher binder content, possibly 45-60 vol.% to increase the strength, toughness and the thermal expansion.
- Investigate the high-temperature properties of the above-mentioned compositions.
- Optimize the continuous sintering parameters for the NiCr and NiCrFe bonded TiC.
- Investigate the corrosion resistance further, for longer times and at elevated temperatures.

Figure 1 shows the effect sintering method and heating rate on the microstructure for TiC bonded with 40 vol% IC-264. The vacuum-LPHIP sintered at ORNL has the larger TiC grain size, while continuous sintering at the higher sintering rate produced the smaller TiC grain size, with bimodal distribution. Figure 2 shows the microstructural comparison as a function of heating rate for TiC bonded with 40 vol% NiCr. Again, the higher heating rate produced a noticeable decrease in the TiC grain size. It is believed that the finer grain size of the TiC will give improved scuff resistance.

Status of Milestones

- | | | |
|----|---|-------------|
| 1. | Refine Economic Model and Design for Chosen Furnace Configuration | Completed |
| 2. | Continue Evaluation of Sintering Parameters on Properties of Selected Si ₃ N ₄ Compositions | Completed |
| 3. | Continue Evaluation of Low Cost Si ₃ N ₄ Powders | Completed |
| 4. | Design and Construct Prototype Belt Furnace | Completed |
| 5. | Continuous Sintering of Inter-Metallic Bonded Carbides | On Schedule |

Communications/Visits/Travel

D. E. Wittmer to ORNL to discuss progress with Ray Johnson and Terry Tiegs.

Problems Encountered

None

Publications and Presentations

Fredrik Göransson, "INTERMETALLIC BONDED CARBIDES SINTERED BY CONTINUOUS SINTERING AND BATCH VACUUM-PRESSURE SINTERING," MS Thesis, Southern Illinois University at Carbondale, April, 2000.

Jason, E. Smith, "EFFECT OF TiC AND TiN ADDITIONS ON THE PROPERTIES OF SILICON NITRIDE COMPOSITES," MS Thesis, Southern Illinois University at Carbondale, April, 2000

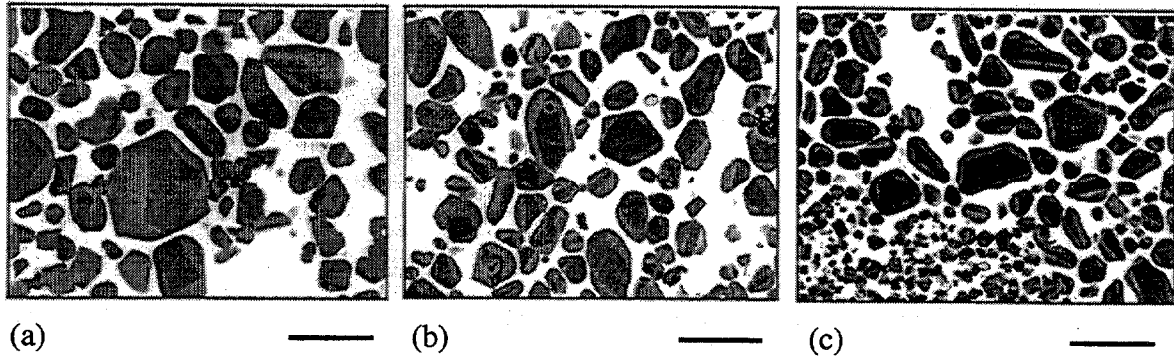


Figure 1. Microstructures of TiC bonded with 40 vol% IC-264, following sintering at 1450°C by (a) vacuum-LPHIP sintering, (b) continuous sintering with a belt speed of 18.3 mm/minute and (c) continuous sintering with a belt speed of 36.6 mm/minute. (Bar = 10 μ m)

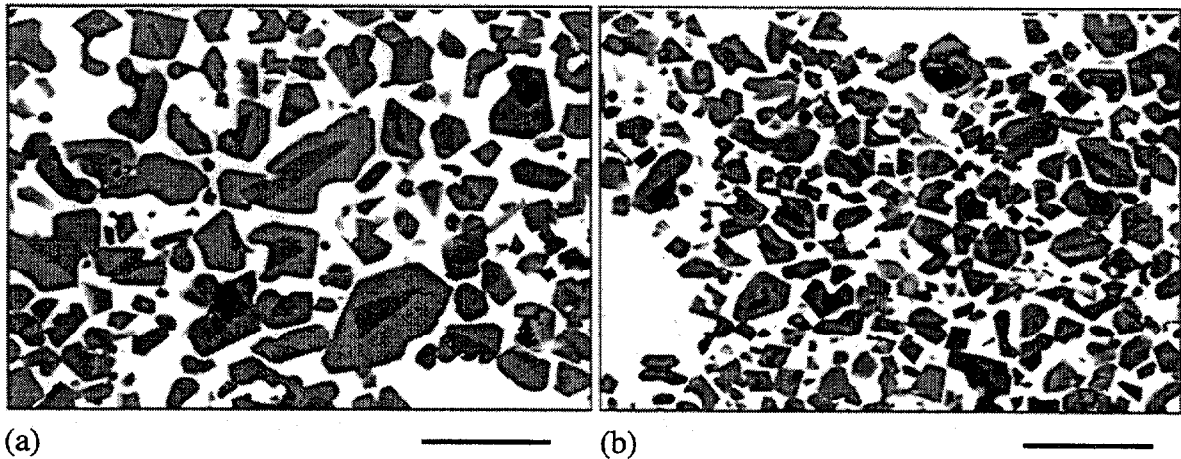


Figure 2. Microstructures of continuously sintered TiC-40 vol% NiCr, sintered at 1450 °C using a belt speed of (a) 18.3 mm/minute and (b) 36.6 mm/minute, showing the finer TiC grains achieved for the higher belt speed. (Bar = 10 μ m)

Table I. Continuous Sintering Results for A3Y9-TiN Using Commercial TiN

Designation	Sintering Conditions		% Target Density	4-Pt. Flexural Strength (MPa)	K _{IC} Fracture Toughness (MPa • m ^{1/2})
	Temperature (°C)	Time (min)			
Baseline A3Y9 Formulation	1790	120	100.0	953 +/- 52	6.5 +/- 0.0
	1775	120	100.0	1003 +/- 139	6.5 +/- 0.1
	1725	120	99.4	1018 +/- 41	6.2 +/- 0.0
TN1 95/5 As-received TiN [†] Pressure Cast & CIPed	1775	120	100.0	798 +/- 44	7.0 +/- 0.2
	1750	120	99.6	860 +/- 143	6.5 +/- 0.0
	1725	120	98.8	874 +/- 30	6.5 +/- 0.0
	1700	120	98.6	783 +/- 81	6.7 +/- 0.1
TN2 95/5 Pre-milled TiN [†] (24h) Pressure Cast & CIPed	1790	120	100.3	988 +/- 68	5.9 +/- 0.3
	1775	120	101.0	992 +/- 45	6.8 +/- 0.1
	1750	120	100.6	963 +/- 85	6.6 +/- 0.2
	1725	120	98.7	803 +/- 83	6.4 +/- 0.1
	1700	120	99.0	811 +/- 57	6.3 +/- 0.3

[†] Commercial TiN provided by H.C. Starck

Table I. Continuous Sintering Results for A3Y9-TiN Using Commercial TiN (continued)

Designation	Sintering Conditions		% Target Density	4-Pt. Flexural Strength (MPa)	K _{IC} Fracture Toughness (MPa • m ^{1/2})
	Temperature (°C)	Time (min)			
TN3 95/5 Pre-milled TiN [†] (32 h) Pressure Cast & CIPed	1790	120	98.9	883 +/- 32	6.3 +/- 0.1
	1775	120	101.1	923 +/- 34	6.6 +/- 0.1
	1750	120	100.9	888 +/- 63	6.4 +/- 0.3
TN4 90/10 Pre-milled TiN [†] (24 h) Pressure Cast & CIPed	1790	120	99.8	849 +/- 25	6.1 +/- 0.0
	1775	120	99.5	838 +/- 55	6.0 +/- 0.0

[†] Commercial TiN provided by H.C. Starck

DIESEL PARTICULATE TRAP DEVELOPMENT

J. C. McLaughlin, D. Butz, R. A. Lowden, and D. P. Stinton
Oak Ridge National Laboratory
Oak Ridge, TN 37831-6063

Objectives/Scope:

Traps and filters are being developed to effectively control diesel particulate emissions from large trucks and other heavy vehicles. The particulate traps are necessary to comply with impending regulations and to alleviate public concerns over particulate emissions. An acceptable particulate trap must be efficient in removing the fine carbon particles from the exhaust gas stream, and must be able to be regenerated (cleaned) while in service. The filters must also be robust to withstand the rigors of vehicle use. Due to the high exhaust gas flows associated with heavy vehicle diesel engines, the filtration systems are large and thus can be difficult to heat resistively for regeneration. These factors necessitate the development of novel filter materials and heating means to produce an acceptable particulate removal system.

A candidate particulate removal system, conceived by Industrial Ceramic Solutions and Microwave Materials Technologies, utilizes a microwave regenerated ceramic filter system. The filter is fabricated from a flat sheet paper product composed of silicon carbide fibers, oxide fiber fillers, and various organic binders. The ceramic paper is formed into a corrugated cylindrical cartridge shape and rigidized employing a ceramic binder. The SiC fibers were included to couple with the microwaves and thus heat to regenerate the filter. Heating was found to be slower than desired and non-uniform. The corrugated structure was then coated with a thin layer of silicon carbide using chemical vapor infiltration to enhance coupling with the microwaves and thus improve heating rate and uniformity. Although initial results have been promising, the composition of the filter media, i.e. quantity of SiC fiber, and thickness and chemistry of the SiC coating, has not been optimized. It is the purpose of this task to optimize the composition and structure of the filter material for strength, coupling, uniformity and efficiency of heating, and filtration.

Technical Highlights:

As described in earlier reports, flat rectangular samples of a ceramic filter paper product, procured from Industrial Ceramic Solutions (ICS) are being infiltrated with SiC employing chemical vapor infiltration. The purpose of the infiltration is to improve the microwave coupling of the product to enhance heating rate and uniformity for use in a diesel particulate trap, and to create a more robust filter medium for use in the demanding service environment of a heavy-duty diesel engine. During earlier deposition experiments it was found that the addition of excess silicon to the reactant gas mixture produced a Si-rich SiC coating that subsequently enhanced heating rate and uniformity for the filter material.

It was found that the silicon content of the SiC layer influenced microwave heating properties of the fibrous filter material. Increasing Si-content improved coupling, heating rate, and uniformity of heating. Altering the Si-ratio in chemical vapor deposited SiC is not trivial, especially in the given furnace configuration and with the selected operating conditions. Additional Si is introduced to the coating by adding SiCl₄ to the methyltrichlorosilane (MTS or CH₃SiCl₃) - hydrogen gas mixture. Difficulties in controlling the flow of SiCl₄ necessitated modification of the gas feed systems for the deposition unit. A vapor source controller designed specifically for SiCl₄ was installed to permit improved control of the gas mixture. Scoping runs using the new equipment were completed to calibrate the controller and examine the relationship between gas and coating composition.

Standard SiC infiltration of the filter material is conducted using a gas mixture containing 225 ccm MTS and 1500 ccm hydrogen. In earlier experiments examining the deposition of Si-rich SiC, it was determined that 100 ccm SiCl₄ added to the standard gas mixture produced desirable results. Deposition runs with times of 1.0, 1.5, and 2.0 hours were made to complete testing of the new vapor controller and explore the deposition of Si-rich SiC on the fibrous filter media. The results are summarized in Tables 1 through 3.

Table 1. Infiltration of Filter Material with SiC plus Silicon (1.0 h run time)

Sample	As-Received (g)	After Infiltration (g)	Wt. Gain (g)	% Wt. Gain
7	2.7807	2.9690	0.1883	6.8
8	2.3733	2.5484	0.1751	7.4
9	2.7914	3.0037	0.2123	7.6
Average				7.2 ± 0.4

Desired SiCl₄ flow: 100 ccm

Actual flow: 98.7 ccm

Table 2. Infiltration of Filter Material with SiC plus Silicon (1.5 h run time)

Sample	As-Received (g)	After Infiltration (g)	Wt. Gain (g)	% Wt. Gain
1	2.7600	3.1803	0.4203	15.2
2	3.2534	3.7808	0.4474	13.8
3	3.3825	3.9657	0.5832	17.2
Average				15.4 ± 1.7

Desired SiCl₄ flow: 100 ccm

Actual flow: 116 ccm

Table 3. Infiltration of Filter Material with SiC plus Silicon (2.0 h run time)

Sample	As-Received (g)	After Infiltration (g)	Wt. Gain (g)	% Wt. Gain
4	2.9210	3.6370	0.7160	24.5
5	2.6035	3.2206	0.6171	23.7
6	2.9539	3.8620	0.9081	23.5
Average				24.0 ± 0.5

Desired SiCl₄ flow: 100 ccm

Actual flow: 120 ccm

Detailed characterization of the infiltrated samples including electron microscopy and x-ray diffraction is planned. Microwave properties and heating rate and uniformity are also to be tested. A prototypical filter component was also coated with SiC for testing and evaluation. A pleated cylinder approximately 40 mm in diameter and 75 mm long made from the filter material was infiltrated with SiC. The sample gained ~12% by weight and permeability, structural integrity, and heating characteristics are to be examined at ICS.

Status of Milestones:

On schedule

Communications/Visits/Travel:

None

Problems:

None

Publications:

None

ADVANCED MANUFACTURING TECHNOLOGY

Durability of Diesel Engine Component Materials

Peter J. Blau and Ronald D. Ott
Oak Ridge National Laboratory

Objective/Scope

The objective of this effort is to enable the development of more durable, low-friction moving parts in diesel engines for heavy vehicle propulsion systems by conducting friction, lubrication, and wear analyses of advanced materials, surface treatments, and coatings. The scope of materials and coatings is broad and includes any metallic alloy, intermetallic compound, ceramic, or composite material which is likely to be best-suited for the given application. Parts of current interest include valves, valve guides, and scuffing-critical components, like fuel injector plungers. Hot scuffing is a primary surface damage mode of interest. Bench-scale simulations of the rubbing conditions in diesel engine environments are used to study the accumulation of surface damage, and to correlate this behavior with the properties and compositions of the surface species. The effects of mechanical, thermal, and chemical factors on scuffing and reciprocating sliding wear are being determined, and the results will be used to refine material selection strategies for durability-critical engine components.

Technical Highlights

(a) *High-Temperature Scuffing of Diesel Engine Components.* The redesign and construction of a new, high-temperature scuffing test system has been completed, but a few remaining calibrations and alignment checks are being performed to ensure that it will be ready to begin baseline tests during the coming months. Basic characteristics of the machine are:

- Contact geometry: pivoting cylinder on flat
- Drive: variable speed, linear-to-rotary drive train
- Loads: variable, dead-weight (minimum 20 N)
- Torque sensing: load cell in the upper drive train linkage
- Temperatures: room temperature up to at least 750° C
- Atmosphere: air
- Lubrication: liquid, solid, or none

Further details of the scuffing apparatus will be provided in future reports.

(b) *Friction and Wear of Metallic Glasses.* Metallic glasses, also known as amorphous metal alloys, have been considered as candidate materials for wear and friction-critical engine components, but no previous research on engine-oil lubricated amorphous alloys has been reported. This prompted the current study.

Specimens of a Zr-based, multi-component metallic glass were specially prepared for this study by Dr. C. T. Liu's group at ORNL. Pin-on-disk tests were conducted in accordance with ASTM

standard G-99 to compare the friction and wear behavior of the metallic glass with that of two, commercial metallic alloys (Stainless steel 303, and Ni-200) tested under the same conditions, all sliding against polished 52100 steel disks. The amorphous alloy's composition (in at%) was 17.9 Cu, 14.6 Ni, 5.0 Ti, and 10.0 Al, with the balance, Zr. The Vickers microindentation hardness numbers for the test specimen materials, in comparison to metallic and ceramic materials, are given in Table 1. Friction and wear results are summarized in Tables 2(a) and (b).

Table 1. Comparison of Vickers Microindentation Hardness Numbers
(data obtained on the materials to be tested here are shown in **bold**)

Material	HV, GPa* [indentation load in N]
Silicon nitride, hot-pressed, type NT-551	16.1 [1.96]
Steel, stainless, type 440C	12.6 [0.98]
Steel, tool steel, type M-50	9.08 [0.98]
ORNL metallic glass, Zr-Cu-Ni-Ti-Al	5.77 [0.98]
Co-based superalloy, Stellite 6B	4.65 [1.96]
Steel, AISI 52100, annealed (disk test specimen)	3.67 [0.98]
Copper, high-purity annealed	0.42 [0.98]

* kg/mm^2 (previously-used HV units) = $101.9 \times \text{GPa}$

Table 2(a). Friction and Wear Data from Unlubricated Tests
(4.95 N load, 0.26 ± 0.02 m/s sliding speed, sliding distance 100 m, room temp.)

Pin Material	Steady State Friction Coeff.	Pin Wear Rate ($\text{mm}^3/\text{N}\cdot\text{m}$)	Disk Wear Rate ($\text{mm}^3/\text{N}\cdot\text{m}$)	Ratio of Pin to Disk Wear
303 St. Steel	0.94	4.99×10^{-4}	5.91×10^{-4}	0.84
Ni-200	1.11	1.07×10^{-3}	9.82×10^{-4}	1.09
Amorphous alloy	0.74	4.68×10^{-4}	4.54×10^{-4}	1.03

Table 2(b). Friction and Wear Data from Lubricated Tests
(as above but lubricated with 15W40 diesel oil)

Pin Material	Steady State Friction Coeff.	Pin Wear Rate ($\text{mm}^3/\text{N}\cdot\text{m}$)	Pin Wear Ratio (dry/lubricated)	Disk Wear Observations
303 St. Steel	0.17	4.73×10^{-9}	1.1×10^5	fine scratch
Ni-200	0.17	1.39×10^{-8}	7.3×10^4	fine scratch
Amorphous alloy	0.20	8.01×10^{-7}	5.8×10^2	roughened track*

* Material was displaced above and below the plane of the disk surface. This was substantiated by profilometry, but there was no clearly measurable wear groove cross-sectional area, and therefore no wear rate could be obtained.

The amorphous alloy's hardness was greater than that of the other two pin materials, and layman's wisdom would suggest it has better wear resistance, but all experienced tribologists recognize that hardness alone does not determine a material's sliding wear behavior. Under unlubricated conditions, both the pin wear and average sliding friction coefficient of the amorphous alloy were slightly lower than the other two materials, but this was not the case under lubricated conditions. Despite its higher hardness, the amorphous alloy's wear behavior was worse than the two other combinations when tested in oil. The reasons for this probably center on the tailoring of tradition engine oil additives to react with ferrous materials to form anti-friction and anti-wear films. Additional work is planned to determine whether sliding contact induced a transformation from the amorphous to crystalline state, as has been reported in past studies of other amorphous alloys.

While not encouraging, these preliminary pin-on-disk results should not rule out the use of Zr-based amorphous alloys in other types of tribosystems. Rather they suggest that a more research is needed in order to establish both the potential and the limitations of amorphous alloys being considered for wear applications.

Future Plans

a) Complete room-temperature baseline tests in the scuffing apparatus and prepare for elevated temperature baseline tests.

Status of Milestones

1) Complete preliminary evaluation of the friction and wear of amorphous alloys and submit report. (June 30, 2000) Status – in progress.

2) Complete design and construction of high-temperature scuffing test system. (June 30, 2000) Status – completed.

3) Complete baseline scuffing tests at room and elevated temperature. (September 30, 2000) Status – on schedule.

Communications/Visitors/Travel

P. Blau presented an invited talk on "Running-in of Surfaces" at a Caterpillar, Inc., workshop on Boundary Lubrication held in Peoria, Illinois on November 1-2.

Problems Encountered

None.

Publications and Presentations

None

NDE of Ceramic Valves for Diesel Engines – Jiangang Sun, William A. Ellingson, (Argonne National Laboratory), and Seung-Kun Lee (Caterpillar Inc.)

Objective/scope

Emission reduction in diesel engines designated to burn fuels from several sources has lead to the need to assess ceramic valves to reduce corrosion and emission. The objective of this work is to evaluate several nondestructive evaluation (NDE) methods to detect defect/damage in structural ceramics valves for diesel engines. There are three tasks to be carried out in this work: (1) Finalize correlation of NDE to machining damage. This limited effort will conclude the earlier work to correlate NDE data with mechanical properties of machining-damaged Si_3N_4 ceramics. Elastic optical scatter method will be used to examine these specimens and the NDE data will be correlated with flexural strength. (2) Correlate NDE data with mechanical properties for fatigue/wear damaged samples. These include rotary fatigue, dynamic fatigue, impact/sliding wear, and possible thermal shock testing. The induced damage will be assessed using various NDE methods including dye penetrant, optical scatter, impact acoustic resonance (IAR), X-ray CT, thermal imaging, and others. NDE data will be correlated with those from characterization tests including mechanical strength, SEM, and others. (3) Conduct NDE studies of full-size engine valves. In this part of the work, full sized ceramic valves will be produced for testing in a single cylinder test engine. These valves will be examined using NDE techniques developed at Argonne.

Technical progress

1. Elastic Optical Scattering NDE for Machining Damage

During this period we received a set of Si_3N_4 ceramic specimens from Caterpillar, Inc. These include four materials, AS800, GS44, CFI, and SN235, and with 12 samples for each material. They are flexure bar specimens in dimensions 3 x 4 x 45-50 mm, and were ground on all four surfaces with a standard machining condition. Figure 1 shows typical specimens for each of the materials. Figure 2 shows optical micrographs of the machined GS44 surface with normal-incident-light (Fig. 2a) and inclined-light (Fig. 2b) sources. The machining lines are evident in Fig. 2a, while some suspected defects and machining damage (those brighter spots and lines) are shown in Fig. 2b. For this group of four Si_3N_4 materials, only GS44 and SN235 have been previously tested for optical transmission. At He-Ne laser wavelength (633 nm), the penetration depth is ~100 μm for SN235 and >400 μm for GS44. The penetration depth for AS800 and CFI is probably between that of GS44 and SN235.

The elastic optical scanned region of the flexure bars is shown in Fig. 3. For each sample, two scans were performed, one on each broad side (50-mm x 4-mm) of the bar. As shown in Fig. 3, the data were collected over a 30 mm by 3 mm region at a resolution of 10 μm . Figure 4 shows typical laser scatter sum and ratio images and Fig. 5 shows detailed sum images for these four Si_3N_4 materials. Based on the theory of optical scattering for the laser scatter system, defect and damage should appear brighter in sum images and darker in ratio images. Suspected spot defects are observed over the entire surfaces of AS800, SN235, and GS44 specimens. Those spots are about 50 μm in diameter and their distributions are especially dense on the GS44 specimen surface. Suspected machining-damage lines are found on SN235, GS44, and AS800 specimens. Those damage lines are typically segmented at <1 mm long, and they are more prominent on the SN235 specimen surface. For the CFI material, the scatter images in Figures 4 and 5 do not show clear defect/damage features. The reason for this results will be further investigated.

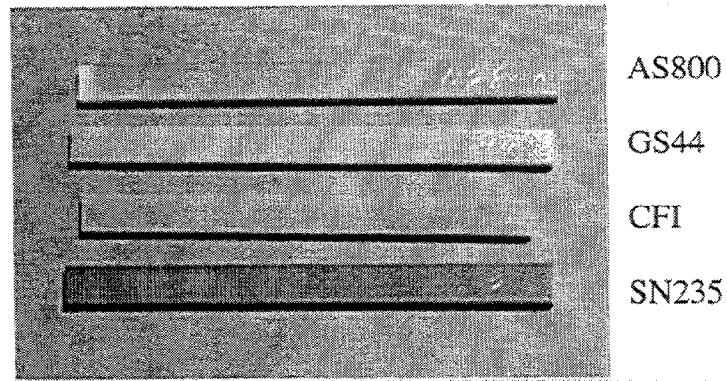


Figure 1. Photograph of fracture-test specimens of AS800, GS44, CFI, and SN235 materials.

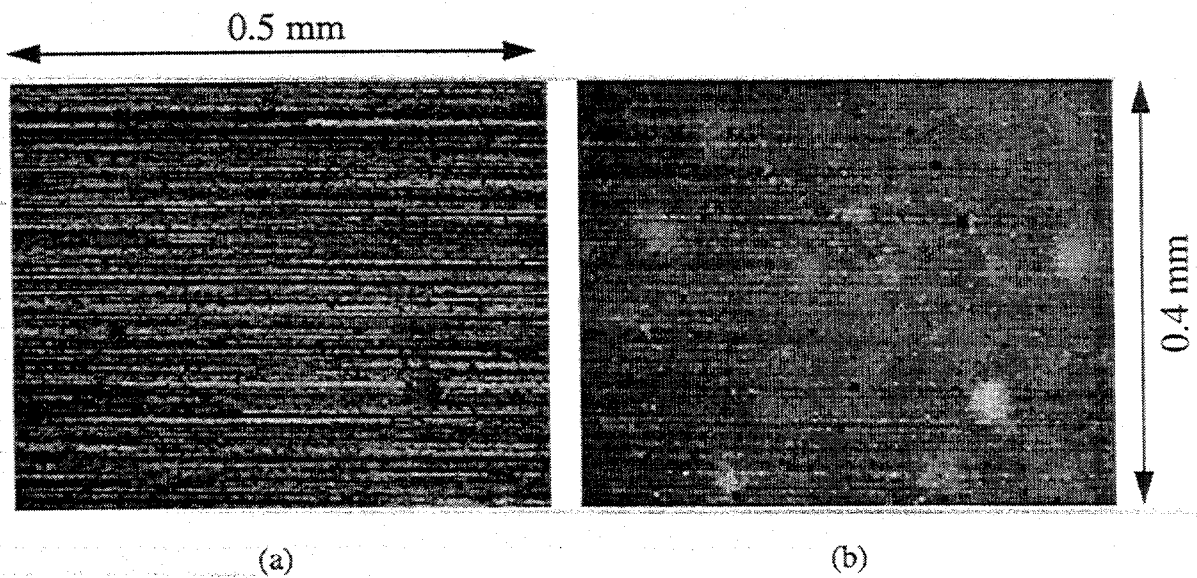


Figure 2. Photo micrographs of GS44 specimen surface with (a) normal-incident light and (b) inclined light sources.

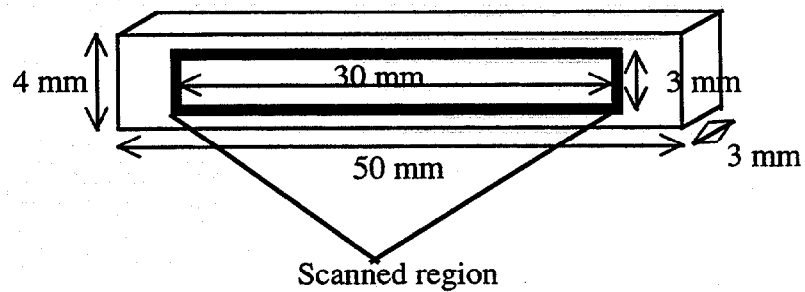


Figure 3. Schematic of the region where optical scattering data were taken.

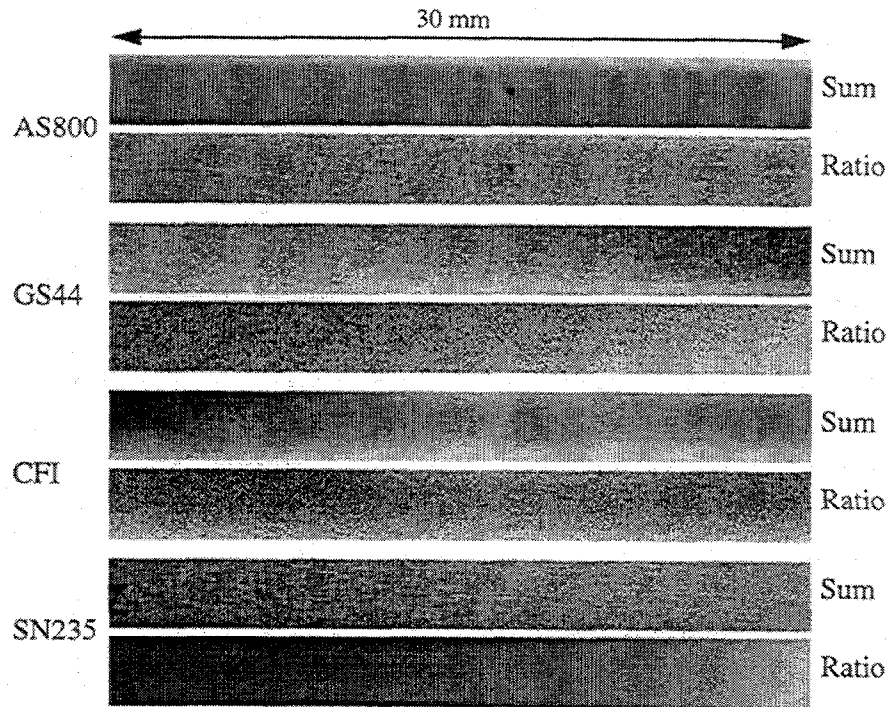


Figure 4. Elastic optical scatter sum and ratio images of the ground surfaces of fracture-test specimens of AS800, GS44, CFI, and SN235 materials.

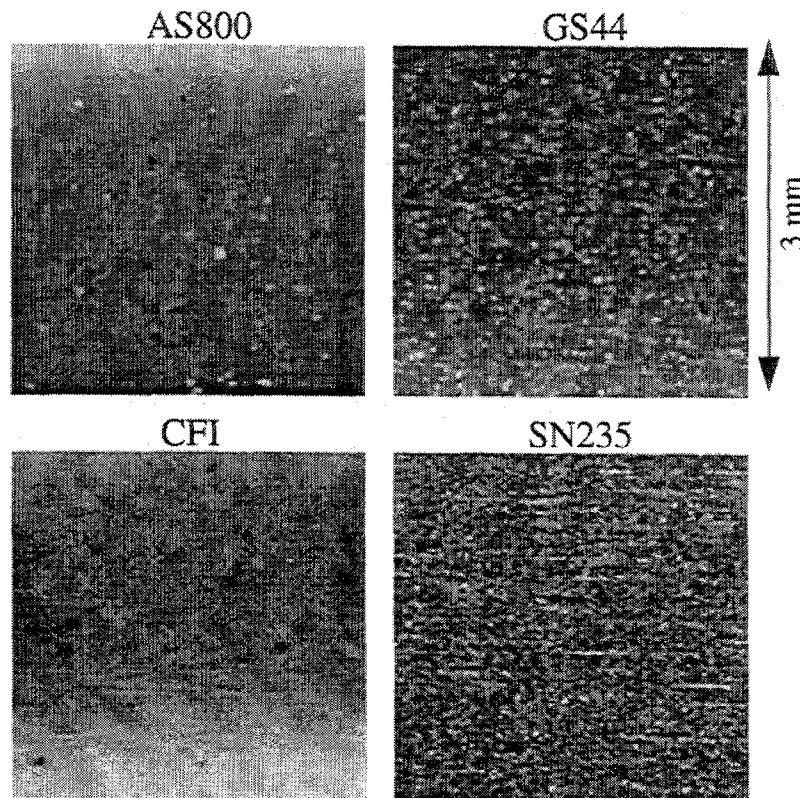


Figure 5. Detailed elastic optical scatter sum images of ground surfaces of fracture-test specimens of AS800, GS44, CFI, and SN235 materials.

Statistical data derived from scattering images of 12 GS44 samples have been obtained. These include the coefficient of variance C_v (standard-deviation/mean), skewness C_s (skew/mean), and their ratio C_v/C_s , and they may provide measures of subsurface microstructural variations between these samples. The plots of these parameters are shown in Fig. 6. The error bars represent the values for each side of the bar with the average between the two values represented as the data point. The large spread for some of samples is probably due to a color variation in the material, similar to that of sample #7 as shown in Fig. 7. These large color variations may be the product of inhomogeneity in the material as a result of processing. Their effect on the bar strength will be determined when the destructive data is received. If this type of inhomogeneity has no effect on strength, the data can be filtered to eliminate this color variation effect.

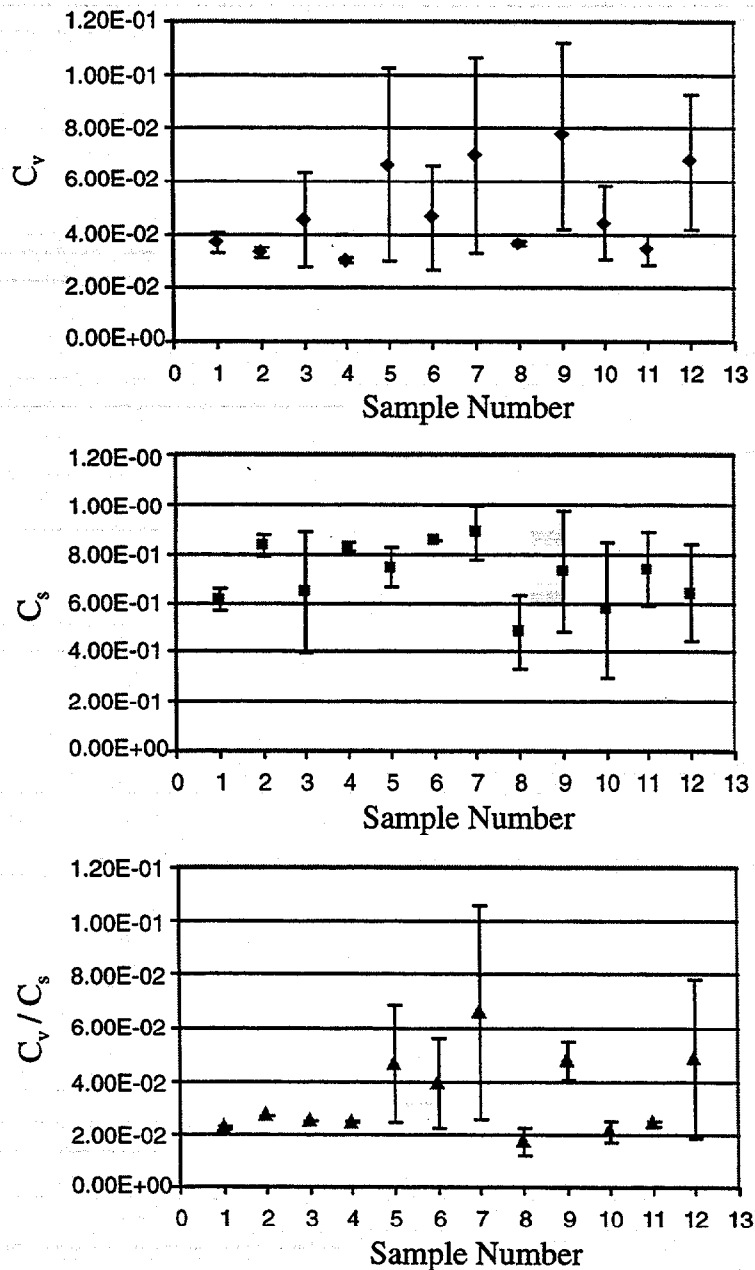


Figure 6. Statistical parameters C_v , C_s , and C_v/C_s for GS44 samples.

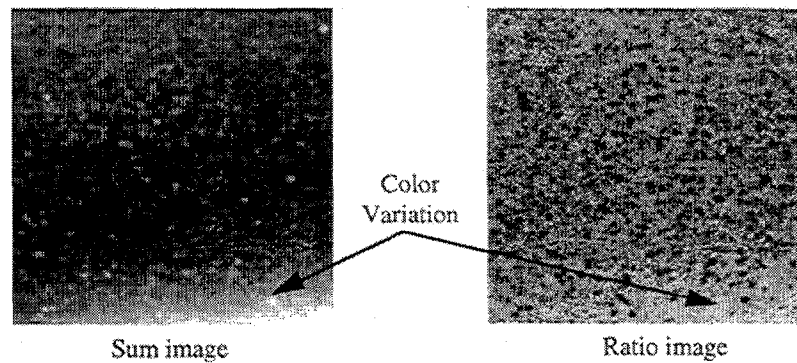
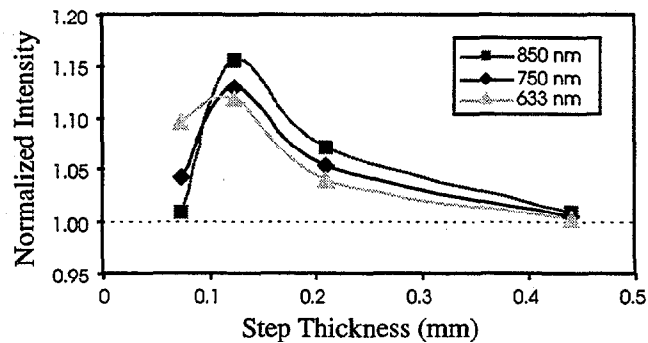


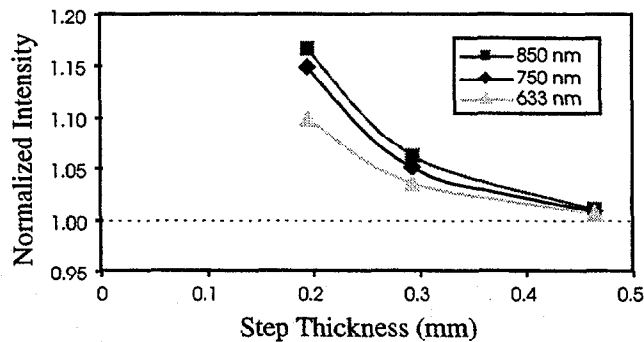
Figure 7. Example of color variation in GS44 sample #7.

2. Study of Laser Wavelength on Elastic Optical Scattering

We continued study of subsurface back scattering from step-wedges as a function of ceramic thickness at several laser wavelengths. As described in our June-July 1999 report, these tests also serve as detection of subsurface lateral cracks at various depths. Figure 8 plots the averaged back-scattered intensity at wavelengths 633, 750, and 850 nm for GS44 and NT164 ceramics as a function of thickness with best-fit lines to an exponential attenuation behavior. It is seen that the back-scattered intensity increases with the increase of the wavelength, except for GS44 with thickness $<120 \mu\text{m}$. This result indicates that longer wavelength light has higher sensitivity on detecting deeper defects within the subsurface of ceramics.



(a)



(b)

Figure 8. Plots of back-scattered intensity as a function of subsurface interface depth and laser wavelength for ceramics (a) GS-44 and (b) NT164.

Status of Milestones

Current ANL milestones are on or ahead of schedule.

Communications/Visits/Travel**Visit:**

1. Dr. S. K. Lee of Caterpillar Inc. visited Argonne on February 17, 2000 to discuss project details.

Travel:

1. W. A. Ellingson and J. G. Sun attended the American Ceramic Society's 24th Annual Cocoa Beach Conference at Cocoa Beach, FL, in Jan. 23-28, 2000.
2. W. A. Ellingson and J. G. Sun visited Caterpillar Technical Center in Mossville, IL on December 15, 1999 to discuss project details.
3. W. A. Ellingson J. G. Sun visited Caterpillar Technical Center in Mossville, IL on October 4th, 1999.

Communication:

1. Discussions have been taking place with Eaton Corporation and St. Gobain Industrial Ceramics to obtain additional machined specimens with carefully controlled machining conditions.

Problems Encountered

None this period.

Publications

None this period.

INTERMETALLIC-BONDED CERMETS

P. F. Becher, C. G. Westmoreland, and S. B. Waters
Oak Ridge National Laboratory
Oak Ridge, TN 37831-6068

Objective /Scope

The goal of this task is to develop materials for diesel engine applications, specifically for fuel delivery systems and wear components (e.g., valve seats and turbocharger components). This will require materials which have a minimum hardness of 11 GPa and a thermal expansion coefficient of between 10 to $15 \times 10^{-6}/^{\circ}\text{C}$ over the temperature range of 25° to 300° C. The material should also have excellent corrosion resistance in a diesel engine environment, flexure strength in excess of 700 MPa, and fracture toughness greater than $10 \text{ MPa}\sqrt{\text{m}}$ to ensure long term reliability. The material should also be compatible with steels and not cause excessive wear of the steel counter face. The upper temperature limit for fuel delivery systems applications is 540° C, and for the other wear applications, the limit is 815° C. Finally, the total material processing costs for these advanced materials should be competitive with competing technologies such as TiN or other ceramic coatings on high-speed tool steels.

Technical Highlights

For improvements in the processing and properties of these cermets have been the focus of recent studies. One approach has been to utilize finer TiC powders (e.g., smaller than the $\sim 2 \mu\text{m}$ TiC powders used earlier) to enhance densification and possibly improve the fracture strengths. Very fine TiC powders are also required for Al_2O_3 -TiC substrates for computer applications, but the special synthesis approaches, which result in a considerable increase in powder costs ($> \$100/\text{kg}$). In addition, these submicron powders must still be milled to break up soft agglomerates to achieve a submicron particle size distribution. Unfortunately, most lower cost commercial TiC powders used in the carbide/hard metals industry exhibit particle sizes in the 1 to $10 \mu\text{m}$ range, Figure 1.

The key requirements for successful powder metallurgical processing of very fine grained TiC cermets are: (1) a simple densification method [e.g., currently pressureless sintering method at modest temperatures ($\leq 1400^{\circ}\text{C}$)] has been developed using liquid phase sintering, and (2) low cost submicron TiC powders with a low oxygen content to promote wetting by the liquid phase.

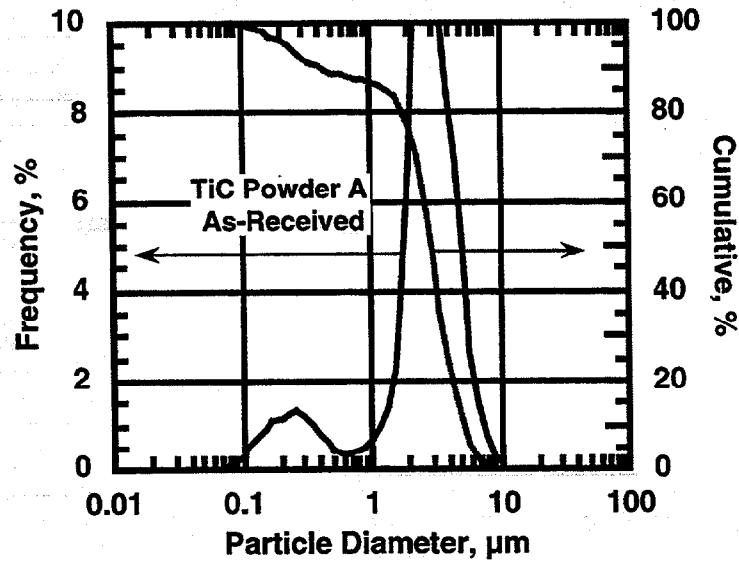


Figure 1. As-received lower cost commercial TiC powders typically exhibit a bimodal particle size distribution with the major fraction (~ 85 %) being between 1 and 10 microns.

The attainment of lower cost submicron TiC powders was addressed by examining attritor milling of such lower cost (~\$35/kg) commercial TiC powders. This involved a series of milling studies: (1) the effects of milling media and (2) milling time. Three different milling media were used: 2 mm spherical ZrO₂, and 4.8 mm and 1.1 mm spherical WC media keeping the volume of TiC powder to media the same. This latter factor meant that the TiC: WC weight ratio was ~ 10:1 while that for TiC:ZrO₂ was nearly 5:1. As seen in Figure 2, milling with the 4.8 mm WC for 6 h yielded a TiC particle size distribution that was similar to that after the 12 h milling with the 2 mm ZrO₂ media, Figure 2. Neither approach produced the submicron TiC size desired, however, the smaller WC media did produce the desired particle size distribution, Figure 2.

The effect of milling time on the TiC particle size distribution was also examined. As seen in Figure 3, extending the milling time typically aided in reducing the particle size and improving the size distributions. On this basis, a 6 h attritor milling time using the 1.1 mm WC media was chosen as standard milling practice.

Obviously, the milling conditions are a critical component to achieving submicron TiC powders, which also must exhibit low oxygen contents in order to achieve good wetting and densification during the subsequent sintering steps. The most recent studies have shown that modifications to the attritor milling steps results in a milled commercial TiC powder whose quality equals that of the expensive submicron TiC powders originally used to fabricate the submicron TiC grain sized cermets, Table I.

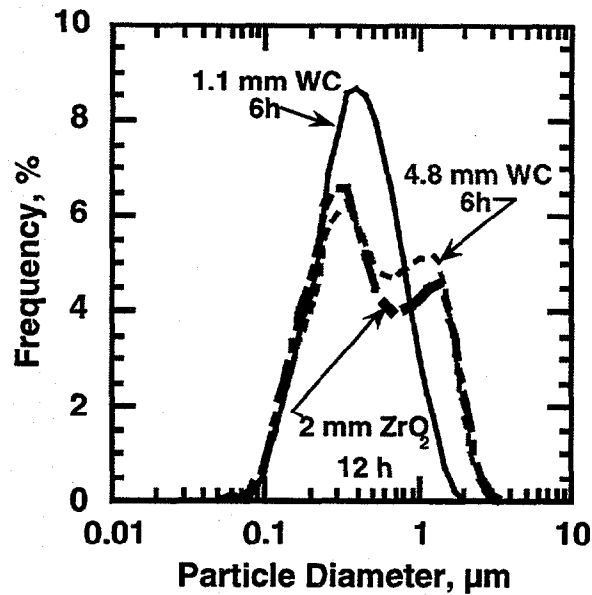


Figure 2. Attritor milling of the commercial TiC powder with 1.1 mm WC media yielded excellent submicron TiC powders (only ~ 5 % of TiC > 1 micron). The attritor milling was least efficient using either the mm zirconia media for ≥ 12 h or the 4.8 mm WC media for 6 h as both left ~ 25 % of the TiC particles with sizes in excess of 1 μm .

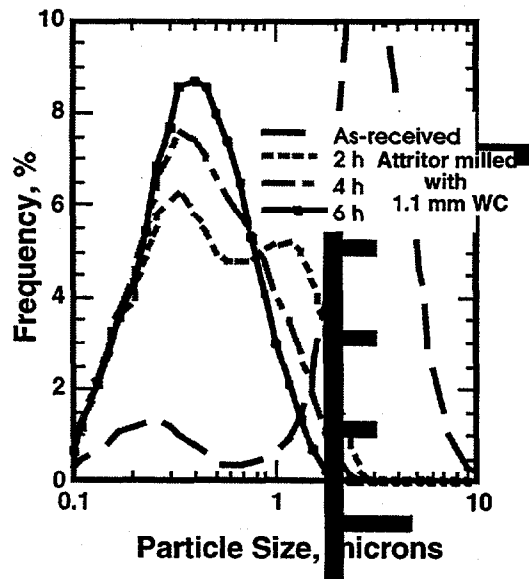


Figure 3. Using the smaller WC milling media, the effect of milling time on the TiC particle size and the shift from a bimodal to a monomodal size distribution is apparent. The response is typical for that of the various milling media used although longer milling times were required to eliminate the bimodal nature of the size distributions.

Table I. Powder Characteristics of Submicron and Commercial TiC Powders.

Powder Grade	As-received		Attritor Milled	
	Mean Particle Size, μm	Oxygen Content wt. %	Mean Particle Size, μm	Oxygen Content wt. %
JNM-007	0.85	1.7	0.43 4 h, isopropanol 2 mm ZrO_2 5 g ZrO_2 :1 g TiC	—
K-02000	2.64	0.5	0.44 6 h, isopropanol 1.1 mm WC 10 g WC:1 g TiC	1.4

Very fine TiC grain size distributions are obtained when the attritor milled submicron TiC powders are employed to fabricate fully dense cermets by vacuum (~ 0.1 torr) sintering at 1400°C , Figure 4. This fine grain size TiC-based cermet referred to in Figure 4 used a Ni_3Al alloy powder to form a binder phase equivalent to 40 vol. %. Thus the process yields the desired average size and the size distribution for the TiC grains.

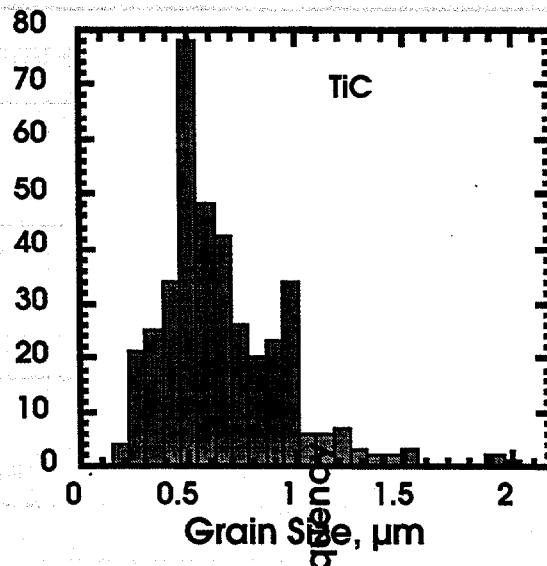
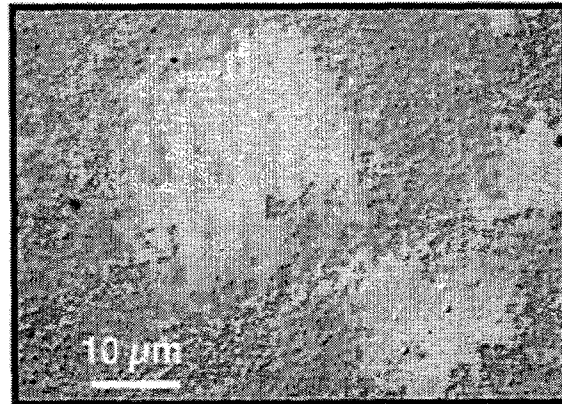
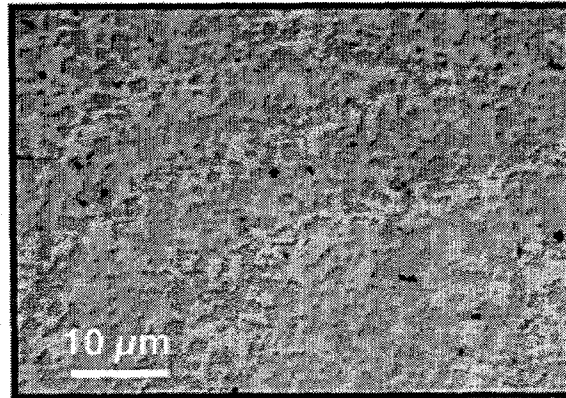


Figure 4. TiC grain size distribution in TiC-40 vol. % Ni_3Al cermet sintered at 1400°C for 60 m reveals submicron nature of TiC grains obtained using commercial TiC powders that were attritor milled for 6 h with the 1.1 mm WC media.

However, it is found that the Ni_3Al binder phase is not uniformly distributed with a large number of large (e.g., 20 to 50 microns across) regions of present in the cermet, Figure 5a. These regions are a result relatively high frequency of the large (> 30 microns) particles present in Ni_3Al powders, which can not be reduced by milling due to the ductility of the Ni_3Al . Size fractionation by sieving or other means can be used to minimize the large particles, but this typically results in a low yield raising the cost of the raw materials.



(a)



(b)

Figure 5. The distribution of the Ni_3Al binder phase in the submicron grain sized TiC cermets fabricated with Ni_3Al alloy powders typically is not uniform with large Ni_3Al regions which are remnants of the original Ni_3Al particles. This can be overcome by using a mixture of fine Ni and NiAl powders that react to form the Ni_3Al phase during sintering.

This nonuniform binder phase distribution has been overcome by using a mixture of (2 Ni + NiAl) powders to form the Ni_3Al during the sintering step. NiAl powders are amenable to particle size reduction during the milling step, and low cost Ni powders with average sizes less than 10 microns are readily available. The resultant improved distribution of the Ni_3Al binder phase in the dense cermet is evident in Figure 5b.

The strengths of the submicron TiC cermets containing 40 vol. % Ni₃Al binder phase using either the alloy powder or the reaction of Ni with NiAl powders measured in four point flexure are very similar, 1033 ± 134 MPa and 1190 ± 149 MPa, respectively.

Status of Milestones

On Schedule

Communication/Visits/Travel

Additional samples of TiC -40 vol. % Ni₃Al cermets prepared and shipped to Cummins Engine for evaluation.

Problem Encountered

None

Publications

None

COST EFFECTIVE MACHINING OF CERAMIC ENGINE COMPONENTS

S. B. McSpadden, Jr.

Oak Ridge National Laboratory
Box 2008, Building 4515
Oak Ridge, Tennessee 37831-6069

Objective/Scope

To develop and demonstrate optimized, cost-effective grinding processes for the production of ceramic components for use in diesel engines.

Technical Highlights

Caterpillar CRADA – As a result of Jeff Bougher's promotion at Caterpillar, Jeff Thiele has now assumed responsibility for the machining work in the Caterpillar CRADA. Work is continuing on this activity. One element of the CRADA is intended to compare the machining effects from surface grinding with those from centerless grinding by correlating the mechanical properties of the two groups of ground specimens with the two machining processes. The tests involve both cylindrical and rectangular flexure specimens made from Ceradyne Si₃N₄ material. Original plans called for machining cylindrical samples using a Dedtru centerless grinding attachment on the Harig surface grinder. During the downsizing operation, in which the cylindrical samples were reduced in diameter from approximately 7 mm to 5.5mm, some of the parts started to chip at the ends of cylinders. After microstructural analysis, it was determined that there is a porous layer on the outer perimeter of the cylindrical parts. These parts were formed to near net shape, and this is the outer reaction zone due to the type of processing for this ceramic (gas pressured sintered). The porous layer needs to be completely removed to ensure that failure occurs from machining damage and not from intrinsic flaws within the material.

After the grinding operations are completed, all specimens will be fractured and the failure mechanism will be determined through fractography. The surface grinding specimens have been cut to size, chamfered, and the experimental surfaces are complete. The cylindrical specimens are still being downsized.

Cummins CRADA – Tom Morris, who was the ORNL principal investigator for the machining portion of the CRADA with Cummins, has elected to accept a voluntary reduction in force. Sam McSpadden will assume responsibility for the machining portion of the work. McSpadden will meet with Cummins personnel in May to review the current status of the CRADA. At that time we will also discuss Cummins' areas of interest for current and future joint research in order to make effective use of remaining CRADA funds.

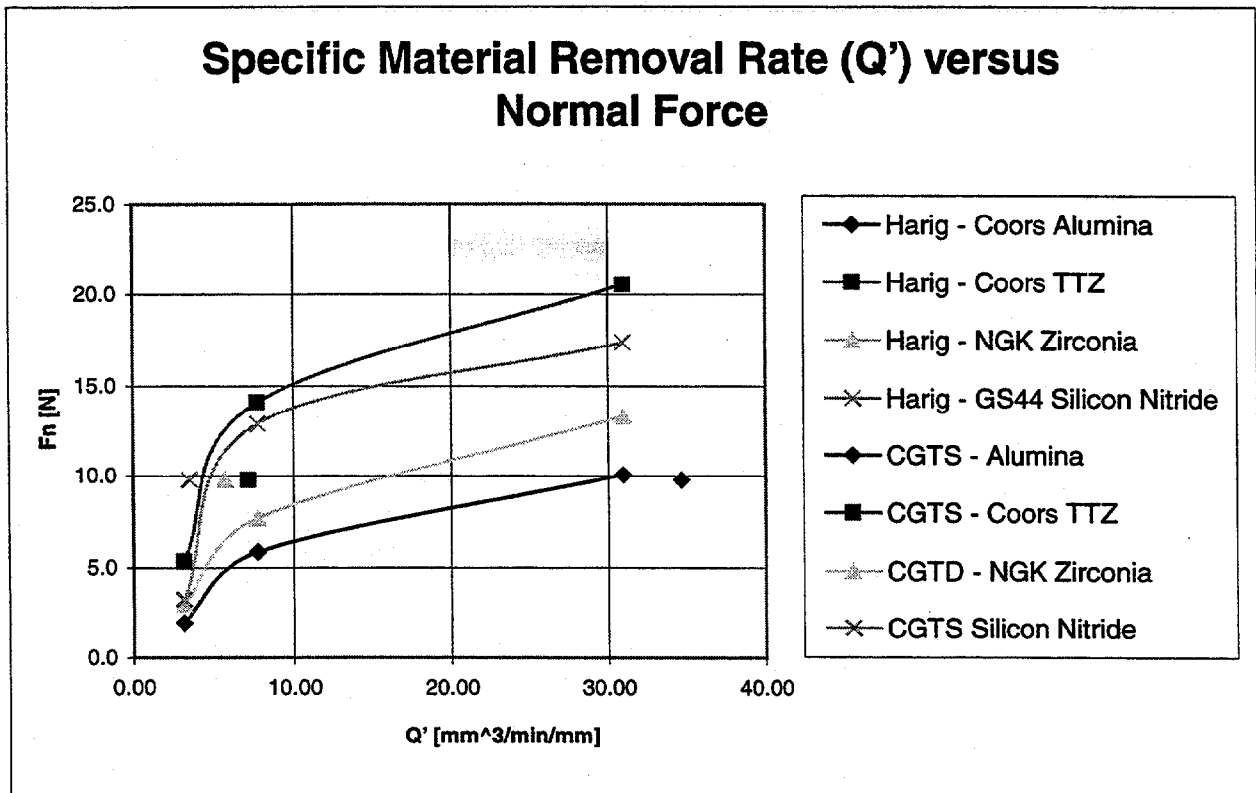
Recent activities in the Cummins CRADA involve the testing of a proprietary grinding wheel for machining zirconia fuel systems components, developing methods of measuring temperature in the grinding interface between the workpiece and the grinding wheel, and evaluating superabrasive grinding wheels that were produced by an innovative and proprietary manufacturing method.

Compact Grindability Test System (CGTS) – The CGTS has been used successfully over the past two or three years, and many small, incremental improvements have been made to the system. The grindability index is determined experimentally using the equation $G=(AL)/(FVT)$, where G is the grindability index, A is the cross-sectional area of the specimen, L is the change in length of the specimen during the test, F is the normal force, V is the velocity of the abrasive media, and T is the time required to perform the test. The grindability index measured by the CGTS is directly proportional to the material removal rate for a given

material. However, if the index is to have any practical significance, it must have a strong correlation with material removal rates achieved on production machine tools such as the Harig surface grinder.

Four different ceramic materials were tested on the CGTS and the same materials were then ground under similar operating conditions on an instrumented Harig surface grinder. The following graph summarizes the test results. A single data point (at a force of 9.8 N) is shown for each material tested on the CGTS. (This point represents an average for numerous replications of the test.) The CGTS is a constant-force device, while the Harig grinder is a constant-speed, variable-force device. It is not feasible to operate the Harig and the CGTS at the same force levels. Therefore the Harig was operated in such a way that the data would "bracket" the desired force reading of 9.8 N, rather than attempting to exactly duplicate the force value. The CGTS predicted that alumina would be the easiest material to grind in terms of specific material removal rate, followed by a Coors zirconia, an NGK zirconia, and an AlliedSignal silicon nitride. The specific material removal rates achieved for the four materials on the Harig grinder are shown as curves determined by three data points. (Again, each of the three points represents an average of several experimental runs.) By locating the CGTS value for each material and moving horizontally along the abscissa until the corresponding Harig curve is intersected, it can be seen that the removal rates predicted by the CGTS for each of the four materials agree reasonably well with removal rates achieved on the Harig grinder.

However, the test does not offer sufficient discrimination between silicon nitride and the two zirconia materials, and these materials are not ranked in the proper order with respect to the actual material removal rates achieved on the Harig grinder. It was discovered that the data obtained on the CGTS is much more repeatable than data obtained on the Harig grinder. This is due to the inability to accurately control the table speed of the Harig. We have recognized for some time that the Harig grinder has severe limitations as a research grinder. We plan to replace this equipment with a much stiffer, much more accurate, instrumented grinder in the near future if funds are available.



The results of this experimental work were prepared in poster form for presentation at the annual American Ceramic Society meeting in April.

Equipment

At the conclusion of a CRADA with Cincinnati Milacron, Inc., a large instrumented centerless grinder was left at the HTML on consignment. The grinder has been at the HTML for a number of years and we do not have sufficient work to justify keeping the equipment. The grinder and related accessories will be returned to Milacron by the end of April. If we are able to proceed with the planned lease of an Elb surface grinder at the beginning of next fiscal year, the grinder will be located in the lab where the centerless grinder is currently located.

The Taylor Hobson Talysurf Series 100 Surface Profile Analyzer was upgraded to add new capabilities and to replace an obsolete computer system that was not Y2K-compliant. The instrument is back in service and the new control and analysis software is a vast improvement over the old system. This instrument is our primary means of measuring surface texture (roughness, waviness, and lay) on machined ceramic components.

Communications/Visits/Travel

Sam McSpadden attended the South-Tec Machine Tool Exhibition in Charlotte, NC. Various state-of-the-art machine tools and dimensional inspection instruments were on display. Discussions were held with representatives of Elb America, manufacturer of the Elb surface grinder, regarding the possible lease of equipment by the HTML.

Publications

Jenkins, V.T., Blau, P.J., McSpadden, S.B., "Correlation of the Grindability Index for Four Ceramic Materials with Surface Grinding Material Removal Rates" (poster presentation scheduled for April American Ceramic Society meeting)

TESTING AND CHARACTERIZATION

NDE TECHNOLOGY FOR FUEL DELIVERY AND INSULATING MATERIALS

W. A. Ellingson, E. R. Koehl, H. P. Engel and H.-R. Lee

Energy Technology Division
Argonne National Laboratory
Argonne, Illinois 60439

Objective/Scope

The objective of the work in this task is to develop important enabling nondestructive evaluation/characterization (NDE/C) technology as part of the materials technology effort related to lower-emission, higher-efficiency diesel engines for heavy vehicles. Specifically the work in this project addresses development of advanced NDE/C technology which will provide data for; a)-materials under development for advanced fuel delivery systems (including injector nozzles), and b)-materials under development for insulating materials for reduced heat loss in the combustion zone. Fuel delivery systems for heavy-duty diesel engines are complex, very expensive and represent a significant portion of the cost of a heavy vehicle diesel engine. High pressures inside these fuel delivery systems contribute to poor fuel delivery and hence poor emissions. Materials development is part of Goal 3 of the heavy vehicle propulsion materials program. Insulating materials are also a significant materials development area because of the improvement in efficiency obtained if reduced heat losses can be obtained. NDE/C technology, which could provide information for cost reduction as part of production as well as provide information as part of engine component surveillance, would be a significant contribution to the goals.

Technical Highlights

Over this reporting period this effort has been refocused and the new statement of work submitted. All future efforts are focused on development of NDE/C technology for materials under development for advanced fuel delivery systems and NDE/C technology for materials under development as insulating materials.

NDE for Fuel Delivery Systems

Several discussions took place this period with various engine manufacturers regarding fuel injectors and materials systems under development to advance these technologies. Cooperative work with Cummins Engine Company is focused on aspects of the ceramic injector pin. These pins, see Figure 1, are machined with high precision and certain aspects of the materials would be desirable to determine either during machining or prior to the machining effort. As part of this work, the Argonne-developed elastic optical scattering method will be employed to determine

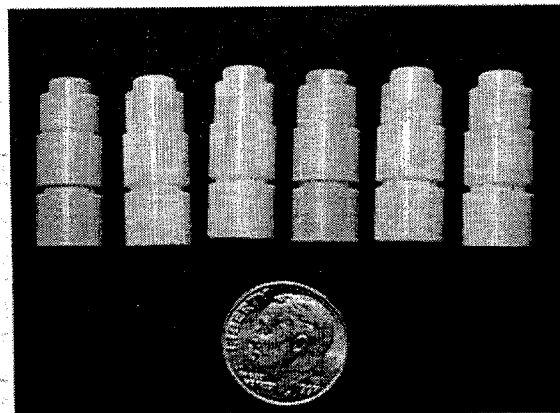


Fig. 1 Photograph of Cummins Engine Company ceramic injector pins under study by NDE/C technology

if such technology, or a variant, could be reliably used to advance the use of the ceramic materials in this application. In order to assess this technology, it is necessary to systematically assess the optical transmission characteristics of the various materials. The approach is to use well-defined step wedges of known thickness to establish the penetration and scatter characteristics as a function of wavelength. Cummins prepared step wedges of the various materials as shown in the photograph in Figure 2 below.

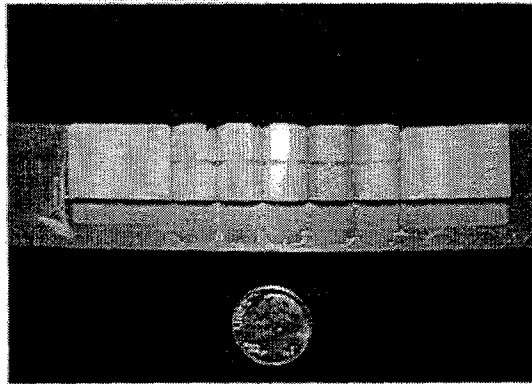


Fig. 2 Photograph of step wedges of various ceramic materials. Note the Wedges are shown still mounted to the steel bar used to hold them during grinding.

We will be reporting on the results from the step wedge experiments in the coming months.

NDE for Insulating Mterials

Discussions were held this reporting period with staff at Caterpillar Inc. about use of ceramics as insulating materials. As now planned, the NDE/C efforts will begin in FY 2001 to be consistent with the work plan at Caterpillar Inc.

TESTING AND EVALUATION OF ADVANCED CERAMICS AT HIGH TEMPERATURE

J. Sankar, A. D. Kelkar and S. Yarmolenko
Department of Mechanical Engineering, North Carolina A & T State University,
Greensboro, NC 27406.

Objective/Scope

The objective of this research is to test and evaluate the long-term mechanical reliability of a Si_3N_4 at temperatures up to 1300°C . The required research includes four (4) major tasks:

Task 1. Cyclic Fatigue Testing of PY6

Cyclic fatigue of GTE-PY6 silicon nitride shall be performed at lower temperatures to investigate $500^\circ - 1100^\circ\text{C}$ characteristics of the material at this temperature range. At these lower temperatures, there may be a true cyclic fatigue effect that enhances failure compared with the static load case.

Task 2. Stress - rupture Study of PY6

Stress-rupture testing of GTE PY6 silicon nitride shall be performed at a lower temperature range of $500^\circ - 1100^\circ\text{C}$. Since there is little information about the time dependent behavior of this material is available at this temperature regime, this task should provide some valuable data.

Task 3. Tensile Testing of GS 44

Pure Uniaxial tensile testing of GS 44 silicon nitride will be carried out at both room and elevated temperature up to 1200°C . The obtained data will be compared with other silicon nitride materials.

Task 4. Stress - Rupture Study of GS 44

Stress-rupture testing of GS 44 silicon nitride will be performed at various temperatures and stresses.

Technical Highlights

During this reporting period, we have performed mechanical testing and finite element analysis of sintered self-reinforced silicon nitride (GS44) under four-point bending.

The mechanical behavior of Si_3N_4 , particularly at high temperatures, is closely related to the microstructures and their stability under stress and in corrosive

environments. Failures of Si_3N_4 components, like those for high temperature operation, are a result of chemical encroachment (oxidation) as well as mechanical fracture (crack initiation and growth). To improve the material performance at high temperature and reduce machining damage, protective barrier coatings (PBCs) have been applied. Knowledge of the thermal mechanical response and failure mechanism of the coated system is essential in selection of an optimal coating system for high temperature applications.

Therefore, in this reporting period, both static and fatigue flexural behaviors of sintered silicon nitride were studied at room and elevated temperatures to determine the effect of temperature and cyclic loading on mechanical properties. This study was carried out to establish a base line data and will pave a way to explore an optimal coating system. An easier and cost effective testing method based on four-point bending was used during the experimental investigation. It was found from static flexural tests that both the failure strength and Young's modulus dropped as the temperature increased. Experimentation also showed that modulus remained constant during flexural fatigue tests at room temperature while the test at 1000°C resulted in a drop of 6-10% during the initial 1000 cycles. A base line finite element model for a sintered silicon nitride bending specimen was developed. The accuracy and validity of the finite element model was validated through comparison of model predictions with experimental data. To characterize the material degradation at high temperature subjected to both a monotonic and cyclic loading, the base line finite element model will be extended by integrating with a damage progressive model. In addition, a thermal-mechanical finite element model for a coated system will be developed in future studies.

MATERIAL

The material used for investigation is sintered silicon nitride, GS-44, provided by Allied Signal. The dimensions for the samples used in the bend test are 3 x 4 x 45 mm. Earlier studies on silicon nitride states it contains small amounts of Y_2O_3 , Al_2O_3 , and other minor constituents as densification aids.

EQUIPMENT AND EXPERIMENTAL PROCEDURES

Four (4) Point Flexural Tests

The American Society for Testing and Materials (ASTM C 1161-94) Standard Test Method for Flexural Strength of Advanced Ceramics at Ambient Temperature and (ASTM C 1211-92) Standard Test Method for Flexural Strength of Advanced Ceramics at Elevated Temperatures were followed as a guide for testing. The experiments were performed with 21 specimens using displacement control at a rate of 0.5 mm/min. All flexural tests were performed using ATS 1605 Series Testing Machine with Series 4231 High Temperature Bend Testing LVDT Extensometer and furnace (up to 1600°C).

Four (4) Point Flexural Fatigue Tests

Fatigue tests were performed under displacement control at a rate of 10mm/min. Cyclic loading frequency depends on loading amplitude (0.35 Hz for maximum load 700 N or 0.5 Hz for 500 N). Data acquisition system collected displacement data for every 5 N with a threshold level of 5 N (i.e. cyclic loading amplitude error of less than 1%). The developed software can analyze and process up to 20 Mbytes data files. The

software can extract, visualize and perform calculation for each cycle. Tests have been conducted at room temperature and at 1000°C.

FINITE ELEMENT ANALYSIS MODELING

A base line finite element model was developed for a generic 4-point bending specimen. While a closed form solution based on a classical beam theory is available to determine both the stress and deflection, it cannot be used for a nonlinear-coated system subjected to a thermal-mechanical loading. In addition, the ignorance of the shear deformation in the classical beam theory may render its prediction inaccurate for the coated system even under the room temperature. To establish a general computational framework for an arbitrary coated flexural test specimen, a base line finite element model was developed and a flexural specimen with a rectangular cross-section was discretized into 864 eight-node solid elements. A concentrated line load underneath each of two bearing cylinders was characterized by a set of discrete forces at 5 nodes on the top surface of the beam. At the location of bottom bearing cylinders, the displacement in the vertical direction is assumed null. From the condition of symmetry, all degrees of freedom at the center point of the beam are fixed to prevent the rigid body motion. The elastic modulus obtained from the experiment was used and the deflection predicted from the FEM was compared with test data.

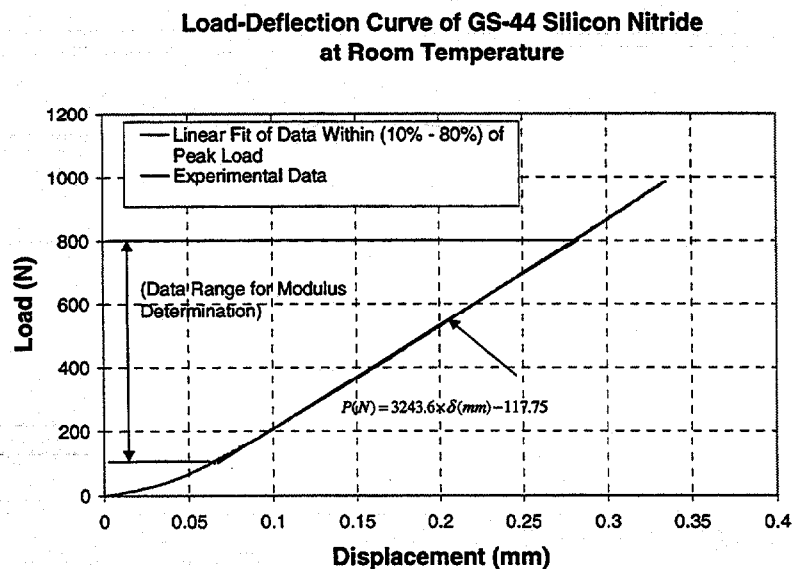


Figure 1. Typical load-deflection curve of GS-44 from four-point flexural test at room temperature

RESULTS AND DISCUSSION

Flexural Tests at Room and Elevated Temperatures

Flexural tests were performed at room and elevated temperatures based on ASTM standard. A load-deflection curve obtained for sample #1 is shown in Figure 1. A linear regression was applied for all test data within the range of 10% to 80% of peak load. For the present peak load of 1000 N (Figure 1), a linear fit was applied within the range of 100 N to 800 N. The resulting slope of the load deflection curve at the room temperature is 3243.6 N/mm. The modulus calculated from the slope of the load-deflection curve,

measured ultimate load, and the flexure strength determined from the failure load under various test temperatures are listed in Table I.

Table I. Results of Flexural Tests of GS-44 at Room and Elevated Temperatures.

#	Temperature (°C)	Ultimate Load (N)	Modulus (E) (Gpa)	Flexure Strength (Mpa)
1	25	984.8	330.2	813
2	25	992.4	315.3	827
3	25	1022.0	319.3	852
4	500	871.8	293.1	719
5	700	820.2	273.8	678
6	800	708.5	244.3	587
7	900	653.1	243.9	539
8	900	719.1	214.6	589
9	900	752.6	245.9	622
10	900	797.9	249.8	664
11	1000	564.4	239.2	470
12	1000	610.7	203.9	504
13	1000	618.5	160.6	507
14	1000	648.0	246.7	540
15	1100	492.5	230.2	406
16	1100	494.1	191.2	406
17	1100	609.6	241.2	509
18	1100	620.5	236.7	517
19	1200	398.4	246.1	332
20	1200	464.8	243.4	380
21	1200	492.3	246.9	405

To further demonstrate the effect of temperature on the failure strength and elastic modulus, both the failure load against temperature and the elastic modulus versus temperature are shown in Fig. 2 and Fig.3, respectively. As shown in Figs 2 and 3, both the failure strength and the modulus drop with the increase of the temperature and the failure strength degrades in a faster rate. A drastic drop of failure strength at the temperature higher than 800°C is mainly attributed to the increase of stress exponent of GS44 from 1 to 2.0 at temperature above 1100°C as indicated in our previous creep analysis report⁶. For instance, at the temperature of 1000°C, the flexure strength is about 60% of the corresponding room temperature value while the modulus is about 73% of the room temperature value. In addition, the modulus degradation curve shown in Fig. 3 seems to be linear with significant scattering at temperatures more than 900°C.

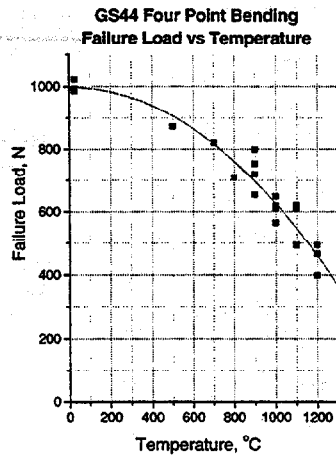


Fig. 2. Failure load vs temperature

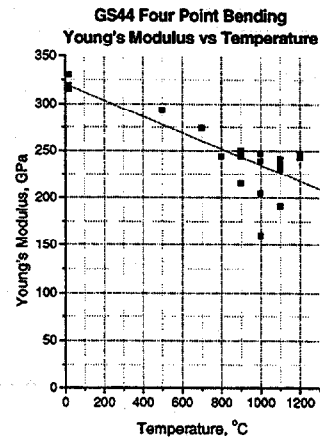


Fig. 3. Modulus vs temperature

Flexural Fatigue

Four fatigue tests were conducted at two levels of peak stress under two different temperatures. A linear ramp waveform was used to simulate the cyclic stress. Figure 4 and Figure 5 show load-displacement loop for first 3 cycles of fatigue test at room and high temperatures, respectively. Hysteresis loop under room temperature shown in Fig. 4 is wider than the tests conducted at high temperature (Fig. 5). The peak load used in fatigue tests at room and elevated temperature is 70% and 80% of the corresponding ultimate flexural load (UFL). As shown in Fig. 5, the modulus determined from the slope associated with the first cycle at elevated temperature is usually lower than that obtained from the slope corresponding to subsequent cycles. We believe that this is probably due to extensometer settling down during its initial cycle.

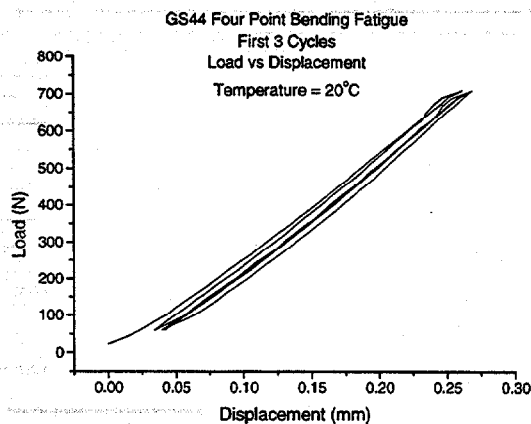


Figure 4. First 3 cycles of four point flexural fatigue test at room temperature (70% UFL)

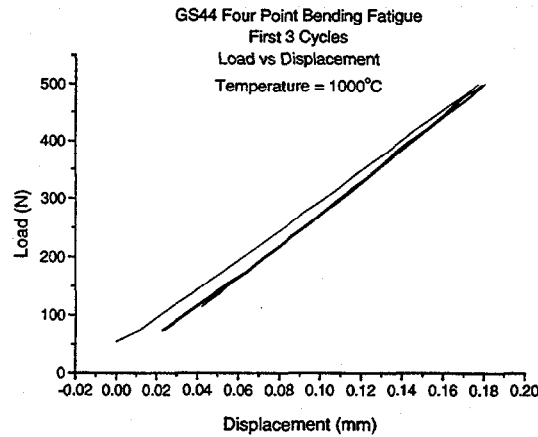


Figure 5. First 3 cycles of four point flexural fatigue test at a temperature of 1000°C (80% UFL)

Two fatigue tests were performed under both the room and high temperatures. The room temperature specimens were fatigued using both 70% and 80% of the ultimate load (~1000 N) and the 1000°C specimen at 80 % of the ultimate load (~625 N). The fatigue test results under both room and high temperatures are summarized in Table II. At lower peak load of 70% of UFL, the modulus dropped 1.3% after 16000 cycles at room temperature, while at a higher peak load of 80% of UFL, the modulus dropped 3.21 % after 3000 cycles at room temperature. Different from the room temperature fatigue results where the modulus remained almost constant, the fatigue tests at 1000°C resulted in a drop of 6-10% during the initial 1000 cycles. To further explore the change of modulus with the cumulated fatigue cycles, a plot of modulus against the number of cycles is given in Figs. 6 and 7 for the fatigue test at room and high temperatures respectively. Despite the oscillation in numerical values of modulus, the average value of modulus remained almost constant at room temperature fatigue (see Fig. 6) while dropped at high temperature fatigue (see Fig. 7)

Table II. Flexure fatigue test results for GS44 at room and 1000°C.

% ULT	Temp (°C)	Initial Modulus (GPa)	Final Modulus (GPa)	% Drop in Modulus	Total Cycles	Failure (yes/no)
70	20	302.3	298.4	1.29	16000	No
80	20	332.9	322.2	3.21	3000	No
80	1000	282.2	253.6	10.13	4000	No
80	1000	260.9	244.4	6.32	4000	No

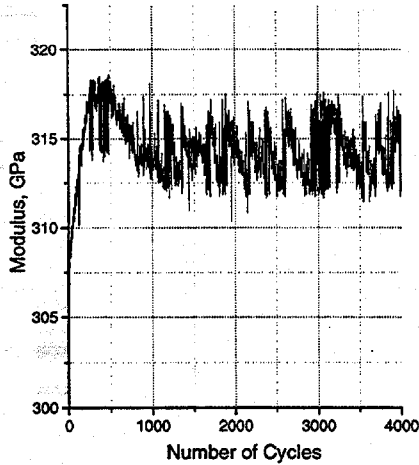


Fig. 6. GS44 fatigue four point bending test (70% UFL at room temperature): modulus vs number of cycles

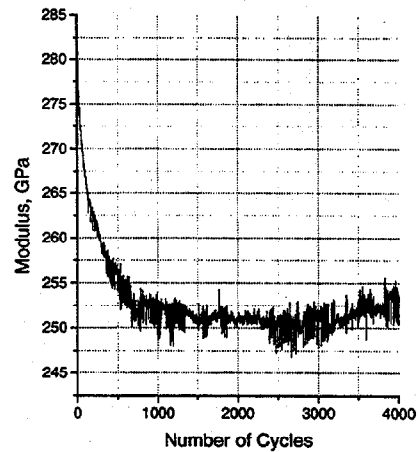


Figure 7. GS44 fatigue four point Bending test (80% UFL at 1000°C): modulus vs number of cycles

Comparison of Finite Element Model Prediction with Experimental Data

A three-dimensional finite element model with 1499 nodes and 864 brick elements was developed to predict the flexural stress and displacement of a bending specimen at room temperature. The developed finite element model will be integrated with a thermal mechanical constitutive model and a damage progressive model to explore both the stress response and damage accumulation under a monotonic and cyclic loading. The accuracy of the present base line model was demonstrated through its comparison with experimental results at room temperature.

The maximum deflection (δ_{max}) under the 4-point bending can be derived from the classical lamination theory given by

$$P = K\delta_{max} \quad (1)$$

where the slop (K) measured from a load-deflection curve is given by

$$K = \frac{768EI}{11L^3} \quad (2)$$

Substituting the slope (K) of $3243.6E+03 \text{ N/m}$ (see Fig. 1), the moment of inertia (I) of $9.0E-12 \text{ m}^4$, and the length (L) of $40E-03 \text{ m}$ in Eq. (2), the resulting modulus (E) of GS-44 at room temperature is 330.3 MPa . An isotropic linear elastic material model with the modulus of 330.3 MPa and the Poisson's ratio of 0.2 was employed in the finite element model (FEM). A comparison of load-deflection curves obtained from FEM and test data is given in Fig. 8. As shown in Fig. 8, an excellent agreement has been achieved with the based line finite element model. The axial stress distribution resulting from a unit load of $P=1 \text{ N}$ is shown in Fig. 9. The resulting maximum tensile stress at the bottom of the specimen is 0.841 MPa . To estimate the accuracy of the finite element based stress prediction, the failure load (984.8 N) associated with Test 1 in Table 1 is employed.

Because of the linear elastic model used, the maximum stress at the failure load of 984.8 N calculated from the FEM result is

$$\sigma_{\max} = 0.841(\text{MPa}/\text{N}) \times 984.8(\text{N}) = 828.22\text{MPa} \quad (3)$$

By comparing Eq. (3) with the flexural strength of 813 MPa listed in Table 1, the resulting error is found to be only 1.8%.

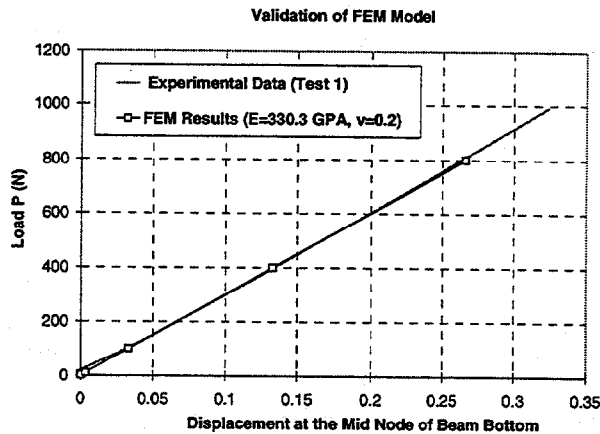


Figure 8. Comparison of FEM results with experimental data (load (n)-deflection (mm) curve)

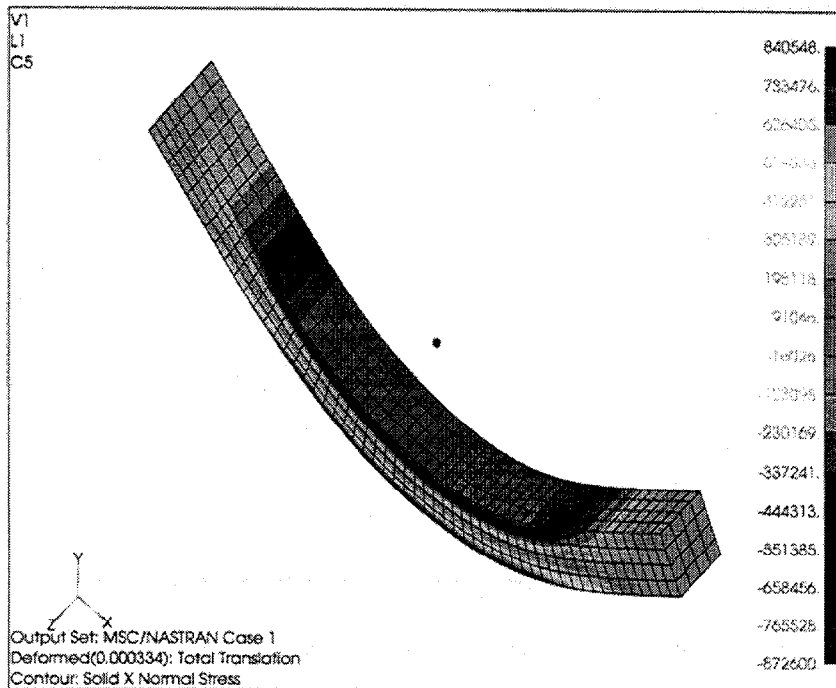


Figure 9. Axial stress distribution under a unit load (P=1N).

CONCLUSIONS

The following conclusions can be drawn from both experimental and numerical studies of sintered silicon nitride specimens under four-point bending:

- 1) The reduction of both the flexural strength and modulus has been observed under static flexural tests due to chemical encroachment at elevated temperature. The rate of drop of the flexural strength at high temperature is severe in comparison with that of the modulus.
- 2) The modulus has remained almost constant during flexural fatigue tests at room temperature while the test at 1000°C has resulted in a drop of 6-10% during the initial 1000 cycles. Thus, the high temperature oxidation plays a dominant role in fatigue damage accumulation.
- 3) The developed finite element model has shown its versatility and high accuracy in predicting both the displacement and stress responses of a four-point bending specimen at room temperature.
- 4) An easier and cost effective flexural testing coupled with a finite element based numerical simulation seems to be an excellent way to explore an optimal coating system in reducing the rate of material degradation and progressive failure of advanced materials for high temperature applications.

Status of Milestones

On schedule.

Communcations/Visitors/Travel

Publications

J. Lua, J. Sankar, S. Yarmolenko, W. Windley III, D. Pai and L. C. Russell, Testing and Finite Element Analysis of Sintered Silicon Nitride Specimens under Four-Point Bending, 24th Cocoa Beach Annual Conference, Jan. 23, 2000. Cocoa Beach, FL.

Q. Wei, J. Sankar, A. D. Kelkar and J. Narayan, Microstructure Changes Associated with Tensile Creep of an in situ Self-Reinforced Sintered Silicon Nitride, MRS 1998 Fall Meeting, Boston, Nov. 30-Dec. 4.1998.

Q. Wei, J. Sankar and J. Narayan, HIGH TEMPERATURE UNIAXIAL CREEP BEHAVIOR OF A SINTERED IN SITU REINFORCED SILICON NITRIDE CERAMICS, 23rd Cocoa Beach Annual Conference, American Ceramic Soc., Jan. 25-29, 1999.

Problems encountered:

None.

Life Prediction of Ceramic Diesel Engine Components

A. A. Wereszczak (ORNL), T. P. Kirkland (ORNL), H. - T. Lin (ORNL), R. A. Ott (ORNL), C. R. Brinkman (ORNL), S. K. Lee (Caterpillar), M. A. Andrews (Caterpillar), and J. Thiele (Caterpillar)

Objective/Scope

The valid prediction of mechanical reliability and service life is a prerequisite for the successful implementation of structural ceramics as internal combustion engine components. There are three primary goals of this research project which contribute toward that implementation: the generation of mechanical engineering data from ambient to high temperatures of candidate structural ceramics; the microstructural characterization of failure phenomena in these ceramics and components fabricated from them; and the application and verification of probabilistic life prediction methods using diesel engine components as test cases. For all three stages, results are provided to both the material suppliers and component end-users.

The systematic study of candidate structural ceramics (primarily silicon nitride) for internal combustion engine components is undertaken as a function of temperature ($< 900^{\circ}\text{C}$), environment, time, and machining conditions. Properties such as strength and fatigue will be characterized via flexure and rotary bend testing.

The second goal of the program is to characterize the evolution and role of damage mechanisms, and changes in microstructure linked to the ceramic's mechanical performance, at representative engine component service conditions. These will be examined using several analytical techniques including optical and scanning electron microscopy. Specifically, several microstructural aspects of failure will be characterized:

- (1) strength-limiting flaw-type identification;
- (2) edge, surface, and volume effects on strength and fatigue size-scaling
- (3) changes in failure mechanism as a function of temperature;
- (4) the nature of slow crack growth; and
- (5) what role residual stresses may have in these processes.

Lastly, numerical probabilistic models (*i.e.*, life prediction codes) will be used in conjunction with the generated strength and fatigue data to predict the failure probability and reliability of complex-shaped components subjected to mechanical loading, such as a silicon nitride diesel engine valve. The predicted results will then be compared to actual component performance measured experimentally or from field service data. As a consequence of these efforts, the data generated in this program will not only provide a critically needed base for component utilization in internal combustion engines, but will also facilitate the maturation of candidate ceramic materials and a design algorithm for ceramic components subjected to mechanical loading in general.

Technical Progress

The flexure testing matrix for the eight silicon nitride ceramics was almost completed during the present reporting period. Originally five grades comprised the matrix; however, NT154, SN235, and SN235P were added during the present reporting period. The updated test matrix is shown in Table 1. Only a few of the longitudinally machined sets for SN235 and SN235P remain to be tested. Both SN235 and SN235P exhibit excellent strength and outstanding fatigue

resistance as summarized in Tables 2-4. For example, the fatigue exponent for SN235 was 164 while that for SN235P was 140 (transversely machined specimens): the next most fatigue-resistant silicon nitride that was examined (KYON3000) half a fatigue exponent less than half these values. Of the eight silicon nitrides examined, the SN235 appears to have the best combination of: room temperature strength; 850°C strength; and 850°C fatigue-resistance. Completion of the test matrix will occur early in the next reporting period.

The two batches of GS44 were examined (Lots C98236 and C99091) in the present study and they yielded bend bars that had different strengths. Additionally, their dilatometry curves were different suggesting that the secondary phases in the two lots were different. More specimens of the C99091 lot were tested in the project, so this GS44 lot has become the focus of the project.

There is consistent evidence to suggest that if the test temperature is above the apparent softening temperature for an amorphous phase in silicon nitride, or if the crystalline phases in a silicon nitride occur below the test temperature, that the silicon nitride will show relatively poor fatigue-resistance. Dilatometry has been completed now in all the silicon nitrides (see Fig. 1) and a common feature to the more fatigue-resistant silicon nitrides (NT154, SN235, and SN235P) at 850°C is that their CTE curves show no significant deflections below 850°C. Furthermore, the strength of Lot C99091 GS44 was relatively unchanged at 500 and 700°C (*i.e.*, below the inflection in its CTE curve) from that measured at 20°C while its strength decreased at 850°C; the inflection point in the CTE curve for GS44 occurred between 700 and 850°C. This project's investigators have characterized this correlation between strength loss and CTE behavior, and soon will be writing a full-length article on the analysis.

Heat capacity, thermal diffusivity, and thermal conductivity measurements were completed with all eight silicon nitrides. Thermal conductivities of AS800, GS44, KYON3000, KYON3500, N7202, NT154, SN235, and SN235P are compared in Fig. 2 as a function of temperature. AS800 has the highest thermal conductivity throughout most of the examined temperature range; however, that for NT154 was the highest above 800°C. N7202 had the lowest thermal conductivity, while the thermal conductivities of KYON3000, SN235 and SN235P were indistinguishably the same.

Phase change as a function of depth in the silicon nitride specimens tested at 850°C was examined. The results showed that the phases as a function of depth in the specimens tested at 850°C did not change (at least 100 microns in from the surface).

GS44 and SN235 bend bar specimens were sent to Caterpillar for exposure tests. Oil ash was deposited on the bend bars and then they are being subjected to high temperatures for a set amount of time. Retained flexure strength will be measured after their exposure. Additionally, pieces from the other six silicon nitride materials are being exposed as well, and microstructural analysis will be performed on all eight silicon nitrides to compare changes in surface microstructure on account of the oil ash deposit.

Several discussions occurred among the investigators pertaining to two issues: the life prediction analysis of an engine component (and how the different silicon nitrides would perform and compare as that component), and the mechanical testing of metal/silicon nitride joints using either tensile or rotary bend fatigue testing. Regarding the latter, the strength and fatigue distributions of the examined silicon nitrides, as well as their generated thermoelastic data, will be combined with component stress analysis (FEA) to predict the survival probability of that component. The chosen component's geometry and boundary conditions will likely be kept generic in nature so that the results from this analysis can, at the same time, aid in the CRADA's proprietary goals while being able to be publicly shared. This application of the data generated in this study to date will further aid in the comparison of the different silicon nitrides and help assess which is perhaps more appropriate for use than the others at certain operating conditions.

Lastly, several proprietary grinding studies as part of this Caterpillar CRADA are underway.

Status of Milestones

All milestones are on schedule.

Communications / Visitors / Travel

A. Wereszczak and H. -T. Lin visited AlliedSignal Ceramic Components, Torrance, CA, on Nov. 4, 1999 to discuss testings of AS800 and GS44 silicon nitrides with Jim Wimmer and several of their other staffmembers.

A. Wereszczak visited Kennametal, Latrobe, PA, on Nov. 16, 1999 to discuss testings of KYON3000 and KYON3500 silicon nitrides with Russ Yeckley and several of their other staffmembers.

J. Thiele of Caterpillar visited ORNL on December 13-17, 1999 and performed various proprietary grinding efforts with R. Ott and the MIRUC in support of the CRADA.

A. Wereszczak attended the 24th Annual Cocoa Beach Conference and Exposition and gave a presentation entitled "High Temperature Inert Strength and Dynamic Fatigue of Candidate Silicon Nitrides for Diesel Exhaust Valves," Cocoa Beach, FL, January 29, 2000.

A. Wereszczak and H. -T. Lin met with Caterpillar's S. K. Lee and P. McCluskey and PNNL's C. Lewinsohn at Cocoa Beach, FL, January 29, 2000 to discuss the project's testing progress and future testing plans.

A. Wereszczak had several conversations with Caterpillar's S. K. Lee during the February-March timeframe about the testing program and results. Additionally, data was shared with AlliedSignal's J. Wimmer, Kennametal's R. Yeckley, Kyocera's D. Carruthers, CFI's G. Wötting, and Norton's V. Pujari.

A. A. Wereszczak had several conversations with M. J. Andrews about identified past strength and fatigue losses in NT551 silicon nitride and how dilatometry results generated with that material are consistent with those observations. The past NT551 strength and fatigue results, along with the NT551 dilatometry data, will be used to supplement the analysis described in the full-length article that the project's investigators are preparing.

Problems Encountered

None.

Publications

"High Temperature Inert Strength and Dynamic Fatigue of Candidate Silicon Nitrides for Diesel Exhaust Valves," A. A. Wereszczak, T. P. Kirkland, H. -T. Lin, and S. K. Lee, to appear in *Ceramic Engineering and Science Proceedings*, Vol. 21, 2000.

“Strength and its Dependence on Secondary Phase Softening in Silicon Nitrides,” A. A. Wereszczak, H. -T. Lin, and T. P. Kirkland, and S. K. Lee, to be presented at the 102nd Annual Meeting and Exhibition of the American Ceramic Society, St. Louis, MO, April 30-May 3, 2000.

“Comparison of Strength and Thermal Properties of Silicon Nitride Ceramics Up To 850C,” A. A. Wereszczak, T. P. Kirkland, H. -T. Lin, and S. K. Lee, to be presented at the ASM Materials Solutions 2000 Conference, St. Louis, MO, October 9-12, 2000.

“Strength and Dynamic Fatigue of Silicon Nitride at Intermediate Temperatures,” A. A. Wereszczak, H. -T. Lin, T. P. Kirkland, M. J. Andrews, and S. K. Lee, in preparation.

Table 1. Silicon nitride test matrix to compare inert strength, high temperature fatigue performance, and effect of machining orientation. ASTM C1161B specimens are being 4-pt flexure strength tested.

Test Condition	KYON KYON							
	AS800	GS44	3000	3500	N7202	NT154	SN235	SN235P
20°C 30 MPa/s Longitudinal	Completed	Completed	Completed		Completed	Completed	Completed	Completed
20°C 30 MPa/s Transverse	Completed	Completed	Completed		Completed		Completed	Completed
850°C 30 MPa/s Longitudinal	Completed	Completed	Completed		Completed	Completed	To be Tested	To be Tested
850°C 30 MPa/s Transverse	Completed	Completed	Completed	Completed	Completed		Completed	Completed
850°C 0.003 MPa/s Longitudinal	Completed	Completed	Completed	Completed	Completed	Completed	To be Tested	To be Tested
850°C 0.003 MPa/s Transverse	Completed	Completed	Completed	Completed	Completed		Completed	Completed
Material's Manufacturer	ASCC	ASCC	Kennametal	Kennametal	CFI	Norton	Kyocera	Kyocera

Table II. Summary of uncensored Weibull strength distributions for silicon nitride specimens longitudinally machined per ASTM C1161.

Material	# of Spmns. Tested	Stressing Rate (MPa/s)	Temp. (°C)	Uncens. Weibull Modulus	± 95% Uncens. Weibull Modulus	Uncens. Chrcctsic Strength (MPa)	± 95% Uncens. Chrcctsic Strength (MPa)
AS800	30	30	20	23.2	17.1, 30.3	707	695, 719
GS44	30	30	20	22.2	16.3, 29.0	959	941, 975
KYON 3000	27	30	20	10.4	7.7, 13.6	847	814, 881
N7202	30	30	20	22.0	16.2, 28.9	775	761, 788
NT154	30	30	20	9.0	6.7, 11.7	706	675, 736
NT551	32	30	20	12.7	9.2, 16.9	1040	1009, 1070
SN235	9	30	20	12.8	6.8, 21.2	999	937, 1061
SN235P	9	30	20	32.6	18.8, 49.6	792	773, 810
AS800	30	30	850	15.1	11.6, 18.8	623	607, 639
GS44	30	30	850	19.1	14.5, 24.2	776	759, 791
KYON 3000	27	30	850	11.9	8.7, 15.7	801	773, 828
N7202	30	30	850	15.6	11.8, 20.0	689	672, 706
NT154	30	30	850	9.3	6.9, 11.9	685	656, 714
NT551	27	30	850	6.3	4.6, 8.2	558	521, 595
AS800	23	0.003	850	6.2	4.4, 8.4	440	408, 472
GS44	21	0.003	850	20.5	13.8, 29.0	590	576, 603
KYON 3000	27	0.003	850	11.7	8.5, 15.4	640	616, 663
N7202	31	0.003	850	10.2	7.6, 13.3	538	518, 558
NT154	27	0.003	850	5.9	4.5, 7.4	618	576, 662

Table III. Summary of uncensored Weibull strength distributions for silicon nitride specimens transversely machined per ASTM C1161.

Material	# of Sprms. Tested	Stressing Rate (MPa/s)	Temp. (°C)	Uncens. Weibull Modulus	± 95% Uncens. Weibull Modulus	Uncens. Chrcstic Strength (MPa)	± 95% Uncens. Chrcstic Strength (MPa)
AS800	30	30	20	19.4	14.4, 25.1	669	656, 683
GS44	30	30	20	17.4	13.1, 22.0	830	812, 849
KYON 3000	27	30	20	14.4	10.4, 19.0	702	682, 722
KYON 3500	21	30	20	14.2	9.8, 19.7	654	632, 675
N7202	30	30	20	18.7	14.3, 23.6	682	667, 696
NT551	30	30	20	9.4	7.0, 12.3	806	772, 839
SN235	15	30	20	23.8	15.4, 33.9	901	879, 923
SN235P	15	30	20	38.1	24.0, 55.8	666	656, 676
AS800	30	30	850	19.1	14.4, 24.4	608	595, 620
GS44	30	30	850	20.2	14.6, 26.8	747	733, 761
KYON 3000	27	30	850	13.2	9.7, 17.2	643	623, 663
KYON 3500	21	30	850	15.0	10.4, 20.4	674	653, 695
N7202	30	30	850	23.7	17.7, 30.5	687	676, 699
NT551	29	30	850	9.8	7.4, 12.5	582	558, 606
SN235	15	30	850	26.7	18.0, 36.7	777	760, 793
SN235P	15	30	850	19.3	12.5, 27.6	631	612, 649
AS800	24	0.003	850	7.8	5.5, 10.6	429	405, 453
GS44	22	0.003	850	22.6	15.7, 30.8	572	560, 583
KYON 3000	27	0.003	850	8.9	6.7, 11.4	569	543, 595
KYON 3500	21	0.003	850	12.7	8.9, 17.2	442	426, 459
N7202	22	0.003	850	9.2	6.6, 12.2	516	490, 542
NT551	30	0.003	850	4.0	3.0, 5.1	374	338, 411
SN235	14	0.003	850	18.5	11.8, 26.8	744	720, 767
SN235P	15	0.003	850	18.2	11.5, 26.8	594	575, 612

Table IV. Summary of uncensored dynamic fatigue exponents at 850°C.

Material	Machining Orientation	Fatigue Exponent
AS800	Longitudinal	22
GS44	Longitudinal	32
KYON 3000	Longitudinal	40
N7202	Longitudinal	33
NT154	Longitudinal	75
AS800	Transverse	22
GS44	Transverse	34
KYON 3000	Transverse	68
KYON 3500	Transverse	20
N7202	Transverse	28
NT551	Transverse	19
SN235	Transverse	164
SN235P	Transverse	140

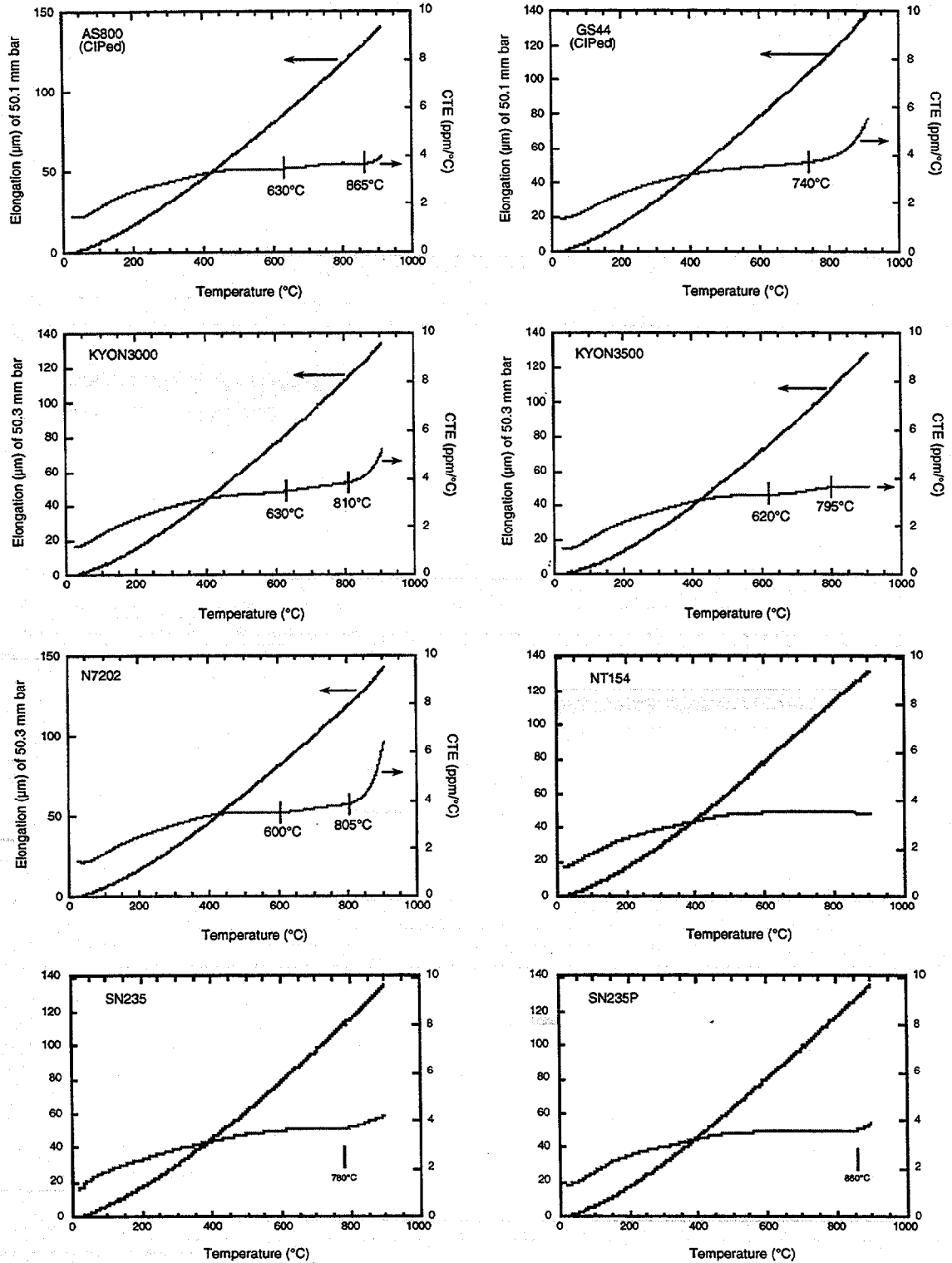


Figure 1. Dilatometry results showed that the coefficient of thermal expansion for many of the gas-pressure sintered silicon nitrides underwent points of inflection.

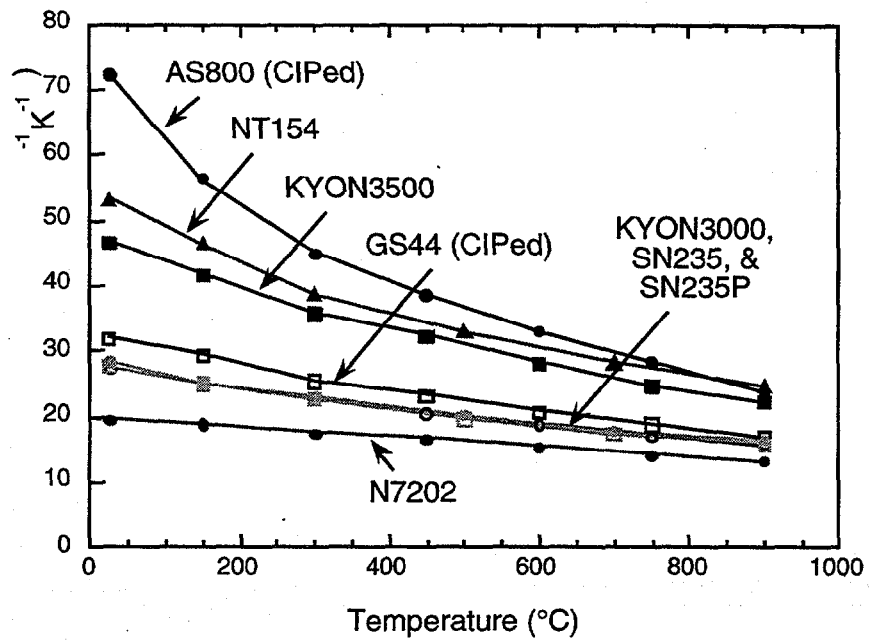


Figure 2. Thermal conductivity comparison of the examined silicon nitrides.

Field Emission Analytical Electron Microscopy for Characterization of Catalyst Microstructures

L. F. Allard, D. A. Blom and T. A. Nolan

OBJECTIVE/SCOPE

The objective of the research is to use analytical and high resolution transmission electron microscopy (TEM) to characterize the microstructures of emission control catalysts and emission particulates. Emphasis is placed on relating microstructural changes to performance of diesel NO_x reduction catalysts, and to determining the sources of contaminants on emission particulates. The research is focused on understanding these changes through TEM studies of experimental catalysts materials reacted in an ex-situ catalyst reactor system especially constructed to allow appropriate control of the reaction conditions and the transfer of the sample between reactor and microscope.

TECHNICAL HIGHLIGHTS

The High Temperature Materials Laboratory has begun studies of diesel emission exhaust catalysts and automotive particulate materials using a new dedicated scanning transmission electron microscope from Hitachi Co. The HD-2000 is on consignment through March of 2001, and will be employed during that time to give advanced analytical capabilities for our program, and will in particular allow us to characterize the distribution and chemistry of fine particles such as catalytic species on oxide support materials at a level unsurpassed by any currently available commercial electron microscope. This instrument has been utilized to give some preliminary information on emission particulates, in support of work over the past several months which has been conducted using the Hitachi HF-2000 field emission TEM for microstructural characterizations.

In studies of motor vehicle exhaust particulate matter (PM), the combination of imaging and analytical information available from TEM examination has provided valuable additional insight into the sources and potential health effects of these particulates. An advantage of TEM observations is the ability to link images of morphology and microstructure to the chemical composition of a very small volume of material. The TEM we are currently using has an analytical spot size of 1 nm, which means we can get composition information at that resolution. The PM we have measured to date has consisted primarily of carbon and oxygen, confirmed by energy dispersive x-ray spectra from the HF-2000. The particulate morphology from a 1993 Mercury Sable showed chains of carbon spheres 20-60nm in diameter, which had a turbostratic structure. A black smoking 1976 Ford F-150, however, produces PM comprising chains of carbonaceous particles having a graphitic structure, with very fine electron dense clusters on the carbon particles. The X-ray spectra acquired from the Ford PM showed strong peaks associated with

the dense clusters corresponding to the elements lead and zinc. The presence of zinc, we believe, is indicative of oil burning, since zinc-containing compounds are added to engine lubrication oil. There is no evidence of separate lead or zinc particles in the PM. We believe that this indicates the presence of lead in the lubrication oil, most likely from the crankshaft bearings. The Mercury Sable was tested at 30°F, while the Ford F-150 was tested at 70°F. At the higher temperature, the oil in the Ford burned much more completely than at the low temperature of the Mercury. We were able to conclude that the PM from the Mercury Sable was due to incomplete oil combustion, from the combination of the presence of Zn and lack of crystallinity in the PM. In contrast the graphitic nature of the PM from the Ford F-150 suggested that oil burned completely in combination with the gasoline. The PM from the Ford had the elements from oil combustion integrated into the chains of material, while the Mercury produced PM which could be attributed just to oil combustion. While both vehicles burned lubrication oil, the resulting PM was different both morphologically and chemically. The health effects of the different PM will most likely vary significantly.

The HD-2000 dedicated STEM was also used to examine the particulate material, and showed beautiful results from high-angle annular dark-field imaging in comparison to corresponding bright-field imaging. The heavy metal clusters on the Ford exhaust particulates were shown in bright contrast, so that the particle sizes and morphologies could be more unambiguously determined. Preliminary x-ray results indicated the great advantage this instrument provides over any other analytical electron microscope for energy dispersive spectroscopy, because of the 20 times larger x-ray acceptance angle which allows much greater data throughput than e.g. our HF-2000 instrument.

We believe we have shown that the characterization of motor vehicle exhaust PM in a TEM is both practical and informative. Beyond characterization of the PM, it is possible to observe biological material in a TEM and learn about the ways in which PM and tissue interact. The use of the new HD-2000 instrument for improved microstructural and microchemical analyses that can be obtained with its advanced analytical capabilities will be reported in future bimonthlies.

MATERIALS AND TESTING STANDARDS

IEA Annex II Management (October 1, 1999-March 31, 2000)
M. K. Ferber (Oak Ridge National Laboratory)

Objective/Scope

The purpose of this task is to organize, assist, and facilitate international research cooperation on the characterization of advanced structural ceramic materials. A major objective of this research is the evolution of measurement standards. This task, which is managed in the United States by ORNL, now includes a formal IEA Annex agreement identified as Annex II between the United States, Germany, Sweden, Japan, and Belgium. The original annex included four subtasks: (1) information exchange, (2) ceramic powder characterization, (3) ceramic chemical and physical characterization, and (4) ceramic mechanical property measurements. In the United States, a total of 13 industrial and government laboratories have participated and contributed their resources to this research. The research in Subtasks 2, 3, and 4 is now complete. In 1990, research in two new subtasks was initiated, including Subtask 5, Tensile and Flexural Properties of Ceramics, and Subtask 6, Advanced Ceramic Powder Characterization. The research in Subtasks 5 and 6 was completed in 1993 and the reports were distributed. Two new tasks (Subtask 7 on Ceramic Machining and Subtask 8 on Ceramic Powder Characterization) were proposed in late FY 1993 and the research is completed (1996). Subtask 7 in the United States included eight companies and three federal laboratories. The report on the results from research performed in the United States on Subtask 7 is complete (the final report has been compiled of all the international research and distributed). Subtask 8 included six companies. The final report for Subtask 8 is complete. In 1996, research in two new subtasks was initiated, including Subtask 9 - Thermal Shock and Subtask 10 - Ceramic Powder Characterization.

Recent Developments

Summary of the Workshop of the IEA Implementing Agreement on a Programme of Research and Development on High Temperature Materials for Automotive Engines, held on 11 October 1999, at IEA Headquarters, Paris, France, follows:

The main objective of this workshop was to discuss the future of our implementing agreement. Dr. Ferber opened the meeting by welcoming all of the participants. This was followed by a series of presentations from several IEA staff members.

Hans Jörgen Koch, who heads IEA's Department on Energy Efficiency, Technology, and R&D at IEA Headquarters, provided an overview on the implementing agreements and the role of the IEA Secretariat. Each implementing agreement is independent in that the executive committee decides on the nature of the activities. The IEA Secretariat provides a platform for conducting this work. It may become involved in organizing joint events and assisting with initiating new activities. Most implementing agreements are composed of multiple annexes. An operating agent, appointed by the executive committee, is assigned to each annex to provide technical assistance and monitoring. This operating agent does not necessarily have to be from a participating country.

Ian Walker, who is responsible for the Energy Technology Data Exchange at IEA headquarters, gave the next presentation, which focused on information management activities. Mr. Walker demonstrated the website dedicated to implementing agreements. He also provided a brief summary on a recent review of our implementing agreement (IA). Based upon this review, the following suggestions for our IA on High Temperature Materials

were made: (1) increase the level of collaboration, (2) increase the materials scope, and (3) prepare a detailed strategy document, which specifies tangible objectives. Mr. Walker also discussed dissemination of information resulting from the various implementing agreements. He proposed that eventually reports could be made available for a nominal fee to parties outside the implementing agreement.

Michael Landwehr, our IEA representative on the Energy End-Use Technologies Committee, provided the third presentation. He first gave an overview on the role of the Energy End Use Working Party (EUWP) in the review and supervision of implementing agreements. For our specific IA, he recommended that we address new topics, increase the number of participants, and reconsider the makeup of our implementing agreement. With the respect to the last topic, Mr. Landwehr indicated that we could add new material activities through new annexes. To facilitate this process, he provided a document summarizing general information for implementing agreements.

The next series of presentations were provided by the various member countries. Japan was represented by Mineo Mizuno from Japan Fine Ceramics Center. Dr. Mizuno stated that Japan wanted to continue under the current annex with the addition of two new subtasks. Subtask 11 would focus on the evaluation of thermal and mechanical fatigue of silicon nitride ceramics. Mechanical fatigue tests would be conducted using four-point bending of flexure specimens while the thermal fatigue tests would utilize cyclic up shock and cooling of disk specimens by laser or gas torch.

Because Dr. Mizuno was not familiar with the proposed subtask on powders, Dr. Said Jahanmir of the National Institute of Standards and Technology (NIST) provided an overview. He stated that Subtask 12 would focus on characterization of powders, granules, and green bodies. In the latter case, issues related to green machining and measurement of binder distribution would be addressed as well.

Sweden was represented by Dr. Robert Pompe of the Swedish Ceramic Institute. He also proposed the addition of two new subtasks to the existing annex. Subtask 11 would focus on the thermal and mechanical characterization of ceramic coatings including thermal barrier and environmental barrier coatings. Thermal fatigue, thermal shock, slow crack growth, and lifetime prediction of silicon nitride turbine components would also be included in Subtask 11. Dr. Pompe indicated that companies would be willing to supply samples at least for the work conducted within Sweden. The proposal was similar to that proposed by Japan.

The proposal for future work from Germany, which was presented by Dr. Rolf Wäsche of BAM, was very similar to that of Japan. In the case of Subtask 11, Dr. Wäsche indicated that three German companies (Siemens, BAM, and FH I-IWS) would participate.

Dr. Jean-Pierre Erauw of the Belgium Ceramic Research Centre presented the Belgian perspective on future work. He stated that at present the powder work was of a more generic interest to the ceramic companies in Belgium and that in general there was not sufficient interest in structural ceramics. He also indicated that in order to be relevant to Belgian interests, it was important to emphasize the standardization activities in the proposed new subtasks. This led to some discussion concerning how research conducted in our implementing agreement should be coordinated with other external standardization activities such as VAMAS. Mr. Landwehr suggested that we should pursue a memorandum of understanding with the parties representing the related VAMAS activities. From the

standpoint of non-powder related work, Dr. Erauw stated that Belgium would be interested in addressing issues of wear and non-destructive evaluation.

Dr. Ferber gave the last presentation in the workshop. The primary goal of this presentation was to summarize the interests of the Department of Energy (DOE) and to suggest the future direction of new activities with respect to the implementing agreement. Dr. Ferber stated that the Office of Heavy Vehicle Technologies (OHVT) in DOE's Office of Transportation Technologies supported continued collaboration within the IEA. However, in order to be better aligned with the mission of the OHVT, any new effort should be directed towards diesel engine technology issues. Dr. Ferber suggested the addition of a new annex entitled, "Advanced Characterization Techniques for Diesel Engine Materials." Possible research topics would include characterization of nano-sized powders, damage assessment techniques, fatigue, reliability, and component assessment. A workshop sponsored by DOE, ORNL, and NIST would be used to define the specific technical details of the new annex.

The results of this Workshop were discussed at the IEA Executive Committee Meeting held on October 12, Paris, France. At that meeting, Michael Landwehr made several recommendations concerning how we could restructure our IA to achieve the goals outlined in the Workshop. For our specific IA, he recommended that we address new topics under the current annex, increase the number of participants (countries), and reconsider the makeup of our implementing agreement. With the respect to the last topic, Mr. Landwehr indicated that we could add new material activities through new annexes. In order to select the most appropriate materials activities, he suggested that the EC should review national government R&D activities, solicit proposals on joint work from potential industrial and government participants, and meet with government technology offices. He also suggested that during this transition period, the EC meet more frequently. Mr. Landwehr completed his presentation by providing several concrete steps that should be taken. These included (1) development of strategy paper, (2) specification of milestones for defining Annex 3, and (3) development of a memorandum of understanding with VAMAS. He also requested that the EC keep the EUWP informed on a regular basis.

Summary of the Executive Committee of the IEA Implementing Agreement on a Programme of Research and Development on High Temperature Materials for Automotive Engines, held on 12 October 1999, at IEA Headquarters, Paris, France, follows:

Dr. Ferber of Oak Ridge National Laboratory, represented the Department of Energy (DOE), the Operating Agent for Annex 2, by chairing the meeting. He welcomed all and thanked the IEA Headquarters attendees for hosting the meeting. There were 12 people in attendance.

The first order of business was to request approval of Dr. Ferber as the Alternate Committee Member for the United States. There can be only one Alternate Committee Member per country. The members of the Executive Committee (EC) unanimously approved this motion.

The next business was to conduct the information exchange, which is required under Subtask 1 of Annex 2. Each country distributed reports as part of the information exchange.

The EC representative from Sweden confirmed that the change in contracting parties had been implemented.

The EC representative from Germany confirmed that the change in contracting parties had been implemented.

The next order of business was to discuss the status of the current subtasks. Dr. Ferber provided a summary for the Subtask 9 effort on thermal shock. Prior to his presentation, he distributed the Subtask 9 report from the United States. The reports from Germany and Japan had been distributed earlier this year. Dr. Ferber's presentation provided a summary of the thermal shock techniques used in Germany, Japan, and the United States. The subsequent discussion focussed on trying to understand the differences in the thermal shock results generated by the three countries. A comparison table was provided. He stated that the final combined report for Subtask 9 would be completed by the end of the year.

Dr. Jahanmir of the National Institute of Standards and Technology (NIST) then reviewed the status of Subtask 10. He stated that the final report would be completed by early February 2000. He next discussed the activities for Subtask 12. The following topics were proposed:

- tighten several existing powder characterization procedures,
- measurement of density gradients,
- evaluate the effect of green machining on strength of green ceramics.

Following the discussion of the current subtasks, the most updated version of Annex 2 was distributed to the EC members. Michael Landwehr, our IEA representative on the Energy End-Use Technologies Committee (EUWP), confirmed that the document was identical to the one on file at IEA Headquarters.

Next Michael Landwehr discussed the results of our workshop held the preceding day. For our specific IA, he recommended that we address new topics under the current annex, increase the number of participants (countries), and reconsider the makeup of our implementing agreement. With the respect to the last topic, Mr. Landwehr indicated that we could add new material activities through new annexes. In order to select the most appropriate materials activities, he suggested that the EC should review national government R&D activities, solicit proposals on joint work from potential industrial and government participants, and meet with government technology officers. He also suggested that during this transition period, the EC meet more frequently. Mr. Landwehr completed his presentation by providing several concrete steps that should be taken. These included (1) development of strategy paper, (2) specification of milestones for defining Annex 3, and (3) development of a memorandum of understanding with VAMAS. He also requested that the EC keep the EUWP informed on a regular basis.

Dr. Ferber discussed the interests of the Department of Energy (DOE) with respect to the future direction of new activities in the implementing agreement. Dr. Ferber stated that the Office of Heavy Vehicle Technology (OHVT) in DOE's Office of Transportation Technology supported continued collaboration within the IEA. However, in order to be better aligned with the mission of the OHVT, any new effort should be directed towards diesel engine technology issues. Dr. Ferber suggested the addition of a new annex entitled, "Advanced Characterization Techniques for Diesel Engine Materials." Possible research topics would include characterization of nano-sized powders, damage assessment techniques, fatigue, reliability, and component assessment. A workshop sponsored by DOE, ORNL, and NIST would be used to define the specific technical details of the new annex.

The next order of business was to solicit suggestions for new work (under Annex 3) from each country. The representative from Sweden indicated because of increased use of biomass, corrosion was now becoming a key concern. Although there is currently an IA on

biomass, it does not deal with material issues. The Belgian representative stated that he would discuss the subject of new work with the ministry. He also said that the powder work could be placed under the new annex. The representative from Germany indicated that he too must contact his ministry for input. The Japanese representative said that our IA could focus on high temperature materials for new energy systems.

Dr. Ferber asked the group whether there was an interest in materials for diesel engines. Representatives from Japan and Belgium stated that there was probably not sufficient interest in this topic. In the case of Japan, pollution from diesel engines was considered too much of a problem. The representatives from Germany and Sweden indicated that they were not sufficiently aware of the needs of the diesel engine community in their respective countries. They stated that they would investigate this further.

The EC then voted to extend the end date of the current annex to February 29, 2000. They also voted to approve the inclusion of Subtasks 11 and 12 in Annex 2. Following discussion of future activities, the extension was to accommodate the two new Subtasks 11 and 12 under Annex 2.

Next the EC discussed the next meeting. Sweden agreed to host the meeting in Malmö, Sweden on June 23, 2000, which is immediately after the 7th International Symposium on Ceramic Materials and Components for Engines to be held in Goslar, Germany on June 19-21, 2000

Subtask 9, Technical Efforts

Kristin Breder, U.S. Coordinator of Subtask 9, has accepted a position at Norton Company, Worcester, Massachusetts, beginning January 2000.

The final report entitled Subtask 9, Thermal Shock Testing of Advanced Ceramics – Final Report-United States was mailed to participants on December 30, 1999. The final report (Subtask 9) is being compiled from the participating countries.

Subtask 10, Characterizing Ceramic Powders

Major responsibility for this subtask in the United States is at NIST, and a detailed report of progress in these subtasks is provided in the section of this report submitted by NIST. The final report (Subtask 10) has been submitted to ORNL for publication.

Status of Milestones - Milestone.411531 [Publish Thermal Shock (Subtask 9) Final Report] due date March 31, 2000, has been changed to June 30, 2000. Milestone 411532 [Publish Powder Characterization (Subtask 10) Final Report] due date March 31, 2000, has been changed to June 30, 2000. Milestone 411533 (Provide reports to ASTM) due date May 31, 2000, has been changed to July 31, 2000. These were changed since more time is needed for final compilation of data from the participating countries (Subtask 9) and the reports will be published on CDs.

Communications/Visits/Travel - Matt Ferber attended the IEA Workshop and IEA Executive Committee Meetings in Paris, France, on 11-12 October 1999.

Publications and Presentations – Ferber, Matt and Kristin Breder, "Subtask 9 – Thermal Shock Testing of Advanced Ceramics – Final Report-United States, October 1999.

Standards for High Temperature Transportation Materials

Said Jahanmir, James F. Kelly and Lin-Sien Lum
National Institute of Standards and Technology
Gaithersburg, MD 20899-8520

Objective/Scope

The objective of the IEA Subtask 10 was to establish the repeatability and reproducibility of test methods used for the characterization of ceramic powders through an international round robin study. Thirty-four laboratories from Belgium, Germany, Japan, Sweden and the U.S. representing industrial, academic and government research organizations participated in this project. The round robin tests were completed in FY 99. Data analysis will be completed in FY 2000 and the final report for this Subtask will be issued. Due to continued interest by all participating countries in this activity, it is planned to extend this project to further evaluate some of the test methods that require refinement. Jointly with the participating countries, plans will be developed for continuation of this project as Subtask 12. Due to the interest in the Heavy Vehicle Propulsion System Materials Program on the development of international test methods for characterization and testing of advance materials for diesel engines, the powder characterization project will be transitioned to VAMAS -- Versailles Project on Advanced Materials and Standards -- during FY 2000. Plans will be established to initiate a new IEA activity focused on test methods and standards for the assessment of reliability of advanced materials used for diesel powered heavy vehicles.

Technical Highlights

This report summarizes the results of an international round robin study on advanced ceramic powders. Thirty-four laboratories from Belgium, Germany, Japan, Sweden and the U.S representing industrial, academic and government research organizations participated in this program. The activities were conducted under the auspices of the International Energy Agency (IEA). The objectives of the IEA Subtask 10 were to evaluate test methods for the characterization of selected properties of ceramic powders through an international round robin study and to determine the repeatability and reproducibility of the test methods. The results will be used to develop recommendations for drafting of national and international standard test methods.

The properties that were measured during this project consisted of: 1) Characterization of powders suspended in water (particle dispersion); 2) Characterization of spray dried powders (flow rate, particle size distribution, and moisture and binder content); and 3) Green body characterization (bulk density and strength). Three powders were studied: silicon nitride, silicon carbide, and aluminum oxide.

1. Dispersion of Powders for Slurry Preparation

The influence of ultrasonication on the state of dispersion of ceramic powders during particle size measurement was assessed. The method involves following the changes in

the particle size distribution as a function of the ultrasonication time used to disperse the powder in dilute suspensions. If deagglomeration occurs by ultrasonication, then the particle size distribution should shift toward the finer size as the ultrasonication time is increased.

The round robin results indicated that the measured diameter of the particles decreased as the ultrasonication time was increased. The longer ultrasonication times (at 128 s) helped to eliminate the potential errors associated with this dispersion procedure.

Many of the labs showed that the suspensions they prepared had agglomerated during the analysis. The agglomerated suspension might indicate that the suspensions were not well dispersed. A well-dispersed suspension is critical in the analysis for particle size.

A critical assessment of the parameters of the dispersion procedure is necessary before this method can be adapted for standards.

2. Characterization of Spray Dried Powder

a. Flow rate

A modified Hall Flow Rate method was used to determine the flow rate of the spray dried granules. The flow rate of a powder helps to determine the rate of filling of a die cavity in the pressing of spray dried powders.

This specific method showed excellent repeatability and reproducibility values for the silicon nitride powder. The data for the silicon nitride powder also indicated that the different types of flowmeter funnels do not affect the measurement methods. However, the silicon carbide powder showed inconsistent results and the powder had flowability problems. This test procedure requires additional work for the silicon carbide powder to determine a more repeatable sample preparation procedure.

b. Size Distribution by Sieving

The size distributions of the spray dried powders were determined by a dry sieving technique. The size distribution affects the flow characteristics, the packing density and the compaction ratio.

An unconventional method was used in the data analysis of the granular size distribution. The method used could be the source of the scatter observed between the labs. Good repeatability was noticed within the labs.

This measurement method needs no additional work. However, a better data analysis method is needed to determine the statistical variations and precision values.

c. Moisture Content

The method of measurement of mass loss after drying was used to determine the moisture content of the spray dried powder.

The data showed excellent precision values for the silicon nitride powder. However, variations in the data were observed for the silicon carbide and many of the labs had difficulties in duplicating their data. The inconsistent method of the moisture removal of silicon carbide powder may have been the source of the variations.

The sample preparation procedure for the silicon carbide powder should be reexamined and improved; for example, a higher oven temperature and a longer heating time may eliminate the measurement problems.

d. Binder Content

The binder content of the spray dried powders was determined through the method of mass loss after binder burn out.

The round robin data showed excellent repeatability and reproducibility values for the silicon nitride powder. However, the data for the silicon carbide powder produced data scatter. This specific predefined procedure is not robust for the silicon carbide powder used in the tests. The scattering could be due to the inconsistent and incomplete binder removal.

Additional work may be required to improve the binder removal procedure for the silicon carbide powder with close attention paid to the sample preparation for the powder. The procedure could be modified to add longer length of heating times and higher furnace temperature.

Subsequent to the completion of the final report for Subtask 12, plans were developed for IEA Subtask 12 and a draft proposal has been prepared for transition of the powder characterization project to VAMAS.

Status of Milestones

On Schedule

Communication/Visits/Travel

S. Jahanmir. IEA Executive Committee Meeting. October, 1999.

Problem Encountered

None

Publications

None

Ceramic Mechanical Property Test Method Development

George D. Quinn (National Institute of Standards and Technology)

Objective/Scope

This task is to develop mechanical test method standards in support of the Propulsion Systems Materials Program. The test methods should meet the needs of the DOE engine community but should also consider the general USA structural ceramics community as well as foreign laboratories and companies.

Draft recommendations for practices or procedures shall be developed based upon the needs identified above and circulated within the DOE ceramics engine community for review and modification. Round-robins will be conducted as necessary, but shall be well-focused, limited in scope, and complementary to IEA round-robins. Procedures developed in this program will be standardized by ASTM and/or ISO.

Technical Highlights and Results

I. Summary

In this semiannual period, progress continued on refining the flexure strength test for cylindrical test specimens. Extensive fractographic analysis on Ceradyne SRBSN was performed to compare fracture origins in specimens prepared by different machining conditions. Emphasis was on detecting machining damage induced by a variety of machining procedures. This work is in conjunction with the NIST Ceramics Machining Consortium.

The ISO Technical Committee 206 draft standard for fracture toughness by the SCF method was revised extensively and sent to the secretariat. The Rolling Element Bearing Group adopted most of the revisions that we requested in their Silicon Nitride Bearing Ball material's specification. A comprehensive set of biaxial creep data was compiled and sent to Dr. Sung Choi at NASA-Glenn for analysis. The new paper on elastic modulus determination by resonance of rectangular prisms was corrected at the last moment prior to printing by the Journal of the American Ceramic Society.

The basic machining preparation steps of ASTM C 1161 and MIL STD 1942 for standard rectangular bend bars were reviewed since we may wish to update this ~17 year old procedure. The new paper on elastic modulus determination by resonance of rectangular prisms was printed by the Journal of the American Ceramic Society in February.

In this semiannual period, there was progress on several standards. Three International Standards Organization Standards were advanced. We worked on the following formal standards

- | | | |
|----|-----------------|--|
| 1. | ISO DIS 14704 | Advanced (Fine) Ceramics - Determination of Flexural Strength at Room Temperature (NIST-USA convenes) |
| 2. | ISO DIS 14705 | Fine Ceramics (Advanced Ceramics, Advanced Technical Ceramics) - Test Method for Hardness for Monolithic Ceramics at Room Temperature (Convened by Japan, NIST represents the USA) |
| 3. | ISO WD 15765 | Advanced (Fine) Ceramics - Determination of Flexural Strength at Elevated Temperature (NIST-USA convenes) |
| 4. | ISO draft 18766 | Fine (Advanced) Ceramics - Determination of Fracture Toughness at Room Temperature by the Surface Crack in Flexure (SCF) Method (convened by USA-NIST) |
| 5. | REBG-draft | Specification for Silicon Nitride Bearing Balls |
| 6. | ASTM C 1161 | Flexural Strength Revisions |

(DIS = Draft International Standard; FDIS = Final Draft International Standard, WD = Working Draft)

Earlier work in this project has contributed to twelve completed standards:

- | | | |
|-----|----------------|--|
| 1. | ASTM C 1161-90 | Standard Test Method for Flexural Strength of Advanced Ceramics at Ambient Temperature |
| 2. | ASTM C 1198-91 | Dynamic Young's Modulus, Shear Modulus, and Poisson's Ratio for Advanced Ceramics by Sonic Resonance |
| 3. | ASTM C 1211-92 | Standard Test Method for Flexural Strength of Advanced Ceramic at Elevated Temperature |
| 4. | MIL HDBK 790 | Fractography and Characterization of Fracture Origins in Advanced Structural Ceramics |
| 5. | ASTM C 1239-94 | Standard Practice for Reporting Strength Data and Estimating Weibull Distribution Parameters |
| 6. | ASTM C 1322-96 | Standard Practice for Fractography and Characterization of Fracture Origins in Advanced Ceramics |
| 7. | ASTM C 1326-96 | Standard Test Method for Knoop Indentation Hardness of Advanced Ceramics. |
| 8. | ASTM C 1327-96 | Standard Test Method for Vickers Indentation Hardness of Advanced Ceramics. |
| 9. | ASTM PS 070-97 | Standard Test Methods for the Determination of Fracture Toughness of Advanced Ceramics |
| 10. | ASTM E-1875-98 | Standard Test Method for Dynamic Young's Modulus, Shear Modulus, and Poisson's Ratio by Sonic Resonance |
| 11. | ASTM E-1876-98 | Standard Test Method for Dynamic Young's Modulus, Shear Modulus, and Poisson's Ratio by Impulse Excitation |
| 12. | ASTM C 1421-99 | "Standard Test Methods for Determination of Fracture Toughness of Advanced Ceramics |

2. Fracture Toughness

2a. ASTM Standard C 1421-99

A November, 2000 ASTM symposium on fracture resistance testing is being organized by Mr. Quinn in cooperation with Jon Salem at NASA-Glenn and Mike Jenkins at the University of Washington. This symposium has been fully subscribed. It will be a good opportunity to inform the ceramic and engineering community about the new fracture toughness standards. We also have scheduled a talk on the fracture toughness standards for the American Ceramic Society Conference in St. Louis in April.

2b. Standard Reference Material 2100 for Fracture Toughness

All work completed in 1999.

2c. Draft International Standard, SEPB Method, ISO Technical Committee TC 206, Fine Ceramics

This document is approved for Final Draft International Standard (FDIS) balloting. It is harmonious with the ASTM standard in most respects.

2d. Draft International Standard 18766, SCF Method, ISO Technical Committee TC 206

Extensive work was allocated to this topic in this semiannual period. A revised draft was prepared by Mr. Quinn, the convener, and sent to the TC 206 secretariat for distribution either for review or ballot as a "Committee Draft."

The ISO draft is the second one for this topic and incorporates changes made in response to input from the Japanese and, to a lesser degree from the English, at the June 1999 meeting of ISO Technical Committee 206 in London. The ISO draft is largely derived from ASTM standard C 1421 which was created with support from this DOE program and which was approved in April 1999. Although the SCF method is not included in the Japanese standard JIS R 1607, the Japanese delegation was receptive to including it in the TC 206 program. The European Community plans to adopt verbatim the ISO SCF method as one of the procedures in their European Standard in CEN Technical Committee 184.

A new annex to the ISO draft has the first venture into ceramic R-curve characterization by any method in any standard in the world. We incorporated some of Dr. Kouichi Yasuda's concepts plus elements derived from outstanding work done in Germany at the Technical High School, Darmstadt (Stech and Rödel) and at the Research Center, Karlsruhe (Fett and Munz). In response to a Japanese request, the SCF draft was modified to make it more similar in appearance to the SEPB draft that they had prepared for TC 206. This was a reasonable request and users will in the future be able to put the two documents

together side by side and recognize the similarities. On the other hand, there were a few crucial technical points that we did not change. For example, the Japanese requested that if slow crack growth was active, that a lab ambient outcome at their standard 0.5 mm/min crosshead rate be accepted as the "standard." The USA stance is that if slow crack growth is active, then the best estimate of fracture toughness is obtained either under inert atmosphere conditions or at very fast loading rates. If stable crack extension is detected on the fracture surface, then the critical crack size and not the precrack size should be used to compute fracture toughness.

3. Flexure Strength at Room Temperature - New Semi articulating Fixture Design

No activity this period. All work is complete, but a report and engineering drawings must be prepared.

4. Diametral Compression

No activity this period. There was no technical activity this period, but in response to a request from Kristin Breder at ORNL a compilation of a few key references was made. This work is on hold pending further intensive fractographic analysis to determine why our earlier test specimens did not fracture from volume flaws in the middle of the specimens. We remain optimistic that this method can be refined and made into a user friendly, standardized test.

5. Flexure Testing of Cylindrical Ceramic Specimens

Figure 1 shows the new fixture design developed as part of the NIST Machining of Ceramics Consortium. Since there is interest within the DOE Heavy Duty Diesel community for such testing, we accelerated the development of these fixtures in this program. A paper is in preparation for the Journal of the American Ceramic Society which will feature the new fixtures.

Fractographic analysis of fractured Ceradyne SRBSN rods was performed this period in conjunction with the NIST Machining of Ceramics Consortium program. Over 160 rods have now been examined carefully with optical microscopy and a large sample by scanning electron microscopy. Fracture sites have been evenly distributed within the fixture gage section, attesting to the success of the fixture design.

At the ASTM Committee C-28 meeting in Kansas City in November, Mr. Quinn made a 15 minute presentation about this project. The ASTM Committee concurred with the suggestion that a task group be created. We intend to have a draft or at least an extended outline ready before the next meeting of C-28 in April, 2000. A master review paper on cylindrical flexure strength testing is about half finished. Our plan is to finish the detailed fractographic work for the Machining Consortium project and then focus on the manuscript and the ASTM draft standard in the Spring of 2000.

Figure 1 shows the outcomes of the comprehensive analysis for Ceradyne SRBSN 147-31N silicon nitride 6 mm diameter rods tested on the new NIST four-point flexure fixture with 40 mm x 80 mm spans. Thirty specimens which were centerless transverse ground with a 320 grit wheel were compared to thirty rods which were longitudinally ground with the same wheel.

The transverse ground rods were appreciably weaker, but had a larger Weibull modulus (21.9). Fractography confirmed that machining damage were the fracture origins in every case except at the high strength end of the distribution, where some sintering flaws were detected. The machining flaws were 15-35 micron deep subsurface semi elliptical cracks. Initially it was difficult to find and confirm the machining damage in this self-reinforced silicon nitride which has elongated silicon nitride grains intended to enhance fracture toughness. We previously measured the fracture toughness in this material by the surface crack in flexure method in some rectangular bend bars. We created 50-70 μm deep semi

elliptical flaws. A toughness of 5.4 MPa \sqrt{m} was obtained, but fractographic interpretation of the artificially created flaws was also difficult. Note that the artificial flaws were not much larger than the machining flaws created in the rods. It is likely that this material has a rising R-curve, and large crack fracture mechanics specimens (e.g., chevron notch, or single edged precracked beam) probably would produce greater fracture toughness values.

In contrast, the longitudinally ground rods had much larger strengths, averaging over 800 MPa. The Weibull modulus (14.6) is very respectable. Fracture origins were almost always natural sintering flaws and machining damage was not controlling.

This work in this task is primarily intended to refine methodologies for cylindrical rod flexure strength testing, but the work also will certainly benefit machining studies.

Rectangular bars cut from the Ceradyne rods have also been tested in the Consortium program and are being carefully analyzed by comprehensive fractographic methods. Our goal is to compare the strengths and fracture flaws in rectangular and round rods from the identical material.

6. Flexure Testing of Segmented Cylindrical Ceramic Specimens

No progress this period.

7. Rolling Element Bearing Group (REBG) Silicon Nitride Bearing Ball Specification

A final set of minor revisions to the REBG draft Materials Specification for Silicon Nitride Bearing Balls was sent to Jeff Wickwire, at the Defense Contacts Management Center, located at Newbrook Machine Corp, Buffalo. The REBG dissolved and reestablished itself as a formal ASTM Committee. The REBG had intended to publish the specification as a REBG-100 specification and distribute it on their web site, this was not done in time. As soon as the new the new ASTM Committee F-34 was established, ASTM exercised their copyright authority and insisted the specification be only released by ASTM. Thus, the draft will now have to wend its way through the ASTM system, but this should not be too difficult, since over the last year or so this author has suggested a number of revisions to the REBG draft to bring it closer in style to and ASTM standards.

The materials specification sets limits on certain key property requirements that must be met for a particular silicon nitride. The draft specification was almost completed and includes a suite of materials requirements including density, color uniformity, surface finish, surface flaws, hardness, flexure strength, and fracture toughness. There are three possible ball classes. Class I is the highest grade for extreme performance requirements and Class III the lowest grade for low duty applications. The document is 14 pages long and includes citations of 10 ASTM test method standards, 6 of which were developed in large part due to work in this DOE program. These include ASTM C 1161, flexure strength; C 1198 and C 1259, elastic modulus; C 1327, Vickers hardness; C 1239 Weibull modulus; and C 1421, fracture toughness.

The REBG was an association of bearing manufacturers, bearing users, and the Department of Defense. The members of the silicon nitride bearing ball subcommittee include the US Department of Defense (US Air Force Wright Patterson AFB, Defense Center Supply, Richmond; and the Defense Contracts Management Center, Buffalo), Norton Advanced Ceramics, Hoover Precision

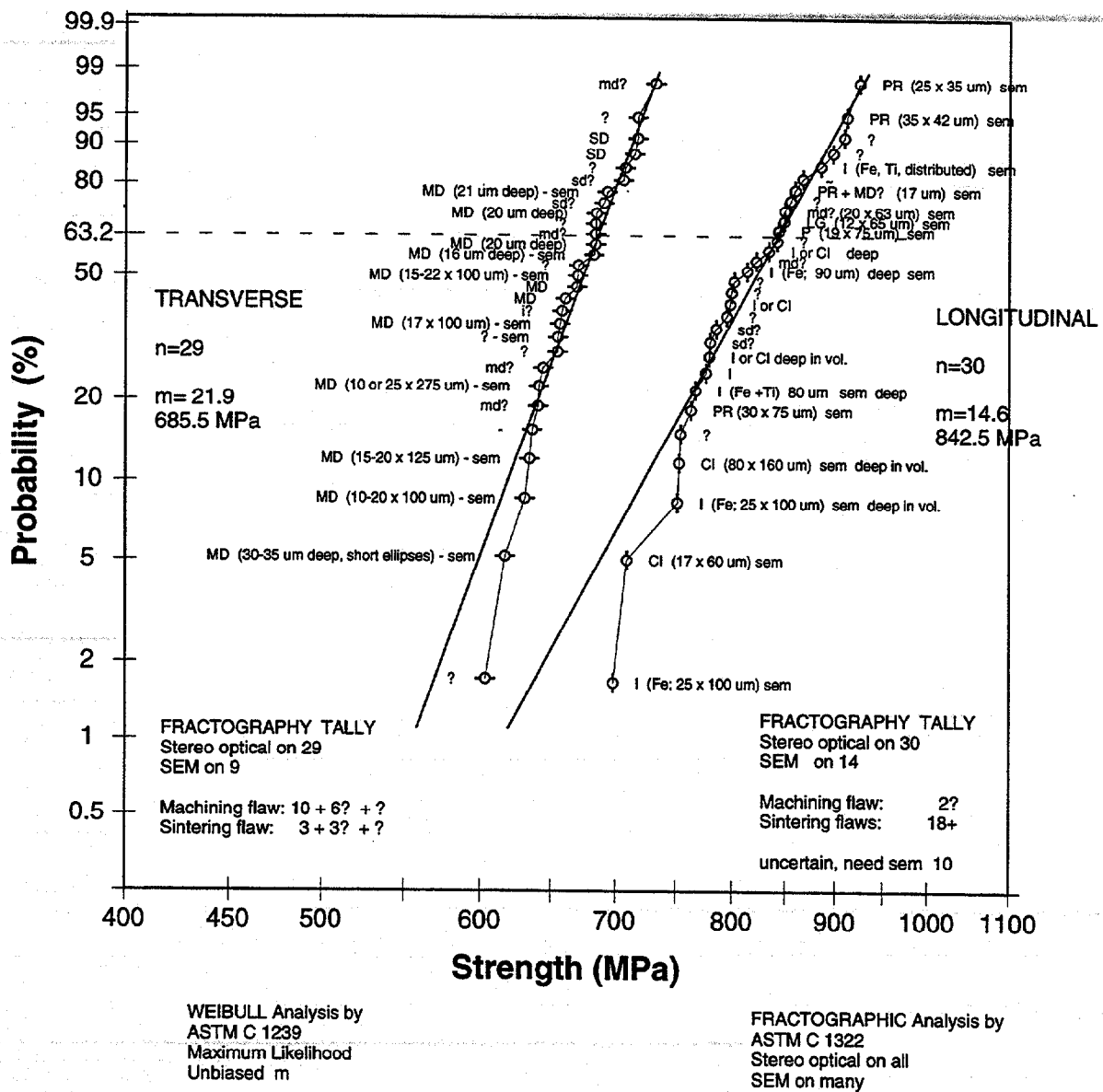


Figure 1 Strength distribution for 6 mm diameter x 100 mm Ceradyne SRBSN rods fractured in 4-point flexure with 40 mm x 80 mm spans. Rods were either transverse ground or longitudinally ground with a 320 grit wheel. The transverse rods are weaker than the longitudinally ground rods, but have a larger Weibull modulus. Each data point is labeled with the fracture origin type. The longitudinally ground specimens fractured from sintering flaws such as: CI, compositional inhomogeneity; I, Inclusion; PR, Porous Region; sd, unidentified sintering flaw; or md, machining damage. Flaw sizes in μm are shown when available. In contrast, the transverse ground specimens fractured from semi elliptical machining damage cracks whose size is shown in μm (depth x length). A few of the latter specimens at the high strength portion of the distribution failed from sintering flaws.

Products, Enceratec (Cummins-Toshiba), ESK, Pratt and Whitney, SKF, MPB, MRC, the Aerospace Corp, Quasar International, Hughes, Winsted Precision, Draper Lab, and NIST. We were not able to attend their November meeting due to the scheduling overlap with ASTM Committee C-28 meeting in Kansas City.

The new ASTM committee F-34, Rolling Element Bearings will have their first meeting on April 25-27, 2000 in Phoenix, Arizona. This unfortunately conflicts with the ASTM Committee C-28, Advanced Ceramics and American Ceramic Society meetings scheduled for the same time in St. Louis, Mo

The first draft of the new ASTM version of the silicon nitride bearing ball material specification was received and reviewed for the benefit of the new ASTM committee F-34. Mr. Quinn joined ASTM Committee F-34.

8. Other Activities

8a. ISO Technical Committee TC 206 (Fine Ceramics)

WG 2 Flexure Strength at Room Temperature

No progress this period. The "Final Draft International Standard 14704" is being balloted.

WG 3 Hardness

This document, FDIS 14705, is up for ballot as a Final Draft International Standard. All important specifications and tolerances are harmonious with ASTM standards C 1326 and C 1327 from Committee C-28, Advanced Ceramics. During this period, the formal ballot was received and reviewed. We detected some minor editorial mistakes including an error in one equation. We also ascertained that several illustrations showing the indentation tips and microscope crosshairs were not quite right. An affirmative ballot with recommended changes was sent to ISO.

WG 8 Flexure Strength at Elevated Temperature

The working draft for the ISO standard was reviewed at the annual TC 206 meeting in June. A number of revisions were proposed. Most have been included into a new draft and the TC 206 secretariat agreed to submit the corrected document for ballot as a "Committee Draft."

8b. Elastic Modulus by Resonance

We may refine ASTM standards C 1198 and C 1259 for the influence of chamfers. Years ago as part of this project, we helped write ASTM standard C 1198 for the determination of elastic modulus of ceramics by resonance of prism specimens. This standard was adapted to more modern impulse excitation methods which also use beam resonance and standard C 1259 also was prepared.

The resonance method of elastic modulus determination entails measuring the resonant frequency of vibration of a prismatic beam specimen. Elastic modulus is calculated from the beam mass, dimensions, and the resonant frequency. This is a well established, simple methodology which has been codified in the two C-28 standards. The standards require nearly perfect rectangular beam specimens, however, since the equations which relate elastic modulus to the beam dimensions, beam mass, and the resonant frequency assume that the beam has a perfect rectangular geometry. C 1198 and C 1259 recommended against using chamfered bars.

We felt that it would be helpful to extend the applicability of C 1198 and C 1259 to ordinary chamfered ceramic strength specimens. In April 1999, Jeff Swab of the US Army Research Laboratory came to NIST to use our resonance equipment on both chamfered and unchamfered ceramic test bars. Jeff measured the resonant frequencies and found that indeed, the chamfers did affect the results. We

devised a correction factor for the presence of the chamfers and this correction matched the experimental shift almost perfectly. For a standard 3 mm x 4 mm bend bar with the maximum chamfers of 0.15 mm, the correction to E is 0.9%. Larger chamfers incur greater than 1% error. A paper on the analytical and experimental data was written and submitted to the Communications of the American Ceramic Society.

At the ASTM Committee C-28 meeting in November 1999 in Kansas City, we proposed that the two resonance standards be modified to include chamfered specimens. The ASTM committee agreed that revisions to C 1198 and C 1259 could be implemented as an annex. Several members in the audience wondered whether the analysis included chamfer effects on the apparent density. This remark prompted us to thoroughly reexamine the equations in all the old papers and sundry world standards. They all assume that the density is the mass divided by the physical dimensions of the bar. Thus, the commenters at the ASTM meeting were correct and due account of apparent density change must also be made in addition to the moment of inertia correction. In December Mr. Quinn and Mr. Swab hastily revised their manuscript which had been approved by the Journal of the American Ceramic Society. They decided to hold off on the revision to the ASTM standards until after the Journal paper was published. The Journal paper was published in February 2000.

8c Review of biaxial creep data

We recently learned that Dr. John Gyekenyesi and Dr. Sung Choi at NASA-Glenn wished to expand the Cares reliability code to cover not only fast fracture biaxial failure modes, but stress rupture and creep fracture as well. We offered to compile and send some old hot-pressed silicon nitride NC 132 data to NASA Glenn. They felt that the quality of data on this older model silicon nitride was worth the effort and would tie in nicely with their own data bases.

In 1987 and 1988, while Mr. Quinn was an exchange scientist at the German Aerospace Research Institute in Cologne, Germany, a series of biaxial stress rupture tests were conducted on hot-pressed silicon nitride disks. The disks were Norton grade NC 132 and were tested in ring on ring loading at 1200 and 1300°C to times out to several hundred hours. Results were compared to uniaxial four point flexure data collected in the 1980's at the U.S. Army Watertown Arsenal. The uniaxial flexure data was used to construct elaborate fracture mechanics maps. The biaxial disks fractured in a similar fashion to the uniaxial bars, but usually at shorter times due to the greater concentration of flaws. Nonetheless, the basic slow crack growth and creep fracture mechanisms in the biaxial disks were identical to what had been detected with the bend bars. The fracture origin and stress rupture lifetime data results were published in 1990. As far as we know, they remain the only biaxial stress rupture data ever collected for an advanced ceramic at elevated temperature.

Center point **creep deflection** data was collected on these specimens as well, yet was not analyzed in the following decade. Corrections for neutral axis shift due to biaxial creep relaxation was perceived to be a daunting task. To the best of our knowledge, no one has ever analyzed the problem. (The matter was formidable enough in the 1970's and 1980's for uniaxial four-point flexure testing.) The 12 year old files were reopened, dusted off, and the strip chart records annotated and analyzed. All data was forwarded to NASA-Glenn.

8d Review ASTM C 1161 flexure strength "Standard Procedure" for machining specimens

After 17 years in use, the basic specimens preparation procedure of MIL STD 1942 and ASTM C 1161 should be revisited. Is a finishing wheel with 320 grit adequate? Are the depths of cut per pass (.0001") too restrictive and slow? Is the total amount of material to be removed in final finishing (0.060

Table 1 Standard Rectangular Flexure Bar Preparation Procedures

	MIL STD 1942 (1983)* ASTM C 1161 (1990) "Standard Procedures"	ISO FDIS 14704 (2000) "Basic Machining Procedure" "The procedure described below is a general duty, conservative practice."	CEN ENV 843-1 (1995) "Standard Preparation Procedures" "This procedure is recommended when there is no other specified method."
General	All grinding shall be done with an ample supply of filtered coolant. Grinding shall be in at least 2 stages, ranging from coarse to fine rates of removal. All machining shall be in the surface grinding mode parallel to the specimen long axis. No Blanchard or rotary grinding	All grinding shall be done with an ample supply of filtered coolant. Grinding shall be in at least 2 stages, ranging from coarse to fine rates of removal.	All grinding shall have an adequate quantity of coolant at all times. Remove approximately equal amounts of material from opposite faces. All grinding shall be parallel to the specimen long axis. Discontinuous rim wheels shall not be used.
Coarse Grinding	Depth of cut not to exceed 0.03 mm (0.001") per pass. to the last 0.06 mm (.002") per face	Grit size shall not exceed 120 mesh (D 126) Diamond wheel shall be round within 0.03 mm. Depth of cut not to exceed 0.03 mm per pass. Alternatively, a creep feed grinding process may be used for the coarse grinding step.	Grit size shall not exceed 120 mesh (D 126). Use a continuous rim peripheral grinding wheel which is round within 0.03 mm. Depth of cut not to exceed 0.03 mm per pass.
Final Grinding	Grit size (200-500) * 320 - 500 no less than 0.06 mm (0.002") per face Depth of cut not to exceed 0.002 mm (0.0001") per pass Remove approximately equal stock from opposite faces	Grit size 320 and 800 mesh (D46 or finer). no less than 0.06 mm per face Depth of cut not to exceed 0.002 mm per pass. Remove approximately equal stock from opposite faces.	Grit size 320 - 500 mesh (D46 or finer) no less than 0.06 mm. Depth of cut not to exceed 0.002 mm/pass. Final pass shall have zero cut.
Chamfers	4 long edges shall be chamfered 45° 0.12 ± 0.03 mm or rounded 0.15 ± 0.05 mm Must be comparable to finish on the flat faces. Direction shall be longitudinal. If chamfers are oversized, correct the stress. Chamfers not needed in some cases.	same as ASTM C 1161 and MIL STD 1942	Edges shall be chamfered or radiused after the faces are finished. Finish the edges the same way as the faces. Direction shall be longitudinal.
Other	Materials with low fracture toughness and a greater susceptibility to grinding may require finer grinding wheels at very low removal rates.		Alternatively, A creep feed grinding process may be used using the same grit sizes as specified above, and with the final grinding removing at least 0.06 mm or material with final passes of 0.002 and 0 mm! The surface roughness R _{max} measured with a profilometer shall be less than 2 μm.

mm) too much? Can we make the procedure more efficient or should we make it more stringent? Should wheel speeds and wheel trueness and table speeds be added? Questions like these had arisen in the NIST Machining Consortium and also arisen from contacts from the European Community scientists as they prepare their CEN standards. We consequently decided to revisit the entire matter and will ask for guidance from the machining consortium. Recommendations for possible changes will be made at the ASTM Committee C-28 meeting in St. Louis in May. Table 1 was prepared to show the current procedure as well as the European and ISO analogues.

Status of Milestones

A list of proposed changes to the milestones in this project was sent to ORNL in early April for review. Many of the old milestones are out of date and not relevant. For example, the shift in emphasis to cylindrical rod flexure strength testing has caused us to defer work on diametral compression.

Problems encountered

None this period, except that the attention paid to the REBG, ISO, and ASTM resonance-chamfer activities have limited our progress on other elements. Work on diametral compression and segmented cylinder testing has been deferred while we focus on completing the flexural strength of cylindrical rods project.

Publications/Presentations

1. G. Quinn and J. Swab, "Elastic Modulus by Resonance of Rectangular Prisms: Corrections for Chamfers," J. Am. Ceram. Soc., 83 [2] 317-320 (2000).
2. G. Quinn, presentation "Proposal for Revisions to ASTM Standards C 1198 and C 1259" Elastic Moduli by Beam Resonance," ASTM Committee C-28 meeting, Kansas City, November 1999.
3. G. Quinn, presentation "Proposal for a New ASTM task Group on Flexural Testing of Cylindrical Rods, ASTM Committee C-28 meeting, Kansas City, November, 1999.

Communications/Visits

Mr. Quinn attended the meeting of ASTM Committee C-28 in Kansas City in November. Jeff Wickwire of Defense Contract Management Center was contacted repeatedly regarding the REBG silicon nitride ball specification. A set of drawings of 4-point flexure fixtures was sent to John Petrovic at Los Alamos National lab. Information on testing cylindrical flexure specimens was sent to Tom Yonushonis of Cummins. Mr. Quinn visited the U.S. Army Research Laboratory in Aberdeen in December to coordinate the corrections to the resonance-chamfer-elastic modulus paper. Ring on ring biaxial creep data on hot pressed silicon nitride, grade NC 132, was compiled and sent to Sung Choi at NASA-Glenn for analysis. Dr. Curtis Martin of the Naval Surface Warfare Center, Carderock visited NIST to consult on fracture toughness testing and NIST SRM 2100.

The Oak Ridge Report: "Strength and Fatigue of NT 551 Silicon Nitride and NT 551 Diesel Exhaust Valves," by Andrews, Wereszczak, Kirkland and Breder arrived and was read cover to cover. This work was very helpful since it dealt with similar issues to those being studied in this NIST task. How well do rectangular strengths compare to rod strengths, tension specimens, and valve stems? Mr. Quinn contacted Wereszczak, Andrews and Breder to offer congratulations on the work.

INTERNAL DISTRIBUTION

L. F. Allard, Jr.
P. F. Becher
T. M. Besmann
P. J. Blau
R. A. Bradley
C. R. Brinkman
T. D. Burchell
A. Choudhury
D. D. Conger
S. A. David
M. K. Ferber
R. L. Graves
C. R. Hubbard
M. A. Janney
D. R. Johnson (5)
R. R. Judkins

M. A. Karnitz
J. O. Kiggans
E. Lara-Curzio
R. J. Lauf
K. C. Liu
R. A. Lowden
W. D. Manly
S. B. McSpadden
T. A. Nolan
A. E. Pasto
M. H. Rawlins
A. C. Schaffhauser
D. P. Stinton
T. N. Tiegs
S. G. Winslow
R. E. Ziegler
Laboratory Records - RC

Jeffrey Abboud
Gas Turbine Association
1050 Thomas Jefferson St., NW, 5th Floor
Washington DC 20007

B. P. Bandyopadhyay
University of North Dakota
Box 8359 University Station
Grand Forks ND 58202-8359

Donald F. Baxter, Jr.
Advanced Materials & Processes
ASM International
9639 Kinsman Road
Materials Park OH 44073-0002

M. Brad Beardsley
Caterpillar Inc.
Technical Center Bldg. E
P.O. Box 1875
Peoria IL 61656-1875

Ramakrishna T. Bhatt
NASA Glenn Research Center
MS-106-1
21000 Brookpark Road
Cleveland, OH 44135

Bruce Boardman
Deere & Company, Technical Ctr.
3300 River Drive
Moline IL 61265-1792

Donald J. Bray
Advanced Refractory Technologies
699 Hertel Avenue
Buffalo NY 14207

Jeff Bougher
Caterpillar Inc.
Technical Center, Bldg. E
P.O. Box 1875
Peoria IL 61656-1875

Mike Bowling
Cummins Engine Company, Inc.
1900 McKinley Avenue
P.O. Box 3005
Columbus IN 47202-3005

Walter Bryzik
U.S. Army Tank Automotive
Command
R&D Center, Propulsion Systems
Warren MI 48397-5000

David Carruthers
Kyocera Industrial Ceramics
5713 East Fourth Plain Blvd.
Vancouver WA 98661

Ronald H. Chand
Morton Advanced Materials
185 New Boston Street
Woburn MA 01801

William J. Chmura
Torrington Company
59 Field Street, P.O. Box 1008
Torrington CT 06790-1008

William S. Coblenz
Defense Adv. Research Projects Agency
3701 N. Fairfax Drive
Arlington VA 22203-1714

Gloria M. Collins
ASTM
100 Barr Harbor Drive
West Conshohocken PA 19428-2959

Shawn Cooper
FEV Engine Technology
4554 Glenmeade Lane
Auburn Hills MI 48326-1766

Douglas Corey
Honeywell
2525 West 190th Street, MS:T52
Torrance CA 90504

Keith P. Costello
Chand/Kare Technical Ceramics
2 Coppage Drive
Worcester MA 01603-1252

Gary M. Crosbie
Ford Motor Company
P.O. Box 2053, 20000 Rotunda Drive
MD-3182, SRL Building
Dearborn MI 48121-2053

Pamela Cunningham
WETO Technical Library
MSE, Inc.
Industrial Park, P. O. Box 4078
Butte MT 59702

S. Keoni Denison
Norton Company
1 New Bond Street
Worcester MA 01615-0008

Sidney Diamond
U.S. Department of Energy
Office of Transportation Technologies
EE-33, Forrestal Building
Washington DC 28505

Michael Easley
Honeywell
P. O. Box 52181
MS 551-11
Phoenix AZ 85072-2181

James J. Eberhardt
U.S. Department of Energy
Office of Transportation Technologies
EE-33, Forrestal Building
Washington DC 20585

Jim Edler
Eaton Corporation
26201 Northwestern Highway
P.O. Box 766
Southfield MI 48037

William A. Ellingson
Argonne National Laboratory
Energy Technology Division, Bldg. 212
9700 S. Cass Avenue
Argonne IL 60439-3848

John W. Fairbanks
U.S. Department of Energy
Office of Transportation Technologies
EE-33, Forrestal Building
Washington DC 20585

Ho Fang
Applied Materials
2695 Augustine Drive, MS-0962
Santa Clara CA 95054

Dan Foley
Honeywell
MS:1/5-1, 26000
2525 West 190th Street
Torrance CA 90504

Douglas Freitag
DuPont Lanxide Composites
21150 New Hampshire Avenue
Brookeville MD 20833

Richard Gates
NIST
Bldg. 223, Rm. A-256
Rt. 270 & Quince Orchard Road
Gaithersburg MD 20899

Ludwig J. Gauckler
ETH Zurich
Nonmetallic Materials
Sonneggstr. 5
CH-8092 Zurich, SWITZERLAND

Robert J. Gottschall
U.S. Department of Energy
Metal & Ceramic Sciences, ER-131
19901 Germantown Road
Germantown MD 20874-1290

Thomas J. Gross
U.S. Department of Energy
Office of Transportation Technologies
EE-30, Forrestal Building
Washington DC 20585

Changsheng Guo
United Technologies Research Center
Machining Systems, MS 129-46
East Hartford CT 06108

Darryl Gust
Cummins Engine Company, Inc.
1900 McKinley Avenue
P.O. Box 3005
Columbus IN 47202-3005

Nabil S. Hakim
Detroit Diesel Corporation
13400 Outer Drive West, A08
Detroit MI 48239-4001

Alan M. Hart
Dow Chemical Company
1776 Building
Midland MI 48674

Michael H. Haselkorn
Caterpillar Inc.
Technical Center, Building E
P.O. Box 1875
Peoria IL 61656-1875

Deborah A. Haught
U.S. Department of Energy
Office of Power Technologies
EE-23, Forrestal Bldg.
Washington DC 20585

Daniel Hauser
Edison Welding Institute
Microjoint & Plastics Tech. Team
1250 Arthur E. Adams Drive
Columbus OH 43221-3585

John Haygarth
Wah Chang
P.O. Box 460
Albany OR 97321-0460

Gene Huber
Precision Ferrites & Ceramics
5432 Production Drive
Huntington Beach CA 92649-1525

Adam Jostsons
ANSTO
PMB1
Menai, NSW, Australia 2234

Yury Kalish
Detroit Diesel Corporation
Mechanical Systems
13400 Outer Drive West
Detroit MI 48239-4001

Roy Kamo
Adiabatics, Inc.
3385 Commerce Park Drive
Columbus IN 47201

Ralph Kelly
Cincinnati Milacron
P.O. Box 9013
Cincinnati OH 45209

W. C. King
Mack Truck, Z-41
1999 Pennsylvania Avenue
Hagerstown MD 21740

Tony Kim
Caterpillar Inc.
Defense Products Dept., JB7
Peoria IL 61629

Joseph A. Kovach
Parker Hannifin Corporation
6035 Parkland Boulevard
Cleveland OH 44124-4141

Edwin H. Kraft
Kyocera Industrial Ceramics
5713 E. Fourth Plain Boulevard
Vancouver WA 98661

Oh-Hun Kwon
Norton Company
Saint Gobain Industrial Ceramics
1 Goddard Road
Northboro MA 01532-1545

S. K. Lau
B. F. Goodrich Aerospace R&D
9921 Brecksville Road
Brecksville OH 44141

Elaine Lentini
Saint-Gobain Industrial Ceramics
Goddard Road
Northboro MA 01532

Stan Levine
NASA Glenn Research Center
21000 Brookpark Road, MS:106/5
Cleveland OH 44135

Robert H. Licht
Norton Company
Saint Gobain Industrial Ceramics
1 Goddard Road
Northboro MA 01532-1545

E. Lilley
Norton Company
Saint Gobain Industrial Ceramics
1 Goddard Road
Northboro MA 01532-1545

B. J. McEntire
Applied Materials Corporation
3050 Bowers Avenue
Santa Clara, CA 95054

James McLaughlin
Sundstrand Power Systems
4400 Ruffin Road
P.O. Box 85757
San Diego CA 92186-5757

Biljana Mikijelj
Ceradyne, Inc.
3169 Red Hill Avenue
Costa Mesa CA 92626

Carl E. Miller
Delphi Energy & Engine Mgmt. Systems
4800 S. Saginaw Street, MC 485-301-150
P. O. Box 1360
Flint MI 48501-1360

Malcolm Naylor
Cummins Engine Company, Inc.
P.O. Box 3005, Mail Code 50183
Columbus IN 47202-3005

Dale E. Niesz
Ceramic & Materials Engineering
607 Taylor Road, Rm. 204
Piscataway, NJ 08854-8065

Thomas J. Paglia
Coors/ACI
3315 Boone Road
Benton AR 72015

Richard Palicka
CERCOM, Inc.
1960 Watson Way
Vista CA 92083

Vijay M. Parthasarathy
Solar Turbines
2200 Pacific Highway, M.Z. R-1
San Diego CA 92186

Magan Patel
Cummins Engine Company, Inc.
Mail Code 50183
Box 3005
Columbus IN 47202-3005

James W. Patten
 Cummins Engine Company, Inc.
 P.O. Box 3005, Mail Code 50183
 Columbus IN 47202-3005

Joe Picone
 Norton Company
 1 New Bond Street
 Box 15008
 Worcester MA 01615-0008

Stephen C. Pred
 Pred Materials International, Inc.
 60 East 42nd Street, Suite 1456
 New York NY 10165

Vimal K. Pujari
 Norton Company
 Saint Gobain Industrial Ceramics
 1 Goddard Road
 Northboro MA 01532-1545

Fred Quan
 Corning Inc.
 Sullivan Park, FR-2-8
 Corning NY 14831

George Quinn
 NIST
 I-270 & Clopper Road
 Ceramics Division, Bldg. 223
 Gaithersburg MD 20899

Mike Readey
 Caterpillar, Inc.
 Technical Center, Bldg. E
 P.O. Box 1875
 Peoria IL 61656-1875

Jack A. Rubin
 CERCOM, Inc.
 1960 Watson Way
 Vista CA 92083

Robert J. Russell
 Riverdale Consulting, Inc.
 24 Micah Hamlin Road
 Centerville MA 02632-2107

J. Sankar
 North Carolina A&T State Univ.
 Dept. of Mechanical Engineering
 Greensboro NC 27406

Maxine L. Savitz
 General Manager, Technology/Partnerships
 Honeywell
 2525 West 190th Street, MS:1/5-2
 Torrance CA 90504

Jim Schienle
 Honeywell
 1130 West Warner Road
 M/S 1231-K
 Tempe AZ 85284

Gary Schnittgrund
 Transfer Technology
 16401 Knollwood Drive
 Granada Hills CA 91344

Robert S. Shane
 Shane Associates
 1904 NW 22nd Street
 Stuart FL 34994-9270

Subu Shanmugham
 MicroCoating Technologies
 3901 Green Industrial Way
 Chamblee GA 30341-1913

Albert J. Shih
 North Carolina State University
 Mechanical & Aerospace Engineering
 2217 Broughton Hall, Box 7910
 Raleigh NC 27695

Charles Spuckler
 NASA Glenn Research Center
 21000 Brookpark Road, MS: 5-11
 Cleveland OH 44135-3127

Gordon L. Starr
Cummins Engine Company, Inc.
P.O. Box 3005, Mail Code:50182
Columbus IN 47202-3005

Marian Swirsky
Cambridge Scientific Abstract
Commerce Park, Bldg. 4, Suite 804
23200 Chagrin Blvd.
Beachwood OH 44122

Victor J. Tennery
113 Newell Lane
Oak Ridge TN 37830

Malcolm Thomas
Allison Engine Company
P. O. Box 420 (W06)
Indianapolis IN 46206

Marc Tricard
Norton Company
Superabrasives Division
1 New Bond Street, MS-412-301
P. O. Box 15008
Worcester MA 01615-0008

Marcel H. Van De Voorde
Commission of the European Union
Eeuwigelaan 33
1861 CL Bergen
THE NETHERLANDS

Robert M. Washburn
ASMT
11203 Colima Road
Whittier CA 90604

R. W. Weeks
Argonne National Laboratory
Bldg. 362, E313
9700 S. Cass Avenue
Argonne IL 60439

Sheldon M. Wiederhorn
NIST
Building 223, Room B309
Gaithersburg MD 20899

Matthew F. Winkler
Seaworthy Systems, Inc.
P.O. Box 965
Essex CT 06426

Thomas J. Wissing
Eaton Corporation
26201 Northwestern Highway
P.O. Box 766
Southfield MI 48037

James C. Withers
MER Corporation
7960 S. Kolb Road
Tucson AZ 85706

Dale E. Wittmer
Southern Illinois University
Mechanical Engineering Dept.
Carbondale IL 62901

Egon E. Wolff
Caterpillar Inc.
Technical Center
P.O. Box 1875
Peoria IL 61656-1875

Roy Yamamoto
Ethyl Petroleum Additives, Inc.
500 Spring Street
P. O. Box 2158
Richmond VA 23218-2158

R. L. Yeckley
Kennametal, Inc.
P.O. Box 231
Latrobe, PA 15650

Thomas M. Yonushonis
Cummins Engine Company, Inc.
1900 McKinley Avenue
P.O. Box 3005, Mail Code 50183
Columbus IN 47202-3005

S. Charles Yoon
Cincinnati Milacron, Inc.
P.O. Box 9013
3000 Disney Street
Cincinnati OH 45209-9013

Jong Yung
Sundstrand Aerospace
Dept. 789-6
4747 Harrison Avenue
Rockford IL 61125

Zhenqi Zhu
Stevens Institute of Technology
Department of Mechanical Engineering
Castle Point on Hudson
Hoboken NJ 07030

Department of Energy
Oak Ridge Operations Office
Assistant Manager for Energy
Research and Development
P. O. Box 2001
Oak Ridge TN 37831-8600

For distribution by microfiche
as shown in DOE/OSTI-4500,
Distribution Category UC-332
(Ceramics/Advanced Materials).